RICE UNIVERSITY

Three dimensional nanostructured designs for Lithium ion Batteries

by

Sanketh R. Gowda

A THESIS SUBMITTED
IN PARTIAL FULFILLMENT OF THE
REQUIREMENTS FOR THE DEGREE

Doctor of Philosophy

APPROVED, THESIS COMMITTEE

Pulickel M. Ajayan (Chair)
Professor of Mechanical Engineering and Materials Science

Matteo Pasquali
Professor of Chemical and Biomolecular Engineering

Jun Lou
Assistant Professor of Mechanical Engineering and Materials Science

HOUSTON, TEXAS
February 2012

ABSTRACT

Three Dimensional Nanostructured Designs for Lithium Ion Batteries

by

Sanketh R. Gowda

The reversible electrochemistry and the superior gravimetric and volumetric energy storage capacities of lithium ion batteries (LIBs) have propelled them as the dominant power source for a range of portable electronic devices. Thin film LIBs are a class of LIBs that have been extensively used for powering Microelectromechanical systems devices, Radio-frequency Identification tags, biomedical sensors and several other low power electronic systems. Thin film electrodes and electrolytes are characteristic of short lithium ion diffusion paths and hence show fast charge/discharge rates. But the thin film battery technology has the major drawback of possessing low energy per footprint area. The three dimensional design for thin film LIBs has been proposed to improve electrode mass loading per footprint area thereby improving the energy delivered by the device. Hence there is interest in assembling the entire battery (current collectors, anode, electrolyte, and cathode) in a three dimensional (3D) nanostructured architecture. This thesis deals with the development and assembly of nanostructured three dimensional designs for Li ion battery components. Several template-based techniques have been used to fabricate nanostructured materials which serve as building blocks for the 3D energy storage devices. Firstly we have addressed the challenging task of fabricating conformal nanostructured polymer electrolytes around nanowire electrode material. The polymer coatings helped in controlling the secondary electrolyte interphase formation and hence in the improvement of cycling characteristics of the nanowire electrode material. We have also fabricated 3D current collectors with

both ordered and disordered pore structure. Electrodes coated on 3D nanostructured current collectors showed improved rate capability and energy per footprint area. Finally, we have used a bottom up approach to assemble all essential components (anode, electrolyte, and cathode) of an electrochemical energy storage device onto a single nanowire, and have tested a parallel array of such nanowire devices for its electrochemical performance, hence demonstrating the ultimate miniaturization possible for energy storage devices.

Acknowledgements

Firstly, I would like to thank my parents and my brother for their encouragement, care and support over the course of my doctoral studies. I must next thank my advisor, Dr. Pulickel M. Ajayan, who gave me this great opportunity to conduct research in the exciting field of nanotechnology. His creativity has had a profound impact on the way I shaped my doctoral research work. I am grateful to have had the opportunity to engage in scientific discussions with a true pioneer in the field of nanotechnology. Dr. Ajayan placed great amount of trust in me, and allowed me to develop independent critical thinking abilities which continue to help me to this day. Dr. Ajayan provided tremendous amount of freedom to explore different scientific challenges. Just interacting with Dr. Ajayan on a daily basis helped me improve as a person. Dr. Ajayan's openness in talking different topics of science and life in general, lead to very interesting discussions which I will cherish for the rest of my life. Dr. Ajayan is someone I look up to, and has set a great example in the kind of person I want to be. Dr. Ajayan has not only been my research advisor, but also a friend and has helped me through several difficult periods over my doctoral studies, for which I remain grateful.

I want to thank Dr. Matteo Pasquali for his constant support over the course of my Ph.D. I have had the opportunity to interact with him in classes and as a part of my thesis committee, and I am grateful for all the insightful suggestions he has given to improve my work. I am very grateful for his patience

and support throughout my Ph.D. here at Rice. I want to thank Dr. Jun Lou for useful suggestions and help in shaping my thesis work. He has been a constant support over the years and I would like to thank him for the great relationship I was able to develop.

I would like to thank the Chemical and Biomolecular Engineering department for giving me this opportunity to conduct research at Rice University. I would like to thank Dr. Clarence Miller, Dr. George Hirasaki and Dr. Laura Segatori for their constant support through my Ph.D.

I am very grateful to past and current members of my research lab, for being great labmates and helping me all along my doctoral studies. Dr. Arava Leela Mohana Reddy has helped and mentored me through my Ph.D. for which I am truly thankful. I would also like to thank Dr. Robert Vajtai for all the advice and help he has provided me over the course of my Ph.D. Past members, Dr. Fung Suong Ou, Dr. Shaijumon Manikoth have also been great influences and have guided and helped me on several occasions.

I would like to thank all the great friends, staff members and colleagues I was able to interact with over the years. I think my experience was truly satisfactory due to the great times I was able to share with everyone I had a chance to meet at Rice University.

Finally, I would like to dedicate this thesis to my parents and my brother, who have played a major role in helping me pursue the doctoral program and stayed by my side to support me all along.

Contents

List of Figures

List of Tables

Chapter 1: Introduction

1.1. Lithium ion Battery

Batteries are energy storage devices that convert chemical energy stored in electrodes to electrical energy via electrochemical reduction-oxidation (redox) reactions. [1] A battery consists of two coupling electrodes for energy storage (positive and negative electrodes) on respective current collectors, and an ion conductive electrolyte (either solid or liquid). When a battery is connected to a load, the electrochemical potential between the two electrodes drives electrons from the negative electrode to the positive electrode, and induce redox reactions within the electrodes for continuous electron release. There are two types of battery systems: primary and secondary (or rechargeable) batteries. When chemical sources are depleted, primary batteries can not be restored; while secondary batteries have reversible redox reactions and are capable of being restored to their original chemical composition by charging and discharging for over hundreds or thousands of cycles.[2-10]

Since the invention of the first battery by Alessandro Volta in 1800, a variety of battery systems have been developed. Lithium metal is an attractive energy storage source for its light weight (0.53 g/cm^3), high specific capacity (3862 mAh/g), and highest operation voltage (-3.04 V versus Standard Hydrogen Electrode).[7] Upon continuous reversible charge and discharge cycles, dendritic mossy growth forms on lithium surfaces due to uneven Li plating and hence causing short circuits and battery failure; hence, metallic lithium is not widely applied as anode material in rechargeable batteries. Carbon has then been found to safely store lithium and allow lithium intercalation and de-intercalation reversibly. Since SONY developed the first lithium-ion battery adopting carbonaceous electrodes in 1991, lithium-ion battery system has become one of the

most popular battery systems for its high energy density, compact size and light weight.[2,11]

Lithium batteries have both the highest volumetric and gravimetric energy density among known technologies applied, including lead-acid, nickel-cadmium, nickel metal hydroxide and other systems as shown in Figure 1-1.[7]

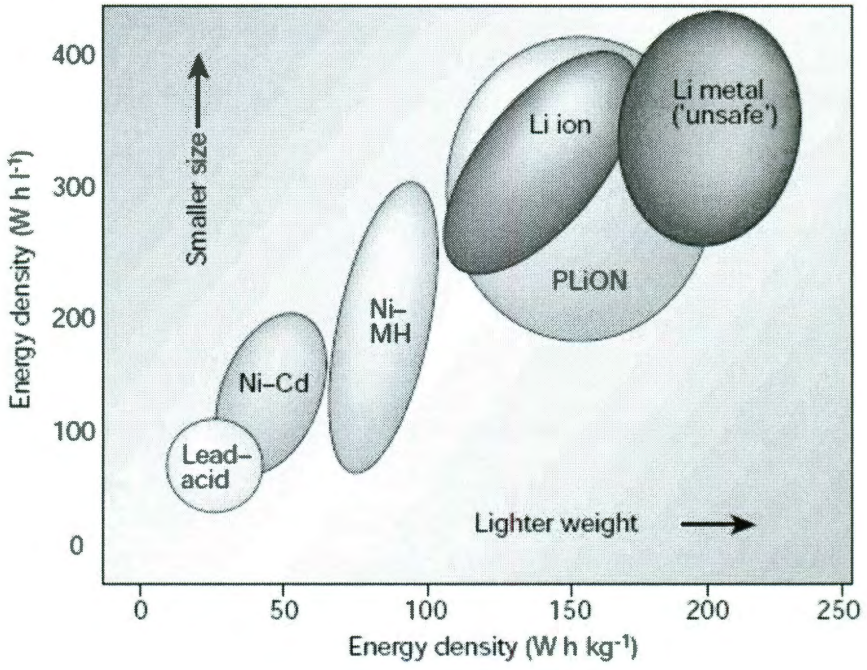

Figure 1-1: Volumetric energy density vs Gravimetric energy density of rechargeable batteries. (Ref. 7)

Similar to any other rechargeable battery systems, i) Lithium battery consists of a lithium metal negative electrode, carbon based cathode and a non-aqueous electrolyte and ii) Lithium-ion battery typically consists of a carbonaceous anode (negative electrode), a lithium metal oxide cathode such as layered $LiCoO_2$ or spinel $LiMn_2O_4$

(positive electrode)[12-22] and a non-aqueous organic electrolyte[23-34] in between. Schematic presentations of both lithium and lithium-ion cell are shown in Figure 1-2. Both of the electrodes work as lithium storage matrix for reversible lithium insertion and extraction; while the electrolyte serves as an ionic pathway for lithium ion transport as well as a separator for the two electrodes. In this thesis we study the Li ion battery system due to its practical applicability standpoint. The energy storage mechanism for lithium-ion battery can be explained as: upon charging lithium stored in cathode is oxidized to lithium ion and released to electrolyte, while lithium ion is reduced and intercalates into anode; upon discharging lithium is oxidized and de-intercalates from anode, and lithium ions are reduced and inserted into cathode matrix.

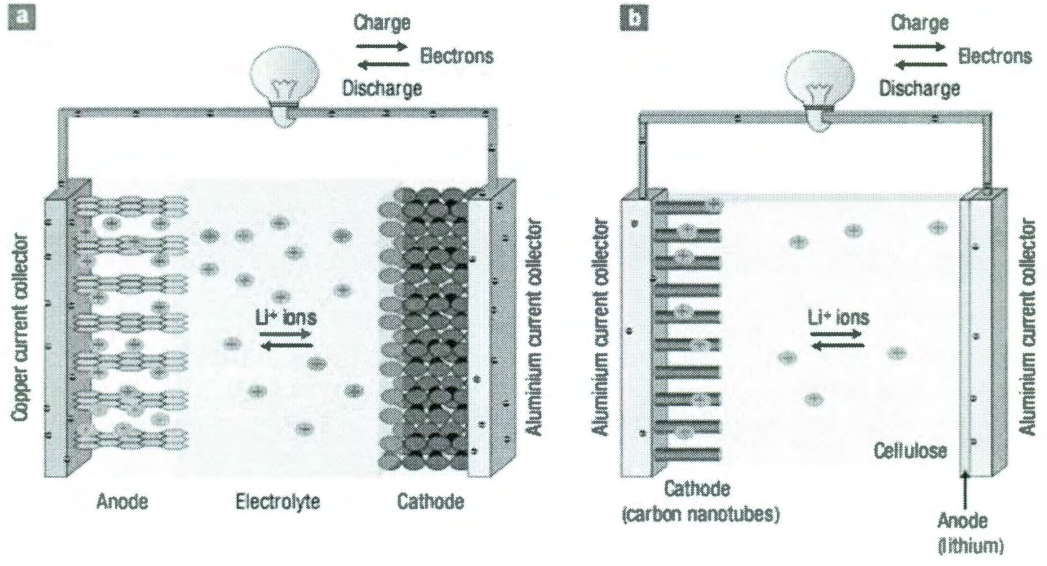

Figure 1-2: a) Schematic of Li ion battery operation b) Schematic of Li metal battery operation. (Ref. 35)

Equation [1-1] and [1-2] are the corresponding reactions for anode and cathode upon charging, and the reactions are reversed during discharging:

Anode reaction:

$$xLi+ + 6C + xe^- \leftrightarrow Li_xC_6 \quad [1\text{-}1]$$

Cathode reaction:

$$LiMn_2O_4 \leftrightarrow xe- + Li_{(1-x)}Mn_2O_4 + xLi^+ \quad [1\text{-}2]$$

Capacity, C-rate, power density and energy density are some important parameters used to define the performance of a Li ion battery. The capacity is defined as the amount of charge transferred during charge/discharge phenomenon represented commonly in mAh units. C-rate is defined as the rate at which the nominal capacity of the electrode material is achieved: 1C – 1 hour to discharge the nominal capacity of the cell. Power density is defined as the rate at which the energy can be delivered using a battery w.r.t the mass of the device and is represented commonly in W/kg units. The energy density is the total energy that is delivered by a battery w.r.t the mass of the device and is represented by Wh/kg units. The lithium-ion battery total capacity strongly depends on capacities of anode, cathode and other cell components. For example, the relationship between the total cell capacities and the anode capacities for standard 18650 lithium-ion battery can be plotted in Figure 1-3 when the cathode capacities are constant at 140 and 200 mAh/g, respectively. Total capacity increases as anode capacity increases up to 1500 mAh/g as shown in Figure 1-3; when anode capacity is over 2000 mAh/g, increase in total capacity is negligible. It can be estimated that current carbon anodes[36-43] with capacity of 372 mAh/g are able to achieve total capacity of 95-120 mAh/g. Therefore, target anode capacity of over 1000 mAh/g is desirable to overcome current capacity threshold and increase total cell capacity by two folds to approximately 200 mAh/g.[44]

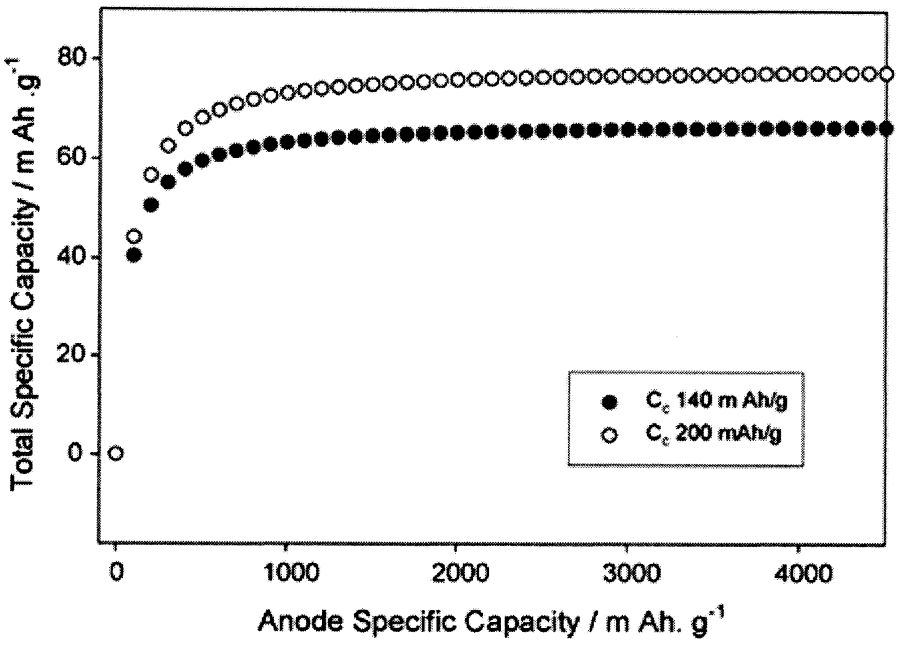

Figure 1-3: Total specific capacity of full cell vs Anode specific capacity. (Ref. 44)

The energy density of the battery depends on the voltage and capacity of the cell. Hence to improve total energy density of the battery, which is the final important metric useful for defining electric vehicle range and portable electronic discharge times, we need to improve cell capacities and cell voltage. Figure 1-4 shows an overview of materials choices that we have for anodes and cathodes to build a Li ion battery with maximum energy density. Apart from basic material choice for the electrodes and electrolyte, material morphology and particle size also play an important role in the overall battery performance.

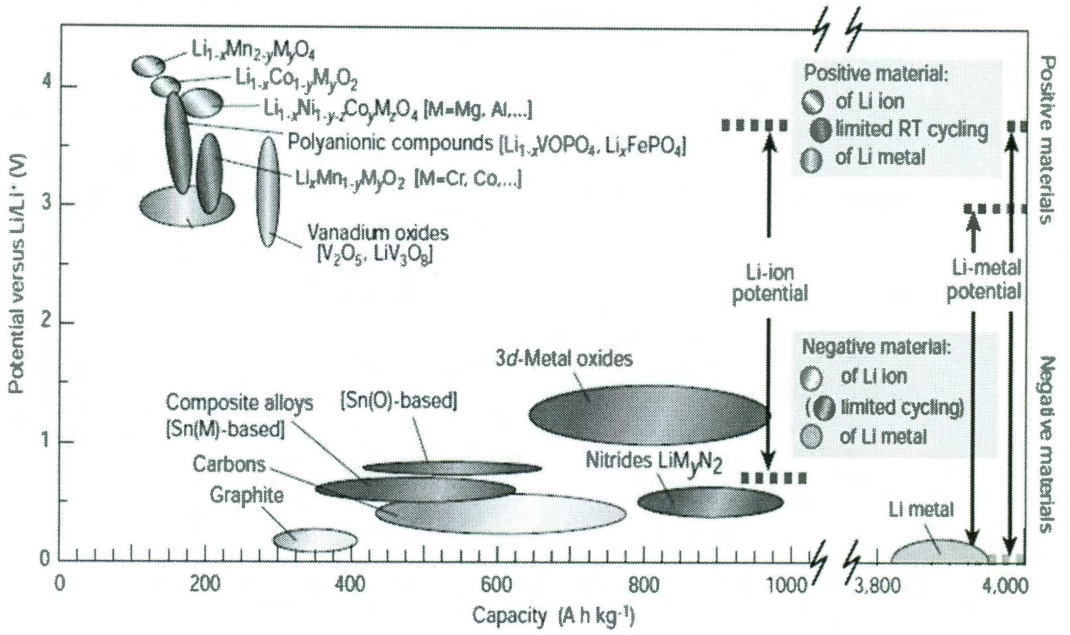

Figure 1-4: Potential (V) vs Capacity (Ah/kg) for different anode and cathode materials

1.2 Nanostructured Materials for Li ion battery

Several potential advantages and disadvantages are associated with the development of nanostructured electrodes for lithium batteries. Some of the advantages include (i) better accommodation of the strain of lithium insertion/removal, improving cycle life; (ii) new reactions not possible with bulk materials; (iii) higher electrode/electrolyte contact area leading to faster charge/discharge rates; (iv) short path lengths for electronic transport (permitting operation at higher power); and (v) short path lengths for Li^+ ion transport (permitting operation at higher current rates or power). A few disadvantages include (i) an increase in undesirable electrode/electrolyte side reactions due to high surface area, leading to self-discharge, poor cycling and calendar life; (ii) inferior packing density of particles leading to lower volumetric energy densities unless

special compaction methods are developed; and (iii) potentially more complicated and expensive synthesis procedures.[45]

Metals/alloys that store lithium are among the most appealing and competitive candidates for new types of anodes (negative electrodes) in lithium-ion batteries due to their high theoretical capacities.[46-56] Several number of metals and semiconductors, for example aluminium, tin and silicon, react with lithium to form alloys by electrochemical processes that are partially reversible and of low voltage (relative to lithium), involve Lithium atom per formula unit, and in particular provide a specific capacity much larger than that offered by conventional graphite.[57] For example, the lithium–silicon alloy has, in its fully lithiated composition, $Li_{4.4}Si$, a theoretical specific capacity of 4,200 mAh/g compared with 3,600 mAh/g for metallic lithium and 372 mAh/g for graphite.[58-65] Unfortunately, the accommodation of so much lithium is accompanied by enormous volume changes in the host metal plus phase transitions. The mechanical strain generated during the alloying/de-alloying processes leads to cracking and crumbling of the metal electrode and a significant loss of capacity to store charge, upon mere few cycles charge/discharge. [66-70]

There have been several attempts to mitigate the side effects of volume expansion upon cycling in alloy based electrodes to preserve the electrode integrity. Among them, the active/inactive nanocomposite concept represents one attractive route. Several researchers have discussed this approach, which involves intimately mixing two materials, one reacting with lithium whereas the other acts as an inactive confining buffer.[71-80] Within this composite, the use of nano-size metallic clusters as lithium hosts considerably suppresses the associated strains, and therefore improves the reversibility of the alloying reaction. By applying this concept through different composite systems

such as Sn–Fe–C, Sn–Mn–C or Si–C, several research groups have demonstrated that these electrodes show a considerable improvement in their cycling response in lithium cells.[49-53] The Si–C nanocomposites have attracted considerable interest because they show capacity as high as 1,000 mAh/g for more than 100 cycles.[53]

Figure 1-5 shows interesting results for a Si-C composite fabricated by chemical vapor deposition technique to obtain stable cycling at a specific capacity of ~ 1500 mAh/g.[81] The important point to notice in this work is that the composite even though nanostructured in nature is made up of microparticles improving the tap density of the overall poweder leading to higher volumetric energy densities. Improvements in performance may also arise because the materials avoid cracking, thus maintaining better conduction pathways, or because they incorporate conductive additives such as carbon. The alloy performance can also benefit from nanostructuring. For instance, thin amorphous silicon films deposited on a specially roughened copper foil surface by a sputtering process were shown to have close to 100% reversibility at capacities larger than 3,000 mAh/g.[69-70] An excellent capacity retention was also noted for silicon electrodes prepared with a nanopillar surface morphology because size confinement alters particle deformation and reduces fracturing.[44] Silicon nanowires have also obtained recent interest due to their ability to show improved cycling characteristics due to better strain handling within space between nanowires.[82] Figure 1-6 shows the cycling characteristics of the Si nanowires and the associated scanning electron images after cycling. The retention of the nanowire structure implies mitigation of cracking induced by the nanostructured morphology of the electrode material.

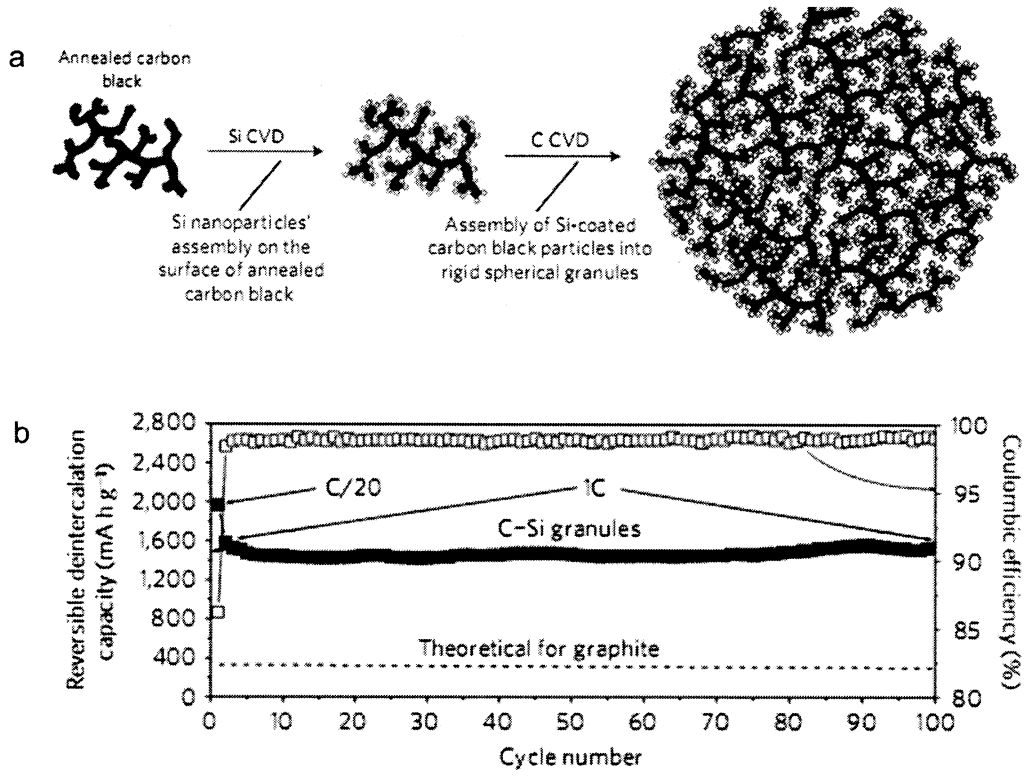

Figure 1-5: a) Schematic of Si/C nanocomposite fabrication process, b) Electrochemical performance of Si/C nanocomposite. (Ref. 81)

One of the greatest disadvantage of primary nanoparticles is the possibility of significant side-reactions with the electrolyte, leading to safety concerns (one of the most critical issues for lithium batteries) and poor calendar life. But if the materials fall within the stability window of the electrolyte or at least limit the formation of the solid–electrolyte interface (SEI) layer, then the many advantages of nanoparticles may more easily be exploited. Such an example is $Li_{4+x}Ti_5O_{12}$ ($0 < x < 3$, 160 mAh/g, 1.6 V vs Li^+/Li). No evidence has been reported for a significant surface layer formation (presumably because the potential is sufficiently high compared with lithium), and this material can be used as a nanoparticulate anode with high rate capability and good capacity retention.

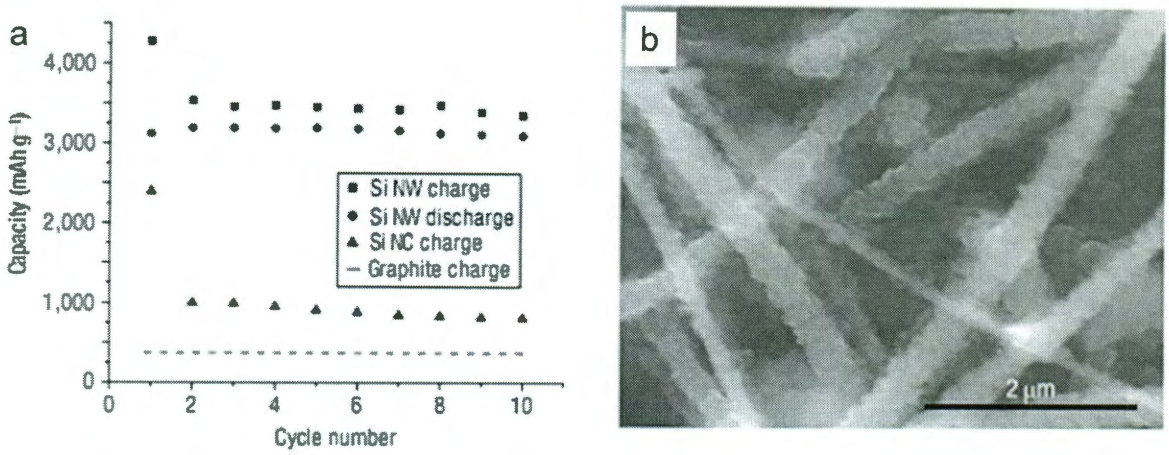

Figure 1-6: a) Cycling characteristics of Silicon nanostructures and graphitc carbon, b) SEM image of silicon nanowires post cycling. (Ref. 82)

Controlling the nanoparticle shape as well as size can offer advantages. This is illustrated by recent results on TiO2-β nanotubes or wires. Such materials have been synthesized by a simple aqueous route and in high yield, with diameters in the range of 40–60 nm and lengths up to several micrometres. The TiO2- β polymorph is an excellent intercalation host for Li, accommodating up to $Li_{0.91}$TiO2- β (305 mA h g–1) at 1.5–1.6 V vs Li^+/Li and with excellent capacity retention on cycling (Figure 1-7). Interestingly, the rate capability is better than the same phase prepared as nanoparticles of dimension similar to the diameter of the nanowires.[83] Carbon nanotubes have also been explored as anodes.[84-104] The cost of fabrication of nanotubes makes it difficult to incorporate into batteries as anode materials.[105-115] Carbon nanotubes have found more application as conductive additives as the required amounts of material is lot lesser when used as an additive and hence finds more economic feasibility. Now we also look at the cathode materials being nanostructured and examples of the benefits observed upon switching to the nano-dimension.

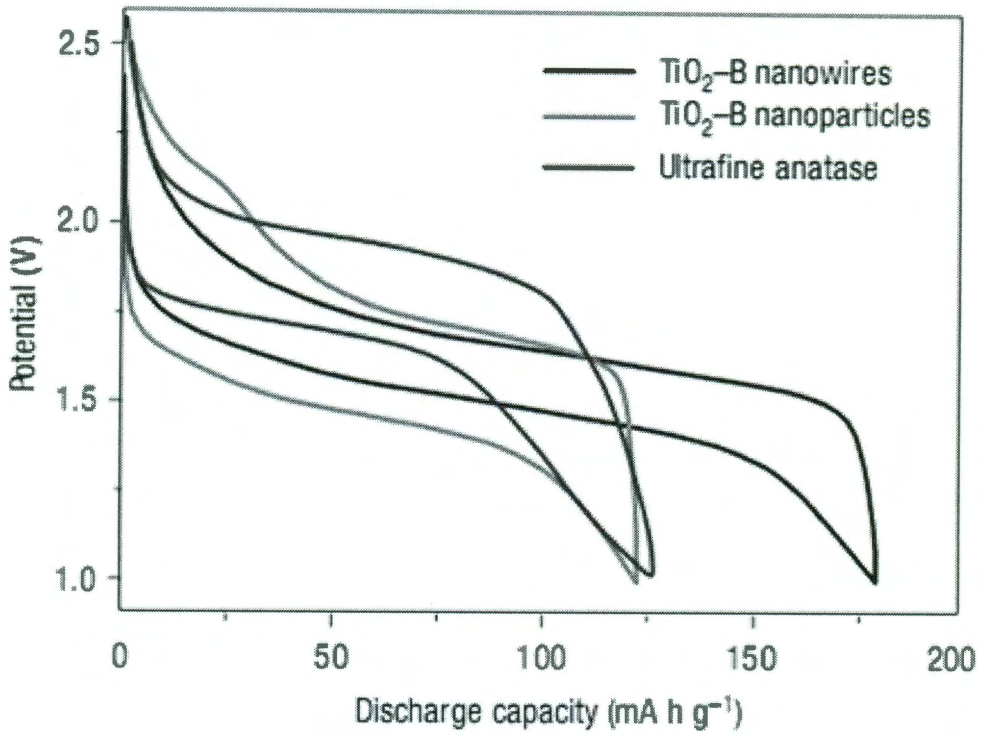

Figure 1-7: Voltage vs capacity curves for TiO_2 nanostructures (Ref. 83)

Recently the optimization of the environmentally benign and low-cost phospho-olivine $LiFePO_4$ cathode material[116-121], that displays a theoretical capacity of 170 mAh/g, as compared with 140 mAh/g for the $LiCoO_2$ electrode used at present ($LiFePO_4$ operates at a lower voltage), has gained tremendous interest. But the insulating character of the olivine had precluded the achievement of the full capacity because, as the electrochemical reaction proceeds, electronically isolated or unutilized areas remained inactive in the bulk electrode. Hence recent research has involved preparing $LiFeO_4$ in the form of carbon-coated nanoparticles through various chemical and physical means.[116] This simultaneously reduces the distance for Li ion transport, and increases the electronic contact between the particles. Procedures of this kind have led to a greatly improved electrochemical response, and the full capacity of the material is now

accessible even under prolonged cycling. A recent success story involving $LiFePO_4$ material is the company A123 systems based in Massachusetts, whose proprietory material is based on doped $LiFePO_4$.[116] The ability to dope the olivine structure with rare earth metals to increase the conductivity significantly to make it useful for vehicular applications has been exploited. Figure 1-8 shows a detailed comparison of the electronic conductivity of the doped electrode as a function of the dopant and the temperature. This example serves to illustrate some of the advantages of materials engineering and nanostructuring for the development of advanced battery electrodes.

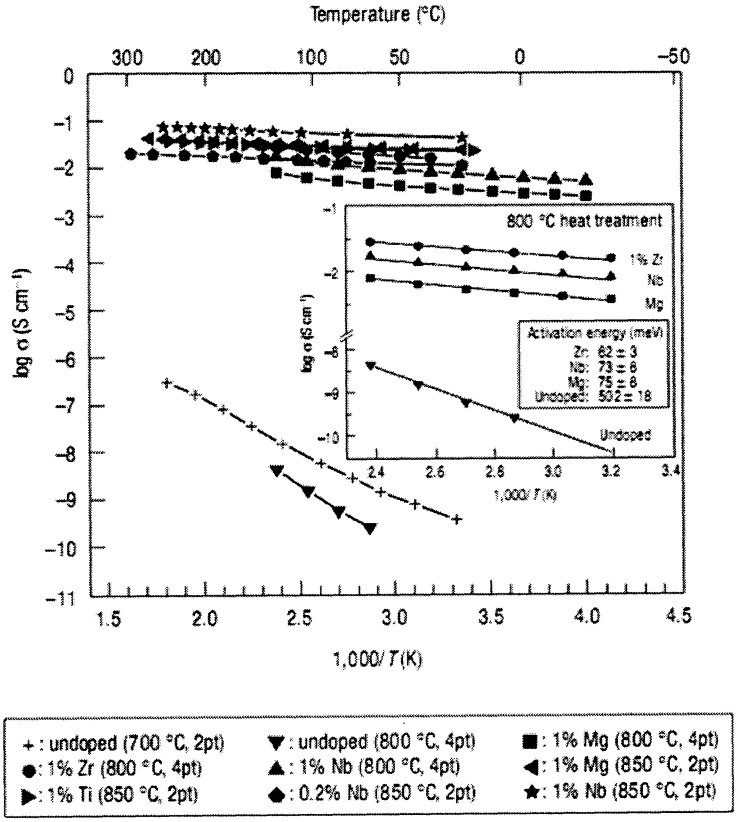

Figure 1-8: Conductivity vs temperature semi-log plots for doped olivine cathode (Ref.116)

1.3. Thin film Lithium ion battery

Lithium ion batteries made up of thin electrodes and separators having an overall device thickness less than 15 μm, are called thin film Li ion batteries.[122-141] They have important applications in a variety of consumer and medical products, and they are useful research tools in characterizing the properties of lithium intercalation compounds in thin-film form. Conventional thin film batteries consist of thin (less than 5 μm thick) films of electrode separated by a thin solid state electrolyte.[142-152] Figure 1-9 shows a schematic of the construction of a thin film Li ion cell. As shown they are generally fabricated onto a substrate with basic components of a battery – current collectors, electrodes separated by a solid state electrolyte. Conventional cathodes such as $LiCoO_2$, $LiMn_2O_4$ have been shown to cycle well against Li foil at very good current rates.

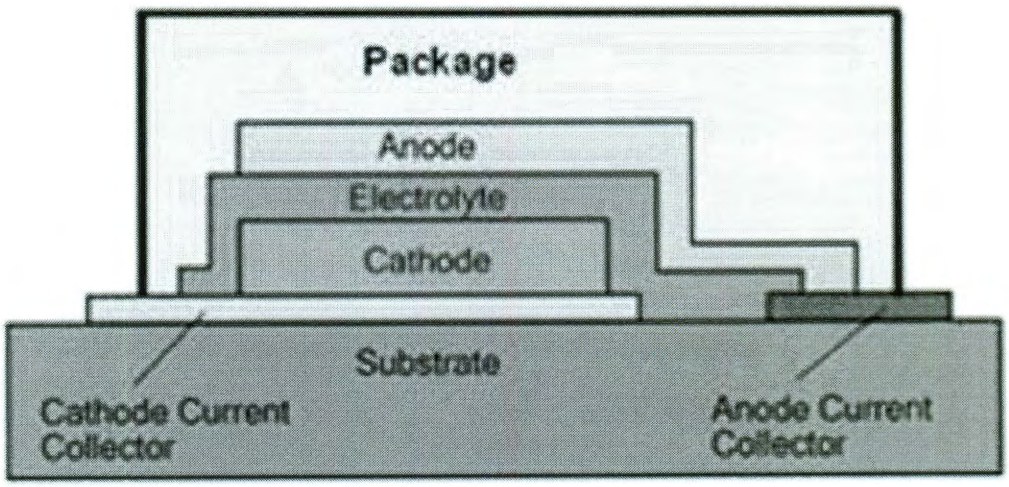

Figure 1-9: Schematic illustration of thin film Li-ion battery

Sn and Si based alloy anodes have been used for thin film batteries. Solid state electrolytes such as LiPON have been extensively used in thin film Li ion batteries and

recently even solid polymer electrolytes are receiving attention. The key advantage the thin film batteries have over their bulk counterpart is that they have very fast rate capability. This is attributed to the fact that the electrode films, in which the slow process – solid state Li ion diffusion, occurs, are very thin. Li ion electrodes have diffusivities within electrode in the order of 10E-9 – 10E-12 cm^2/s.[150] Hence to operate batteries at reasonable current rates, one needs to reduce the thickness of the electrodes to allow for fast Li ion diffusion and hence complete electrode utilization. As shown in the schematic representation of Figure 1-10, if the electrode gets thicker the Li ion diffusion does not take place within the entire electrode at a reasonable current rate leading to unutilized electrode material. Hence the capacity obtained from the electrode material is limited only to the top section of the electrode film as shown in the schematic.

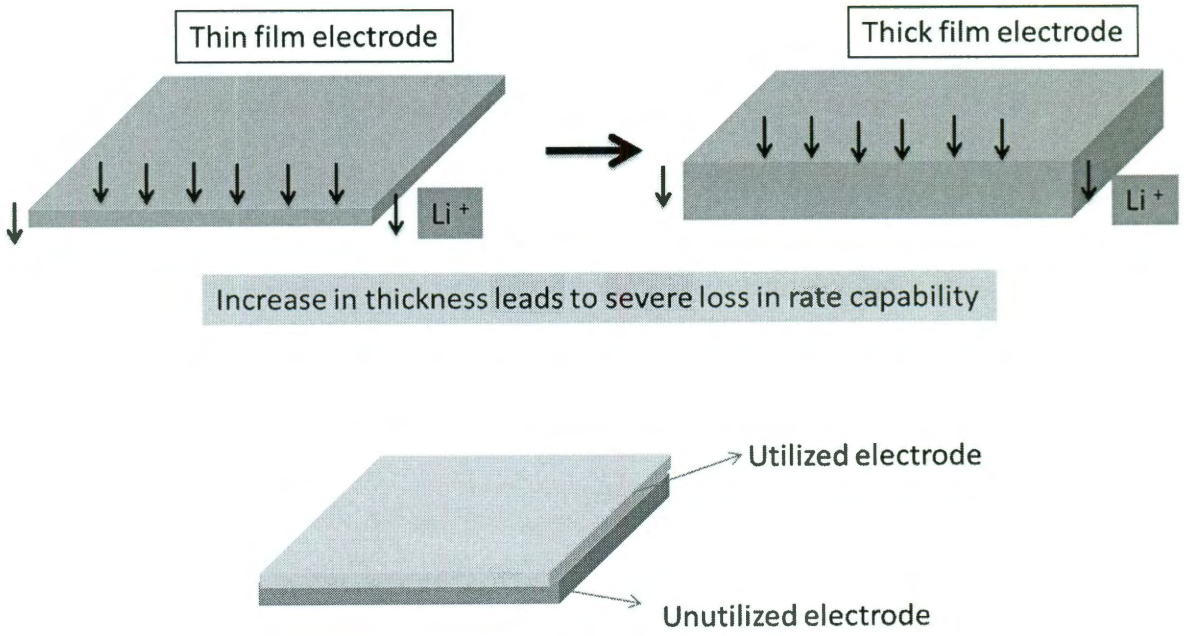

Figure 1-10: Schematic illustration of electrode utilization in thin film Li-ion battery

Firstly Li metal based thin film batteries were extensively studied. But their applications have been limited to low temperature use due to the low melting point of Lithium metal. Responding to the need for thin-film batteries that can tolerate heating to 250°C–260°C so they can be integrated into circuits using the solder reflow process, research groups around the world have also synthesized several inorganic anode materials that result in thin-film lithium-ion cells which are stable at these temperatures.[135,140] Bates and co-workers at Oak Ridge National Laboratory have conducted detailed studied on thin film Lithium and Lithium ion batteries and have shown excellent cycling characteristics thousands of cycles and operation at very good rate capabilities upto 20 mA/cm^2.[140]The long cycle and shelf life of these batteries results from the properties of the glassy lithium phosphorus oxynitride ("Lipon") electrolyte which is stable from 0 to nearly 5.5 V and has an acceptable conductance in thin-film form.[146]

For the cathode materials $LiCoO_2$ and $LiMn_2O_4$ have been studied quite extensively. Polycrystalline films of $LiCoO_2$ deposited by rf magnetron sputtering exhibited a strong preferred orientation or texturing after annealing at elevated temperatures. For films thicker than about 1 μm, more than 90% of the grains were oriented with their (101) and (104) planes parallel to the substrate and less than 10% with their (003) planes parallel to the substrate.[140] Extensive studies of $Li/LiCoO_2$ cells have been conducted to study the electrochemical performance. Figure 1-11 At low currents, the discharge capacity corresponds to about 0.5 Li per CoO_2 or 137 mAh/g corresponding to areal capacities of the order of ~60-70 $\mu Ah/cm^2$. The total capacity loss of the cell with the micron thick $LiCoO_2$ cathodes having a capacity of 65 μAh was less than 2% after more than 4000 cycles at discharge rates of 0.1 and 0.6 mA/cm^2. Thicker $LiCoO_2$ cathodes have also been studied and they discharged at rates from 0.1 mA/cm^2

to 1.5 mA/cm^2. At 1 mA/cm^2, the capacity loss per cycle was 0.02% and at 1.5 mA, 0.05% per cycle. The total capacity loss measured at 0.1 mA/cm^2 after more than 3800 cycles was found to be less than 0.08%. Some integrated circuits are fabricated using solder reflow (surface mount) assembly in which the IC is heated to 250–260°C for a short time causing all of the components to be soldered at once. Due to the low melting point of lithium, 180°C, lithium batteries fail when heated to these temperatures, and hence metallic anodes with a high melting point and that are less reactive have also been investigated.[140]

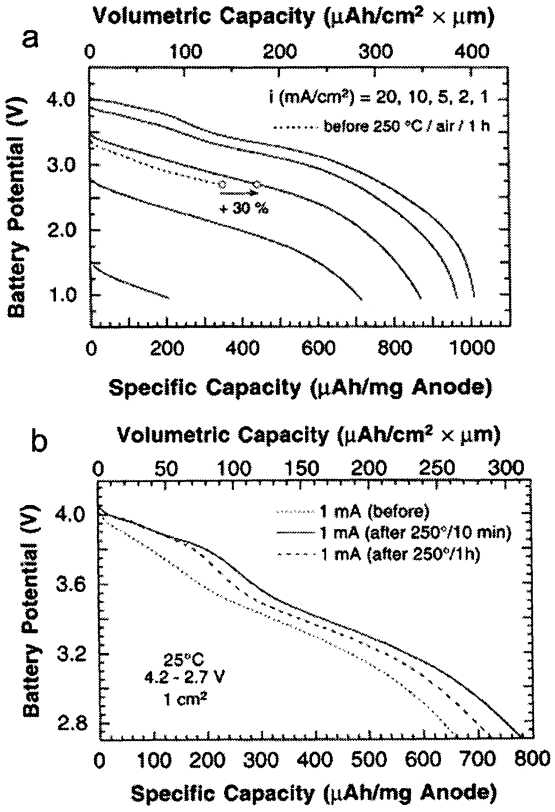

Figure 1-11: (a) Voltage vs Capacity curves for Li/$LiCoO_2$ cells at different current rates (b) Voltage vs Capacity curves for Li/$LiCoO_2$ cells at different annealing conditions. (Ref. 140)

Bates and co-workers have also conducted detailed studies on the alloy based anode material Lithium silicon tin oxynitride (Li_ySiTON). The lithium-ion thin-film battery was of the construction SiTON/Lipon/$LiCoO_2$, where the $LiCoO_2$ cathode serves as the positive electrode the initial lithium source. The thin film battery showed reversible capacities of ~600 mAh/g of SiTON at current rates of 0.1 mA/cm^2 (Figure 1-11). The rate capability of the battery was also tested for higher current rates such as 1, 5, 10 and 20 mA/cm^2. It was observed that excellent capacity retention of ~95% was observed for current rates upto 10 mA/cm^2 and capacity retention of 30% was observed for a current rate of 20 mA/cm^2. Even at high temperature treatments in air, as high as 250 °C, the battery showed no degradation due to improved stability of the anode and electrolyte (Figure 1-11). As this temperature being higher than the solder reflow conditions on microcircuit board, the batteries were deemed as suitable for microelectronic applications.

1.4 3D design for Li ion battery

One of the major drawbacks with 2D thin film Li ion batteries is the low energy per unit area delivered due low electrode mass loading per unit area. In recent years there has been the realization that improved battery performance can be achieved by reconfiguring the electrode materials currently employed in 2D batteries into 3D architectures. Some of the envisioned approaches are reviewed in more detail in this section. The general strategy of this approach is to design cell structures that maximize power and energy density yet maintain short ion transport distances. While many possible architectures can achieve this goal, a defining characteristic of 3D batteries is that transport between electrodes remains one-dimensional (or nearly so) at the microscopic level, while the electrodes are configured in complex geometries (i.e.,

nonplanar) in order to increase the energy density of the cell within the footprint area. A 3D matrix of electrodes (in a periodic array or an aperiodic ensemble) is necessary to meet both the requirements of short transport lengths and large energy capacity. Improvements in energy per unit area and high-rate discharge capabilities are two of the benefits that could be realized for these 3D cells.[153-164]

One of the most common 3D designs is that, consisting of interdigitated electrodes shown in Figure 1-12a. The anode and cathode consist of arrays of rods separated by a continuous electrolyte phase. The spatial arrangement of the anode and cathode arrays determines the current-potential distribution. Clearly, the short transport distances lead to a much lower inter-electrode ohmic resistance as compared to traditional planar battery configurations. A principal feature for the interdigitated configuration is that the arrays need to be periodic. A variation on this approach is to use interdigitated plates rather than rods (Figure 1-12b), which is analogous to stacking 2D batteries with parallel connection. There is no particular reason that the electrolyte must serve as the continuous phase in 3D battery architectures. Another 3-D design that has been proposed, utilizes a concentric arrangement where the rod array is composed of one of the active electrode materials and is then coated by an electrolyte layer. The other electrode material then could fill the remaining free volume and serves as the continuous phase, as shown in Figure 1-12c. Another option for 3-D design is that of a completely aperiodic 3-D battery configuration, where the electrolyte layer is formed around a random 3-D network of electrode material (Figure 1-12d). This design strategy also represents a concentric configuration in that the electrolyte envelops the electrode material while the other electrode material fills the mesoporous and macroporous spaces and surrounds the electrolyte. Short transport-path characteristics between the insertion electrodes are preserved with even this arrangement. In contrast to the other 3-D

designs, all battery components, anode, cathode, and electrolytes are continuous throughout the sponge-like structure.

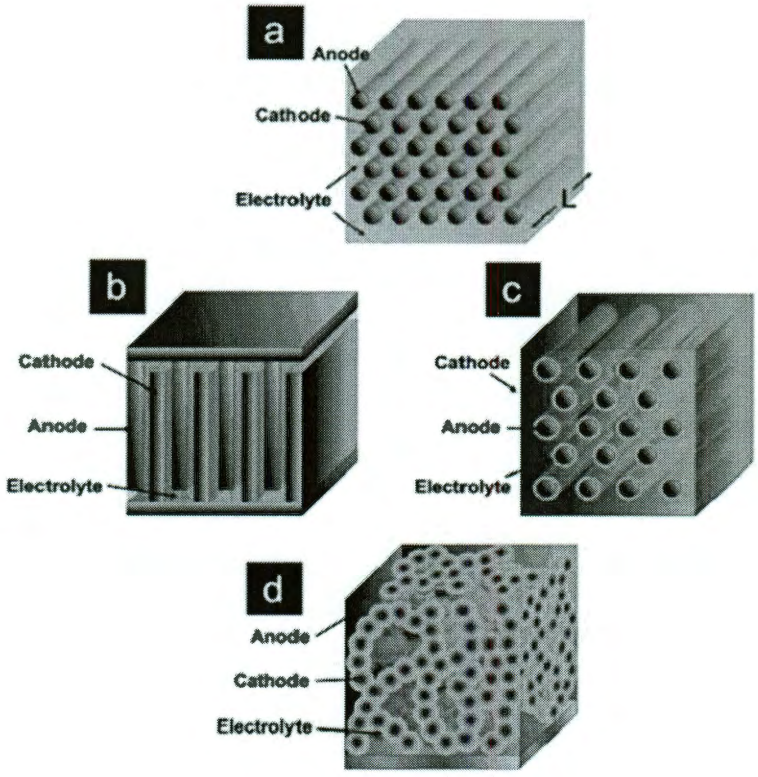

Figure 1-12: Schematic illustration of different three dimensional (3D) designs for electrochemical energy storage devices. (Ref. 153)

For improvement in power density or rate capability, reducing the thickness of the solid electrolyte plays an important role. Hence it requires the fabrication and understanding of cells in which the cathode and anode are separated by a conformal thin-film electrolyte, in the range of few tens of nanometers in thickness. White et al., have considered several potential phenomena, not normally considered in battery design, that will be operative when the electrodes are placed in such close proximity to

one another in their model. Their explanation is based on a closed cell model as depicted in Figure 1-13, which contains LiCl as the electrolyte.

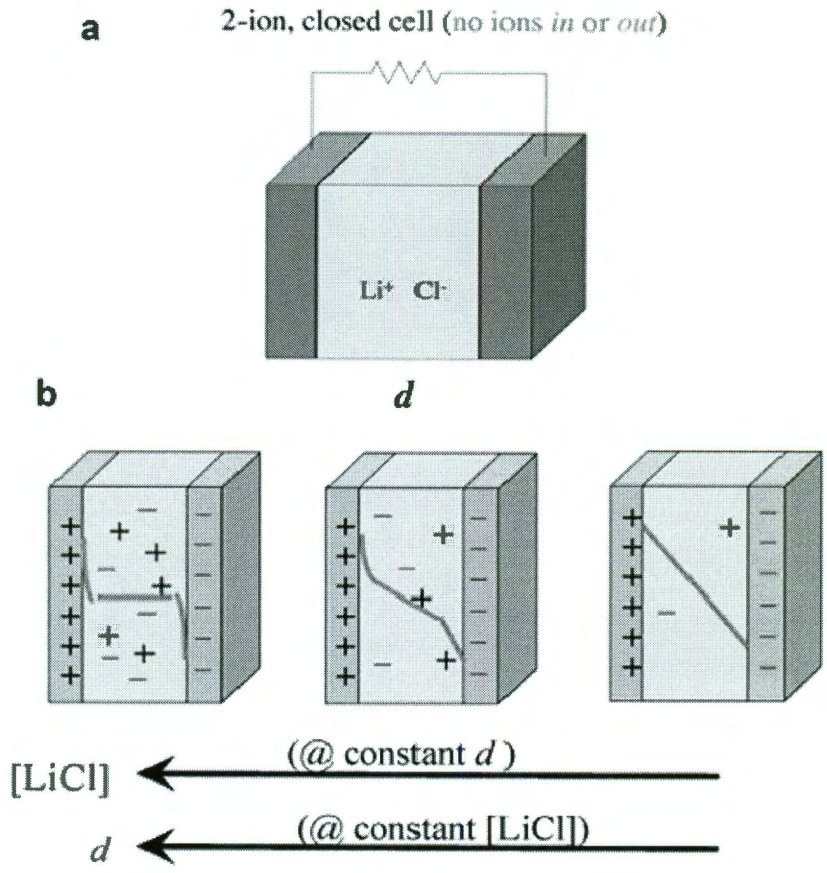

Figure 1-13: Dependence of potential profile across the electrodes as a function of distance between the electrodes, d, and the concentration of the electrolyte, LiCl (Ref.153).

According to the 2-D model the cathode and anode are assumed to be separated by 10 nm. It is important to note that at distances in the regime of 10 nm, electron tunneling between the surfaces will be negligibly slow. The decay length associated with the tunneling effect would be ~ 1 Å. Thus, the electrodes were assumed not to be

electronically coupled. Hence normal redox reactions at the cathode and anode are expected during battery operation. At shorter distances, e.g., 1 nm, the electrodes would spontaneously discharge via direct tunneling between the cathode and anode, a process equivalent to shorting the battery. Thus, the researchers propose a theoretical lower limit on the thickness of the battery separator depending on the electrolyte system. From the results of this work it is shown that although the cathode and anode are not electronically connected at 10 nm separation, their presence is known to each other through the electrical fields that originate from their respective surface charges. As shown in Figure 13, the overlap of the electrical double layers becomes more significant as either the distance between the electrodes, d, is reduced or the concentration of the electrolyte is decreased. Hence the role of the electrolyte concentration has been quantitatively expressed through the Debye length, 1/k, which can be estimated for a 1:1 electrolyte at room temperature using the expression, $1/k\ (nm) \sim 0.3/[LiCl]^{1/2}$, where [LiCl] is the molar concentration (M) of the electrolyte. In essence, 1/k represents how well the electrolyte shields the solution interior from the electrical charge of the electrode surfaces. Thus, two electrodes separated by 10 nm in a 10 mM LiCl solution will clearly be in electrostatic contact through their overlapping double layers.[153,165-171]

The consequence of overlapping double layers on battery operation has only been recently considered and very few reports exist demonstrating these effects. Hence it can be inferred that the electric fields will certainly have an effect on the transport of ions through the electrolyte, as migration will be important in the strong fields of the double layers. Whether transport of Li ions is impeded or enhanced by the field will depend on signs of the electrode charges (determined by the potentials of zero charge, an ill-defined quantity for most battery electrode materials) and whether the battery is being charged or discharged. At small electrode separations, the number of ions in the

electrolyte between the electrodes is quite small. For instance, the average nearest neighbor distance between cations in 10 mM LiCl solution is ~2 nm.[153] Thus, on average, only a few Li+ ions are located between cathode and anode at any position on the electrode surfaces. The number of ions is assumed to be so small in this situation that the battery behaves virtually like a capacitor, with the separator being a dielectric material, resulting in a linear potential drop between the electrodes (Figure 13). In addition, even if migration from the electrical double layers is neglected, the small separation distance between the electrodes will result in enormous diffusional fluxes. It has been proposed that if sufficiently high these, diffusional fluxes could lead to breakdown of electroneutrality and formation of a space-charge layer in the electrolyte. Much research efforts are needed to explore and quantify these ideas.

1.4.1 3D designs using templates

Ordered templates have been used as a building block to construct elements of three dimensional battery components. The use of porous membranes as templates for electrode structures was pioneered by Martin and coworkers, and this approach has since been extended to include numerous electrode compositions and geometries and applications beyond energy storage, including sensing and separations. In the template approach, chemical and electrochemical routes have been used to fill in the cylindrical, uniform, unidirectional pores of a free-standing membrane with electrochemically active materials and structures. The pores in such membranes may be either random, as in "track-etched" polycarbonate, or an ordered array, as in electrochemically prepared alumina membranes. The pores in these membranes can be as small as 10 nm and range upward into the hundreds of nanometers and micrometers. Various strategies are used to produce electrode structures within the membrane pores, including sol-gel

synthesis, CVD, electrodeposition, and electroless deposition. With careful control of the synthetic conditions, the pores are either filled completely or preferentially coated at the pore walls, producing hollow tubes. Following infiltration with the desired electrode material, the membrane is subsequently removed under conditions that do not disturb the active material, leaving an array of either solid nanofibers or nanotubes attached to a current collector like the bristles of a brush. In this case there is very limited interconnectedness between the nanofibers, except at the current collector base. Using this approach, template-synthesized electrodes have been prepared not only from metals, but from TiO_2, V_2O_5, $LiMn_2O_4$, SnO_2, TiS_2, carbon and various conducting polymers.[155,160,161] Dewan and Teeters infiltrated alumina membranes to template a device: a V_2O_5 xerogel-carbon battery using a poly(ethylene oxide)-lithium triflate electrolyte.[155] Many of the templated electrode ensembles described above function as high-performance battery electrodes in lithium-containing electrolytes. The fibrous morphology of these templated electrodes reduces the solid-state transport distances for lithium ions participating in the charge-storage reaction. This feature facilitates not only good cyclability but also rapid charging and discharging. For example, template-synthesized SnO_2 electrodes deliver gravimetric capacities that are orders of magnitude higher than a thin-film control electrode when discharged at greater than a 50C rate.[18] The void spaces between the individual electrode fibers also provide room for expansion during electrode cycling, which is a particular problem for SnO_2, because a Sn metal phase alloys with electrogenerated Li metal, with accompanying large volume changes. Template strategy has also been used to fabricate 3-D current collectors for Li ion batteries. Simon and co-workers used the alumina template to demonstrate the high rate capability of Fe_2O_3 based anode for Li ion batteries (Figure 1-14).[168] High current rates were obtained for low electronic conductivity oxide electrodes due to the 3-D design.

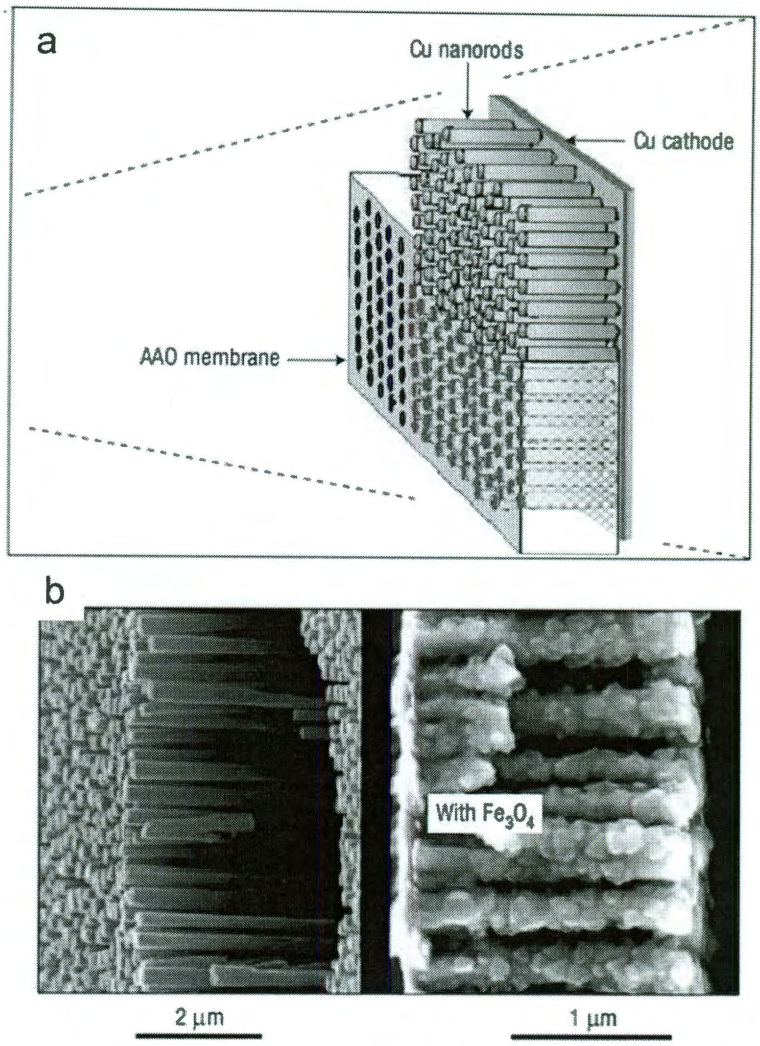

Figure 1-14: (a) Schematic illustration of template assisted process of current collectors deposition and (b) SEM image of Cu nanorods current collectors and Fe2O3 coated Cu nanorods (Ref.168).

Recently Braun and co-workers have used a polystyrene based template to fabricate a three dimensional $LiMnO_2$ cathode with ultrafast charge/discharge current rates.[167] As shown in Figure 15 the three dimensional Ni network is fabricated first followed by the coating of the active cathode material. Current rates as high as ~1100C

have been reported using this periodic templated 3-D approach. Most of the prior literature has focused on building individual electrodes in the 3-D format using templates. Yet, there exists few reports for the fabrication of all three components of an energy storage device, namely, anode, cathode and electrolyte onto a single nanostructure and evaluation of its performance.

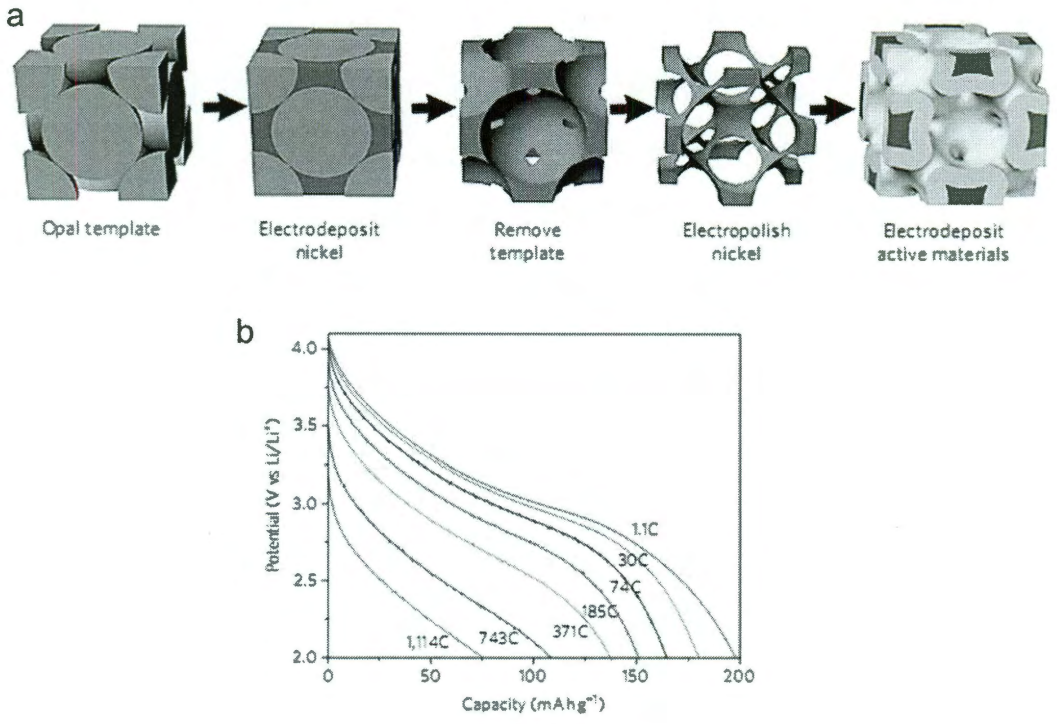

Figure 1-15: (a) Schematic illustration of fabrication of periodic porous network b) Rate capability of porous cathode (Ref.167)

1.4.2. 3D design aperiodic

To exploit higher surface areas possible with a disordered network design, researchers have built Li ion batteries around foam like aperiodic templates. Sol-gel methods have been used to synthesize monolithic gels that are composed of a 3-D

interconnected network of nanoscale particles, continuously intermingled with a phase of fluid-filled pores.[153] The processing of these wet gels to render the dried forms must be carefully controlled so that the highly porous architecture is retained. Annealing times have to be controlled to maintain the porous structure after electrode formation. Also the direct evaporation of typical pore-filling fluids creates capillary forces at the liquid-vapor interface, resulting in pore collapse and a partially densified porous solid known as a xerogel. This structural collapse is avoided if the pore fluid is removed under supercritical conditions where no liquid-vapor interface is ever established. Figure 1-16 provides an overview of the different types of gels that can be formed and their respective microstructures. Gels processed by supercritical fluid extraction, usually with CO_2 as the pore fluid, are denoted as aerogels. In an alternative to supercritical drying, the pore fluids in a wet gel are replaced with a low-surface tension, nonpolar liquid, such as an alkane, which is then allowed to evaporate under subcritical or ambient-pressure conditions. The resulting solids, denoted as "ambigels" (for ambient-pressure-dried gels), do exhibit a moderate degree of densification but retain a large fraction of pore volume, with pores usually in the mesopore size range. The densification that accompanies ambient-pressure drying provides for more mechanically strong monolithic forms than those for comparable aerogels. A fourth scheme of pore-fluid removal utilizes a freeze-drying process to render highly porous "cryogels". Aerogels and related structures have the important characteristics of extremely high surface area and a through-connected, aperiodic network of porosity. Additionally, these solids can be cast and molded into a range of shapes and forms or cast as thin films on planar supports. An important attribute that seems to set these aperiodic architectures apart from the mesoporous ordered solids, even the nominally 3-D porous ones, is proven performance in rate-critical applications. The rapid flux of molecules through the aerogel architecture avoids

the potentially devastating loss of rate capability through 1-D channels if a blockage occurs. Aerogels have already demonstrated orders of magnitude faster current rates for energy storage devices than other pore-solid architectures.[153-155]

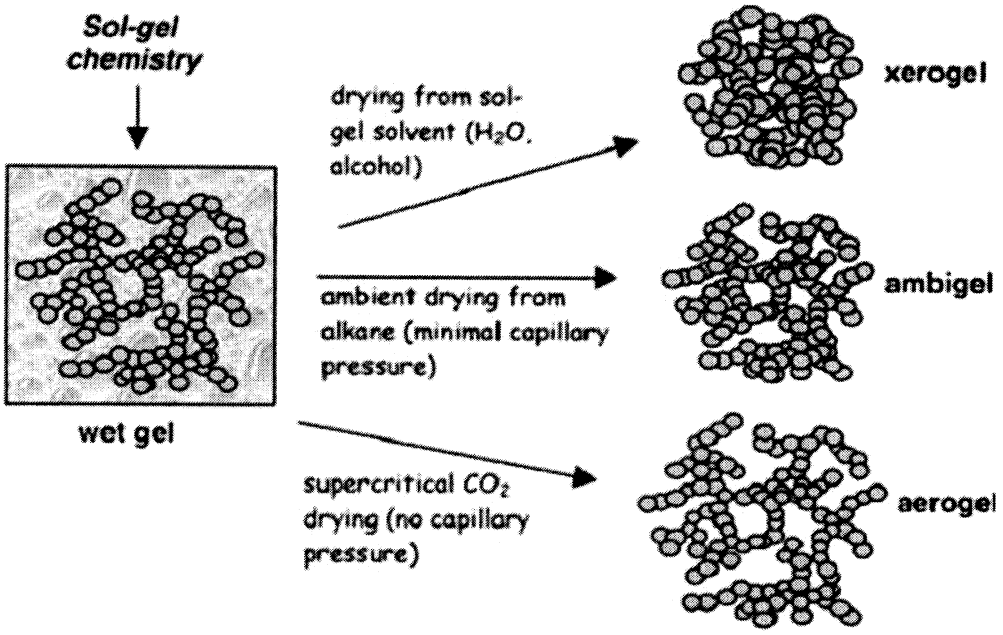

Figure 1-16: Schematic of disordered porous networks (Ref.153)

Aerogels that are electronically conductive have been prepared from a range of transition metal oxides, including vanadium oxide, manganese oxide, molybdenum oxide, and tin oxide. The nanostructured oxide forms have shown improved performance as Li ion insertion electrodes in conventional electrochemical cells. Vanadium pentoxide aerogel electrodes have been shown to accommodate the reversible electrochemical insertion of up to four Li ions per V_2O_5 unit. In addition to higher overall capacities, aerogel electrodes deliver more energy (capacity) under high charge-discharge current

rates than do conventional materials. This is due to combined enhancement of ion accessibility and improved mass distribution of electrode resulting in faster solid state Li ion diffusion. Carbon aerogels are typically derived from the reaction of resorcinol have been converted to highly conductive, monolithic carbon structures that retain the characteristics of an aerogel by pyrolyzing in inert atmospheres at high temperature. The synthesis of carbon aerogels offers considerable flexibility as the pore-solid organic architecture can be adjusted by simple changes in the initial reaction conditions of the polymer gel. Through such variations, carbon aerogels can be prepared in either predominantly mesoporous or macroporous forms. Carbon aerogels are being exploited as electrodes for electrochemical capacitors, where the high surface area, through-connected porosity, and electronic conductivity of the aerogel promote rapid chargedischarge reactions.[149] They are also being used as template networks around which 3-D Li ion battery electrodes are being built. Fabrication of fully interepenetrating 3-D battery has also been demonstrated where all essential components of a Li ion battery have been built around an aperiodic design. Yet, the complexity of fabrication and the difficulty of detecting shorts within the network makes this a challenging approach to build interpenetrating 3-D batteries.

1.5. Scope of thesis

This thesis focuses on fabrication and characterization of nanostructured three dimensional designs for Li ion batteries. The fabrication of ordered nanostructured materials using template approach is exploited, to demonstrate important 3-D designs for Li ion batteries. The thesis attempts also to address some of the key hurdles preventing the use of nanomaterials for Li ion batteries. Nanostructured three dimensional designs, both periodic and aperiodic in nature, are fabricated and studied

for the electrolyte, electrode and current collector. Chapter 1 provides an literature overview in relevant research topics such as 3-D Li ion batteries and nanostructured materials for Li ion batteries. In chapter 2 the challenging task of fabricating nanostructured solid electrolytes separating electrodes for the realization of fully interpenetrating 3D Li ion battery is addressed. Conformal pin-hole free polymer separators are fabricated around nanowire based electrodes. In Chapters 3 and 4 the enhancement of electrochemical performance by the fabrication of three dimensional current collectors for the negative electrode and positive electrode materials of the Li battery, has been discussed. In Chapter 3 a current collector design that incorporates both aperiodic and periodic current collector designs are incorporated into one current collector design to maximize the advantages of order and disorder, has been fabricated and studied. In Chapter 4 a 3-D tubular design to build a suitable current collector substrate for high capacity silicon anode has been discussed. Chapter 5 deals with the fabrication of nanowire energy storage device achieved by the assembly of all segments of a hybrid electrochemical energy storage device, anode, cathode and electrolyte onto a single nanowire. They are tested as parallel array of devices. This represents the ultimate miniaturization of electrochemical energy storage devices. Chapter 6 summarizes the key findings of the thesis.

Chapter 2: Conformal nanostructured polymer electrolyte for Li ion battery

2.1. Introduction

Various 3D battery architectures have been proposed to address effective power delivery in micro/nano-scale devices and for increasing the stored energy per electrode footprint area. One step towards obtaining 3D configurations in batteries is the formation of core-shell nanowires that combines electrode and electrolyte materials. One of the major challenges however in creating such architectures has been the coating of conformal thin nanolayers of polymer electrolytes around nanostructured electrodes. In this chapter we show conformal coatings of 25-30 nanometer Polymethylmethacralate (PMMA) electrolyte layers around individual Ni-Sn nanowires used as anodes for Li ion battery. This configuration shows high discharge capacity and excellent capacity retention even at high rates over extended cycling, allowing for scalable increase in areal capacity with electrode thickness. Our results demonstrate conformal nanoscale anode-electrolyte architectures for efficient Li-ion battery system.

2.2. Experimental Details

2.2.1. Fabrication of Ni-Sn nanowires and film

Alumina templates (ANODISC 13) were purchased from WHATMAN which had an average pore diameter of around 200 nm. A thin (200 nm) copper layer was sputtered onto the branched side of the alumina template which served as the electrical contact for the electrodeposition of nanowires. An aqueous solution of 0.2M $CuSO_4$ and 0.1M H_3BO_3 was prepared for the electrodeposition of Copper nanorod current collectors. A 20 mL aqueous solution of 0.075M $NiCl_2$, 0.175M $SnCl_2$, 0.5M $K_4P_2O_7$, 0.125M Glycine

and 5mL L^{-1} NH_4OH was prepared for the electrodeposition of Ni-Sn nanowires.[1] The electrodepositions were carried out in a three electrode cell consisting of a Pt counter electrode, Ag/AgCl reference electrode and the Au-coated alumina template working electrode using an AUTOLAB PGSTAT 302N potentiostat/galvanostat. First a short copper nanorod current collector segment was grown potentiostatically at -0.7V for 90s. The alumina template was removed from the cell and cleaned with large amounts of DI water followed by drying in vacuum for 4 hours. After drying, the Ni-Sn nanowires were electrodeposited using a galvanostatic method at a current density of 6mA/cm^2, typically for 30 minutes to partially fill the alumina template. A copper foil (Nimrod Hall Copper foil company) of thickness 0.025 mm was used as the substrate for electrodeposition of the planar Ni-Sn film. The same Ni-Sn electrolyte solution as used for the nanowire growth was used to grow planar films on the copper foil current collector. The copper foil was cleaned thoroughly with DI water before electrodeposition. Using the same three electrode setup as used for the Ni-Sn nanowire growth, planar Ni-Sn bulk film was grown on the copper foil to obtain films of same thickness.

2.2.2. Fabrication of planar and conformal Ni-Sn/PMMA nanostructures

After the growth of the Ni-Sn (electrode) nanowires and bulk film, the PMMA based polymer electrolyte/separator was coated onto the electrode. A 2 wt% solution of PMMA in acetonitrile was prepared inside an Argon filled glove box. The PMMA electrolyte was coated onto the Ni-Sn nanowires to obtain two different electrode-electrolyte designs. A thin film of PMMA was coated onto the planar Ni-Sn bulk film by spin coating to obtain the 2D electrode-electrolyte architecture. For the conformal configuration the Ni-Sn grown AAO template was typically first treated with 0.1 M NaOH for 40 minutes to widen the pores of the template. After the pore widening process the PMMA was drop coated

onto the alumina template. After the coating process the template surface was wiped off the excess liquid using a clean tissue paper and dried in vacuum at 25°C for 1h. A thin film of PMMA was allowed on top of the template to ensure electrical insulation between the two electrodes. The structure of the conformal configuration was analyzed by Transmission electron microscopy (FEI Quanta 400 ESEM FEG, JEOL 2100F). The template was dissolved completely in 3M NaOH to release individual nanowires prior to the electron microscopy characterization.

2.2.3. Electrochemical Measurements

The electrochemical performance of the Ni-Sn/PMMA core-shell nanowires was tested by galvanostatic charge/discharge measurements. For the half cell measurements, an electrochemical test cell was assembled in a Swagelok-type cell inside an Argon-filled glovebox using the Ni-Sn/PMMA (planar and conformal configurations) electrode/separator unit as the working and lithium metal foil as the counter/reference electrode. For full cell measurements, the cathode was made of $LiCoO_2$ (SIGMA ALDRICH), carbon black and PVDF binder in the weight ratio of 85: 10: 5. The slurry was prepared by mixing the above mixture of $LiCoO_2$, carbon black and PVDF in Dimethylformamide thoroughly, followed by casting onto an Aluminium foil (Alfa Aesar, thickness of 0.1 mm). The coated cathode was dried in a vacuum oven at 120°C for 24 hours. The conformal nanostructured Ni-Sn/PMMA array was used as anode/separator unit against the $LiCoO_2$ cathode. The PMMA film was soaked in 1 M solution of $LiPF_6$ in 1:1 (v/v) mixture of ethylene carbonate (EC) and dimethyl carbonate (DMC) for 1 h prior to assembly of each of the electrochemical cells. All galvanostatic charge/discharge measurements were conducted using an ARBIN BT 2000 Battery Analyzer. The electrochemical measurements of the uncoated Ni-Sn nanowires were performed in a

Swagelok-type cell using Ni-Sn nanowires as the working electrode, Li metal foil as a counter/reference electrode and 1M solution of $LiPF_6$ in 1:1 (v/v) mixture of ethylene carbonate (EC) and dimethyl carbonate (DMC) as an electrolyte. A glass microfiber filter was used as the separator. The cells were charged and discharged at a rate of 0.12 mA/cm^2 between 1.5 V and 0.02 V vs Li/Li+.

2.3. Results and Discussion

2.3.1. PMMA coated Ni-Sn nanowires

Owing to its high specific capacity, low cost and easy fabrication, Ni-Sn intermetallic nanowires have been chosen as the prototype electrode material.[39] Ni-Sn nanowires were grown inside pores of an anodized alumina template using a galvanostatic electrodeposition method (Figure 2-1).

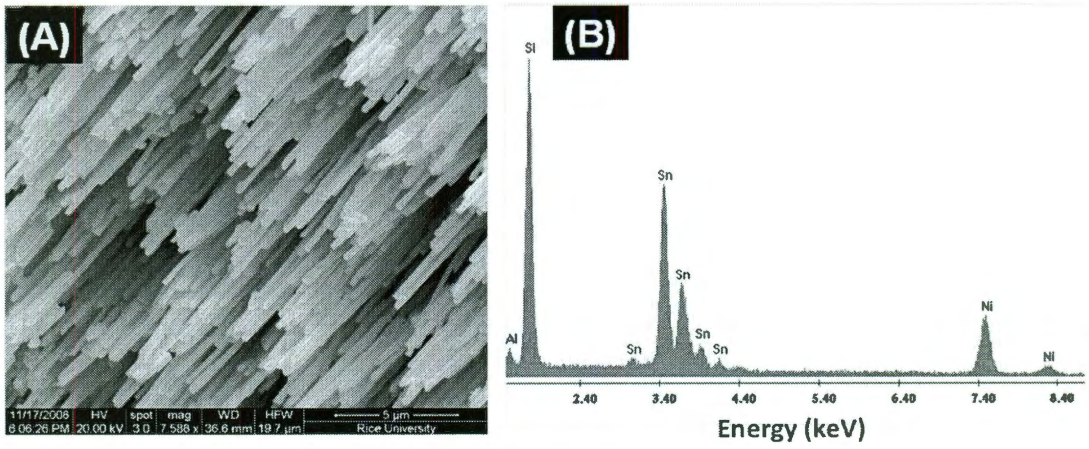

Figure 2-1. (a) SEM image showing uniform diameter of the Ni-Sn nanowires and (b) EDX spectra of Ni-Sn nanowire confirming the presence of elements Ni and Sn.

Spin coating or drop coating followed by wiping the excess solution on the surface of the template was used to coat a thin layer of PMMA onto the Ni-Sn electrode

for the planar and conformal configuration respectively. Using a combination of the above two techniques to grow nanostructured electrode and electrolyte/separator materials in the alumina template, the conformal configuration has been realized for the electrode-electrolyte assembly (Figure 2-2A). Electron Microscopy images of the conformal configurations show the well developed interfaces between the electrode and the polymer electrolyte/separator (Figure 2-2B).

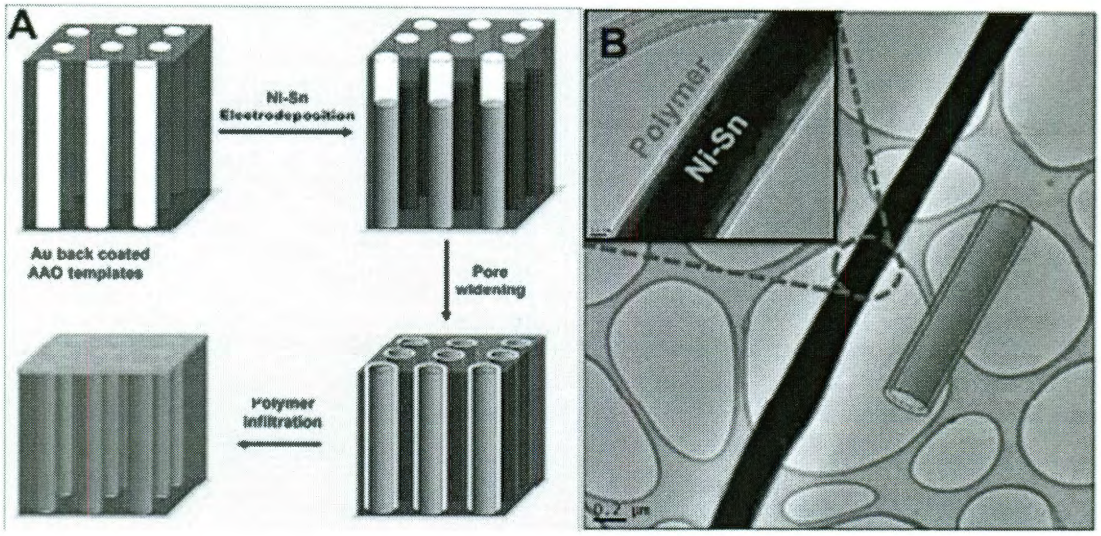

Figure 2-2: (a) Schematic showing the fabrication of the novel nanostructured conformal configuration of the electrode/separator assembly (b) TEM image of the conformal configuration showing the conformal PMMA layer around a ~3μm long segment of a Ni-Sn nanowire.

An entire nanowire was visualized at 24 continuous segments by TEM to confirm the conformal nature of the coating along the length of the nanowire as shown in Figure 2-3. The conformal nature of the PMMA coating around the nanowires was observed for all the Ni-Sn nanowires imaged using TEM. The conformal configuration results in a core-shell nanostructure and has much higher interfacial area compared to the conventional planar configuration. This leads to an electrode volume gain and allows for direct access of Li ions to the entire surface of the cylindrical nanowires. But in the case

of the planar configuration Li ion transport occurs only across the planar interface between the electrode and electrolyte. Hence the conformal configuration of electrode-electrolyte assembly is expected to exhibit superior electrochemical properties compared to the respective planar thin film based configuration.

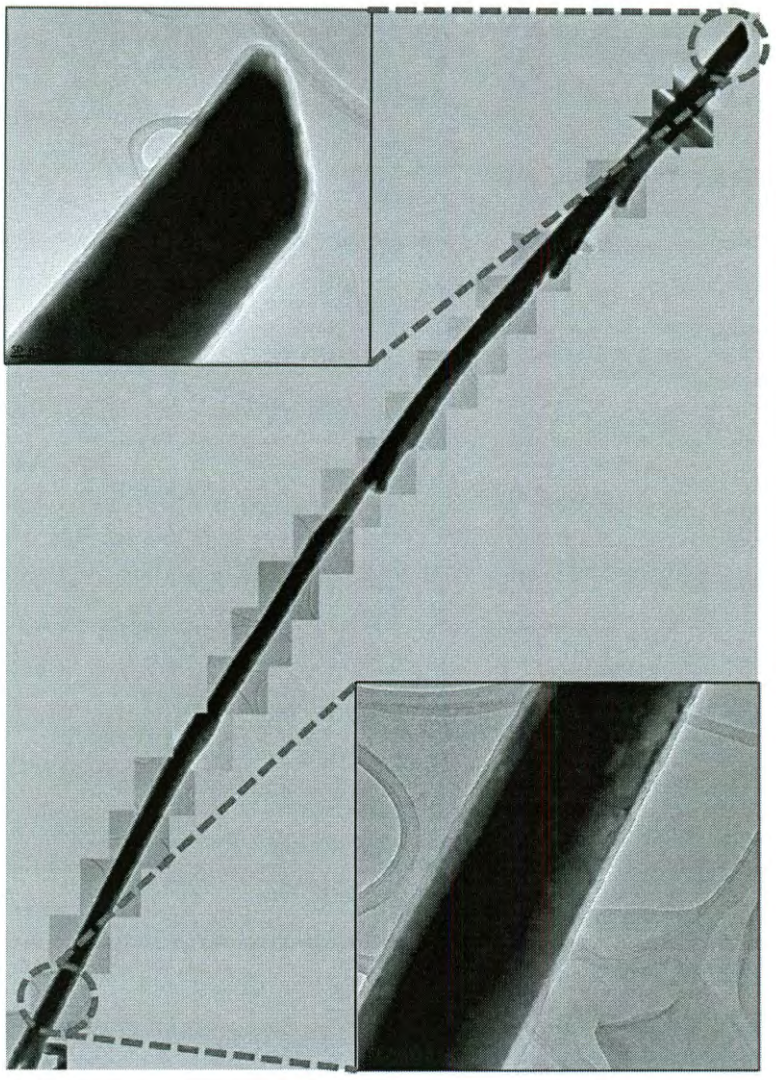

Figure 2-3: TEM image of a 10μm long PMMA coated Ni-Sn nanowire. 24 high magnification images along the length of the nanowire have been put together. High magnification images at two different segments of the nanowire clearly showing the Ni-Sn/PMMA interface (*Inset*).

2.3.2. Electrochemical performance: 2D vs 3D

Ni-Sn/PMMA electrode-electrolyte assemblies with planar and conformal nanostructured configurations were tested for their electrochemical performance in Li half cells by Galvanostatic charge/discharge cycling between 1.5 V and 0.02 V vs Li/Li^+, with Ni-Sn as the working electrode. Conformal PMMA layer soaked in liquid electrolyte solution formed the gel electrolyte and separator. For the conformal nanostructured electrode-electrolyte configuration, nanowires of height 10 μm were electrodeposited in the AAO templates and for the planar configuration a film of same thickness was electrodeposited on a copper foil. The potential vs capacity curves for the two electrode-electrolyte configurations (Figure 2-4A, B) at a current rate of 0.12 mA/cm^2 show typical Li insertion/extraction behavior of tin based intermetallic anodes.

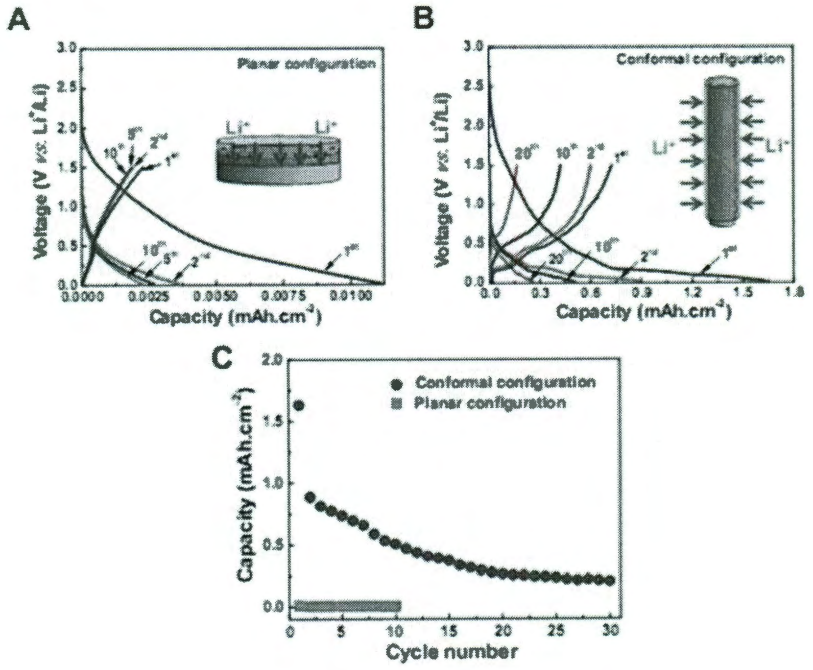

Figure 2-4: Electrochemical performance of Ni-Sn/PMMA assembly in (A) planar (B) conformal configurations (C) cycling behavior of the planar and conformal configuration.

Li ion transport in these configurations has been schematically illustrated in the respective plots. It can be clearly seen that the capacity per unit area of the conformal configuration is higher than that for the planar counterpart. The thin film based planar configuration showed a reversible capacity of ~0.002 mAh/cm^2 respectively after 10 cycles of charge/discharge whereas the conformal configuration was able to retain a reversible capacity of ~0.26 mAh/cm^2 even after 30 cycles of charge/discharge. The novel conformal nanostructured electrode–electrolyte configuration shows an improvement in the reversible capacity by two orders of magnitude. Moving to the third dimension with a conformal nanowire based configuration has resulted in geometrical area gain and an associated electrode volume gain. This leads to shorter transport path for Li ion diffusion between the electrodes. On the contrary in the planar configuration, the Li ions diffuse through the entire length of the nanowire or the bulk film respectively. The slow transport of Li ions through solid state anode materials leads to the development of a concentration polarization which results in a large loss in capacity delivered.[40] In the case of the conformal configuration, the problem of concentration polarization is reduced significantly by the conformal wrapping of PMMA electrolyte around every individual nanowire electrode hence resulting in short radial Li ion diffusion distances. Hence the Galvanostatic cycling results (Figure 2-4C) clearly delineate that the conformal design of the electrode-electrolyte assembly in LIB leads to efficient performance with good cycling characteristics and energy densities compared to conventional planar design.

2.3.3. Rate capability of 3D design

To realize the high rate power capabilities of this novel conformal electrode-electrolyte assembly for 3D nano/micro battery applications, we studied its

electrochemical performance at higher current rates and with increasing heights of electrode segments, maintaining the areal foot print. Ni-Sn/PMMA (gel electrolyte) with conformal configuration and electrode length of ~ 10 μm were galvanostatically cycled in a Li half cell at different current rates of 0.12 mA/cm^2 (0.5C) and 0.3 mA/cm^2 (3C) (Figure 2-5A).

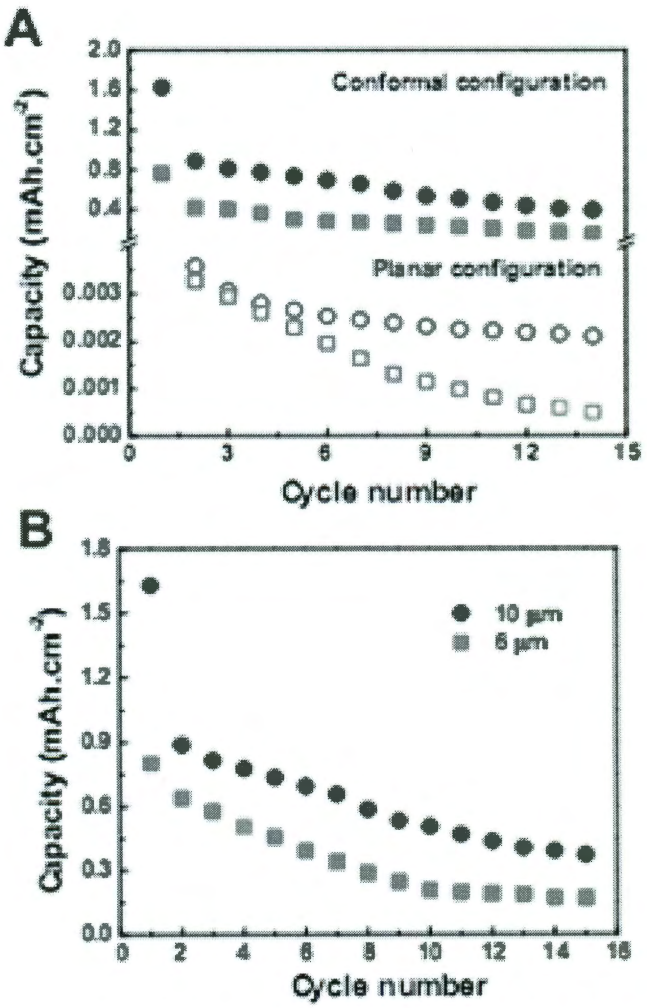

Figure 2-5. Rate capability and capacity retention of conformal Ni-Sn/PMMA assembly.

A planar electrode-electrolyte assembly with same electrode height (thickness) is also tested for comparison. The difference in the initial capacity could be due to the differences in the accessibility of the bulk electrode film. The capacity behavior of planar assembly follows a typical thin film electrode with a constant decrease at higher current rates. Excellent rate capability is observed with the conformal design and shows good capacity retention even at higher current rates. Reversible and steady capacity of 0.15 mAh/cm^2 was achieved at a high current rate of 0.3 mA/cm^2. This can be attributed to the short diffusion distance in the Ni-Sn nanowire due to radial diffusion of Li ions.

Hence an increase in the height of the electrode segment, with the same small foot print area, is expected to result in increased areal capacity along with high power capabilities.[152] To carry out this study, two samples of Ni-Sn/PMMA core-shell nanowires with varying heights of 6 μm and 10 μm were galvanostatically cycled in Li half cell at current rates of 0.06 mA/cm^2 and 0.12 mA/cm^2 respectively. The capacity vs cycle number plot (Figure 2-5B) clearly shows the increase in areal capacity with increasing electrode height. Reversible capacities of 0.17 mAh/cm^2 and 0.37 mAh/cm^2 have been obtained for samples with Ni-Sn height of 6 μm and 10 μm respectively. This further confirms the conformal nature of the polymer coatings around the entire length of the nanowire electrode, as there is no change in the Li ion transport distance. The discharge profiles of the two samples show that fast Li ion kinetics (power capability) is retained even after increasing the height of the Ni-Sn nanowire electrodes (Figure 2-6A and B). In general, Sn-based electrodes suffer from capacity decay with cycling,[165] however, our present study intends to demonstrate the novel conformal configuration of the electrode-electrolyte assembly for 3D nano/micro battery applications and the concept can be extended for other electrode systems as well. Using Li half cell measurements, we clearly show that the conformal design of the electrode-electrolyte assembly brings an

innovative approach to improving areal energy densities of low dimensional batteries yet maintaining their high power capabilities.

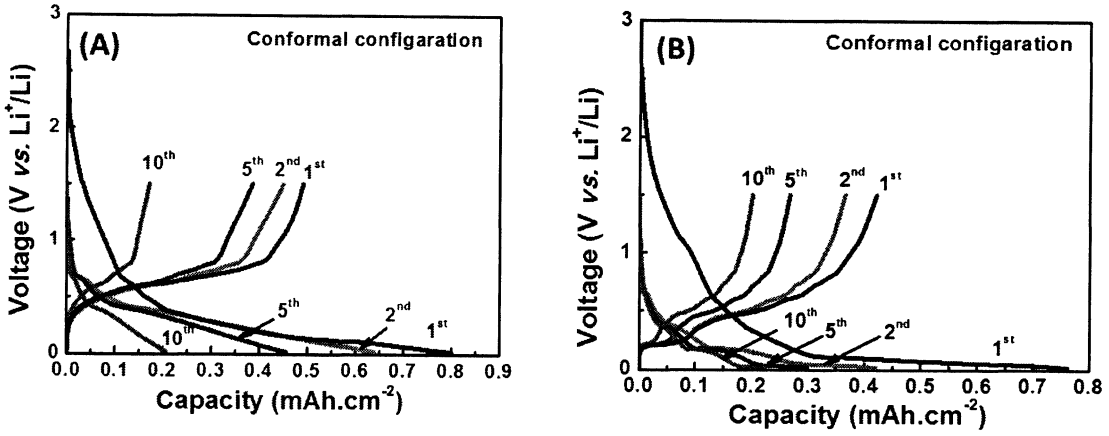

Figure 2-6: Voltage vs Capacity profiles of the (A) Shorter and (B) Longer Ni-Sn nanowire electrodes.

2.3.4. SEI stabilization with PMMA coating

We have conducted control experiments to compare the electrochemical performance between PMMA coated and uncoated Ni-Sn nanowires. Galvanostatic charge/discharge measurements were conducted on coated and uncoated nanowire arrays at a current rate of 0.3 mA/cm^2 (3C) to investigate the rate capability of the two configurations. From the galvanostatic cycling results (Figure 2-7) it is clear that the PMMA coated Ni-Sn nanowires show an improvement in the reversible capacity retention at a high current rate of 3C. Conformally coated Ni-Sn nanowires show a stable reversible capacity of ~0.2 mAh/cm^2 for galvanostatic cycling at fast rates of charge/discharge (3C) upto 60 cycles of charge/discharge. From these results we believe that the conformal PMMA coating could be playing a role in improvement of rate

capability of the Ni-Sn nanowires. The presence of an interfacial reaction between Ni-Sn and the liquid electrolyte leads to the formation of the SEI film on the electrode surface

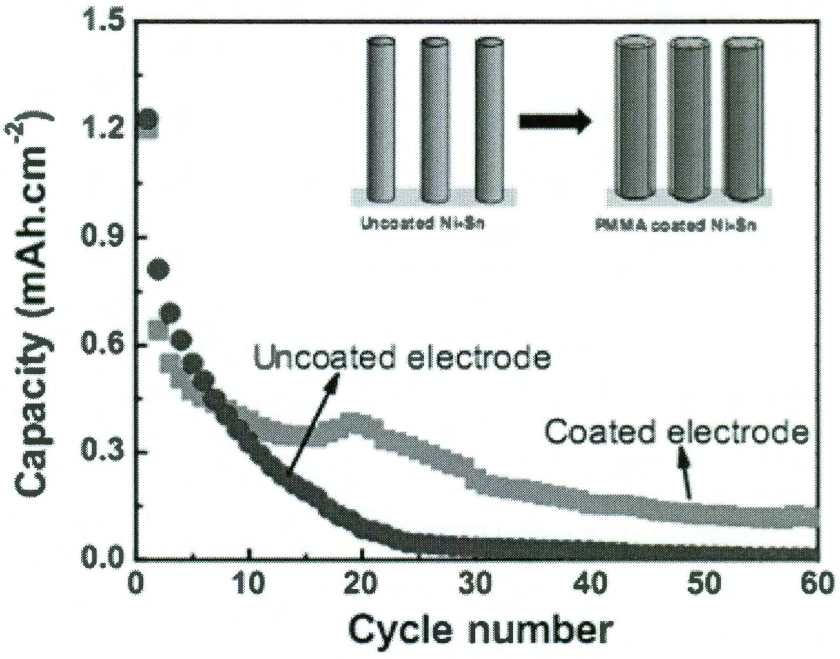

Figure 2-7: Electrochemical performance of conformally coated (PMMA) Ni-Sn nanowires and uncoated Ni-Sn nanowires.

leading to capacity loss over cycling.[120] Recent research efforts have characterized the surface films on intermetallic anodes specifically Ni-Sn based anodes and have discussed the dependence of cycling characteristics on surface reactions.[120,124] Herein, we speculate that the polymer coating around the Ni-Sn nanowires could be helping in stabilizing the SEI film and conceivably suppressing the detrimental surface effects on the electrode leading to the improved cycling characteristics. The exact details of the SEI formation mechanisms and its evolution over cycling are yet to be probed and understood. We believe that the coating of polymers (which also serves as the separator

functionality) around individual electrode Ni-Sn nanowires could open a new direction of research towards improving cycling characteristics of this high volume expansion electrode material without the need of external surface modifications. We have conducted extensive TEM analysis of the conformally coated Ni-Sn nanowires after galvanostatic charge/discharge cycling which also reveals that the PMMA shell is intact around the Ni-Sn nanowires (Figure 2-8). The absence of pinholes even after extended cycling at a high current rate (3C) clearly demonstrates the strength of the electrode-electrolyte interface. Hence the polymer coated electrode nanowires could serve as a great candidate for future 3D Lithium ion batteries.

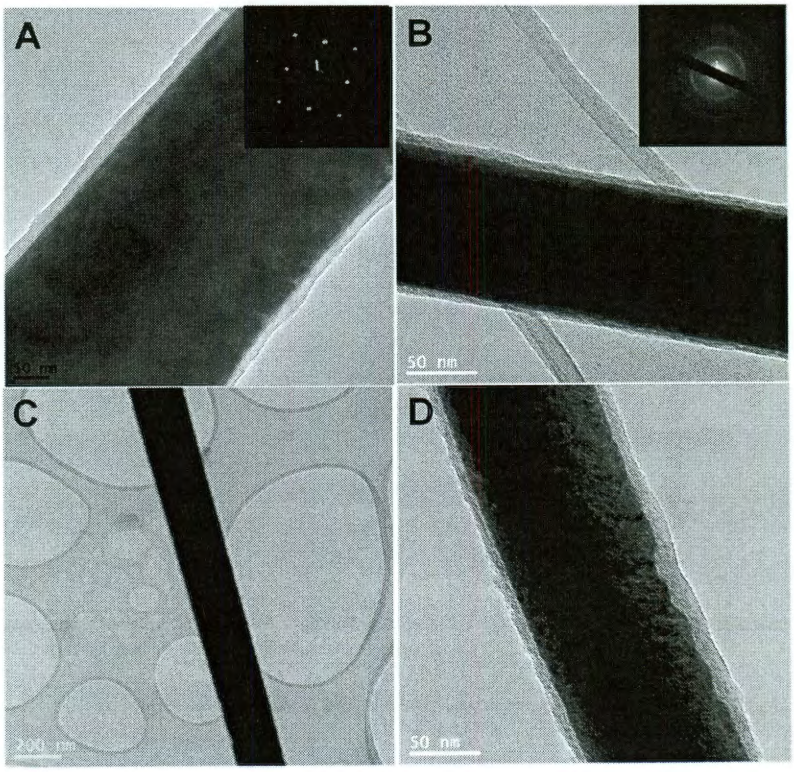

Figure 2-8. TEM images of a PMMA coated Ni-Sn nanowire (A) before cycling (Electron diffraction is shown in the *Inset*) (B) after 15 cycles of charge/discharge (C) and (D) low and high magnification images after 60 cycles of charge/discharge.

2.4. Conclusions

In this chapter we have demonstrated a simple template assisted technique to fabricate nanoarchitectured conformal electrode/electrolyte assembly which can be useful in Li-ion nano/micro battery systems. Thin conformal layer of PMMA deposited around Ni-Sn nanowire electrode provides the separator functionality to the assembly and serves as the gel electrolyte when soaked with liquid electrolyte. The conformal configuration showed excellent electrochemical performance with two orders of magnitude improvement in the reversible discharge capacities, compared to its planar counterpart. High rate capability over extended cycling resulting from the nanoarchitectured conformal electrode-electrolyte assembly has also been demonstrated. The PMMA coating has been observed to stay intact around the Ni-Sn nanowires over extended cycling at high current rates and has shown to improve the cycling characteristics of the bare nanowires. We believe that our general approach could easily be extended to deposit other active electrode materials and polymer separators which could lead to the development of an efficient nanoscale Li ion battery. The conformal configuration of the PMMA coated electrode we have shown here is an important step towards realizing the true 3D nanostructured battery where the anode, electrolyte and cathode are all conformally integrated into the single nanowire assembly.

Chapter 3: Nanoporous gold current collectors for Li ion battery cathode

3.1. Introduction

This chapter describes the fabrication and electrochemical characterization of nanoporous current collector substrates for thin film Li batteries. Conventional thin film battery electrodes have been fabricated on planar current collectors[118,119]. But due to energy per unit area restrictions in planar thin film designs the search for rough 3D structures have gained more importance in the recent past[150-153]. Prior research in the periodic nanorod based current collector proposed by Simon and co-workers has served as a great substrate to build 3D nanostructured thin film Li batteries[120,152,166,168]. The template approach for growing nanorods provide for good control of spacing between individual nanorods for the subsequent deposition of electrode/electrolyte layers. On the other hand the aperiodic foam like structures with pores size less than 10 nm have been used as current collectors and possess lot higher surface area compared to periodic counterpart hence increasing the active mass of electrode accommodated per footprint area. But due to the complexity in the aperiodic porous structure it is very challenging to fabricate subsequent electrode and electrolyte layers without the presence of electrical shorts to realize a fully interpenetrating 3D Li battery.

Herein we demonstrate the use of Au nanoporous nanorods as Li battery current collectors which exhibits two levels of porosity, where i) each nanorod exhibits high surface (pore size less than 10 nm throughout the volume of the nanorod) for better mass accommodation and ii) the space between individual nanorods (pore size ~ 50-100 nm; alumina template controlled) for the assembly of the electrolyte and electrode layers

to fabricate the full 3D energy storage device. Polyaniline cathode material has been used to avoid any low voltage Li ion insertion into the gold nanostructure. The novel electrode/current collector configuration has shown improvement in the discharge capacity per footprint area and rate capability of the polyaniline electrode material.

3.2. Experimental Details

3.2.1. Fabrication of Au nanotubes

WHATMAN alumina membranes (pore diameter = 200 nm) were used for the electrodeposition of Au-Ag alloy nanorods. Before electrodeposition the alumina membranes were cleaned by sonicating them in deionized water for 30 minutes and dried in a vacuum oven at 80°C for 4 hours. A 200 nm film of gold was sputtered onto the branched side of the alumina membrane which served as the electrical contact for the electrodeposition process. Polyaniline nanowires were first grown using a cyclic voltammetry three electrode electrodeposition method with Aniline (0.1M) and Sulfuric acid (0.5M) electrolyte. The electrodeposition was conducted between -0.2V to 1.2V for 80 cycles with an Ag/AgCl (in 3M NaCl) reference electrode. The PANI nanowires were contracted in diameter by annealing the PANI/Alumina membrane in vacuum at 80 °C. Then, gold was electroplated around the PANI nanowires using a TECHNIC Inc Orotemp gold plating solution as electrolyte at a voltage of -0.9 V w.r.t Ag/AgCl in 3M NaCl reference electrode. This was followed by etching of the PANI nanowire using concentrated nitric acid and then the alumina membrane was stuck onto a stainless steel foil using a thin layer of silver paste. The alumina membrane was etched using 3M solution of NaOH and then the Au nanotube film was cleaned thoroughly using DI water and dried in a vacuum oven for 4 hrs at 80 °C.

3.2.2. Fabrication of Au Nanoporous Nanorods

WHATMAN alumina membranes (pore diameter = 200 nm) were used for the electrodeposition of Au-Ag alloy nanorods. Before electrodeposition the alumina memebranes were cleaned by sonicating them in Deionized water for 30 minutes and dried in a vacuum oven at 80°C for 4 hours. A 200 nm film of gold was sputtered onto the branched side of the alumina membrane which served as the electrical contact for the electrodeposition process. Au-Ag alloy nanowires were electrodeposited by a potentiostatic method at -0.9 V (w.r.t Ag/AgCl in 3M NaCl reference electrode) using a 3:1 (v: v) mixture of gold (TECHNIC Inc Orotemp) and silver (TECHNIC Inc RTU) precursor solutions respectively as the electrolyte. A platinum wire served as the counter electrode and the gold coating on the alumina membrane served as the working electrode for this three electrode electrodeposition setup. Electrodeposition of Au-Ag nanorods was conducted for 4 minutes in order to obtain nanorods of height ~500 nm. The alumina membrane was treated with concentrated nitric acid for 10 minutes to remove the silver component in each individual nanorod followed by thorough rinsing with DI water to remove any traces of nitric acid. The alumina membrane was then stuck onto a stainless steel substrate using a thin layer of silver paste and the alumina was dissolved using 3M NaOH. The vertically aligned Au-Ag nanorod array was rinsed again with DI water and dried in a vacuum oven for 4 hrs at 80 °C.

3.2.3. Fabrication of PANI coated Au substrate

PANI was electrodeposited onto the planar and nanostructured substrates using a three electrode galvanostatic electrodeposition setup using the gold substrate as the working electrode, a platinum wire as the counter electrode and the Ag/AgCl in 3M NaCl as the reference electrode. A current density of 1 mA/cm^2 for 2 minutes was applied

using an aniline (0.15M) + Sulfuric acid (0.5M) + Sodium Sulfate (0.5M) electrolyte solution to obtain a film of PANI around each of the three gold based current collectors – i) planar thin film of gold sputtered onto stainless steel foil, ii) vertically aligned array of Au nanotubes on a stainless steel foil, iii) vertically aligned array of gold nanoporous nanorod on a stainless steel foil.

3.2.4. Electrochemical Measurements

All galvanostatic charge/discharge measurements were conducted using an ARBIN BT 2000 Battery Analyzer. The electrochemical measurements for all the three configurations, – i) planar thin film of gold sputtered onto stainless steel foil, ii) vertically aligned array of Au nanotubes on a stainless steel foil, iii) vertically aligned array of gold nanoporous nanorod on a stainless steel foil were performed in a Swagelok-type cell using Ni-Sn thin film as the working electrode, Li metal foil as a counter/reference electrode and 1M solution of $LiClO_4$ in 1:1 (v/v) mixture of ethylene carbonate (EC) and dimethyl carbonate (DMC) as an electrolyte. A glass microfiber filter was used as the separator. The cells were charged and discharged between 3.6 V and 2 V vs Li/Li^+ at current rates 0.04 mA/cm^2.

3.3. Results and Discussion

3.3.1. Nanoporous current collectors

Nanoporous current collectors have been proposed to improve surface area for the accommodation of higher active electrode mass. Figure 3-1 shows the schematic representation of advanced 3D nanostructured configurations for current collectors around which thin film electrodes have been be fabricated. Nanotube based current collectors is expected to exhibit higher surface area for electrode deposition in

comparison to conventional nanorod[7] based current collectors due to the added inner wall surface. Whereas nanoporous nanorod current collectors are expected to show even higher surface area due to the internal pore surface area within each individual nanorod. Due to the different available surface areas for the three current collector substrates (planar, nanotube, nanoporous nanorod) used in this study, corresponding electrode distributions (electrode thickness) varies for each of the cases (planar, nanotubes and nanoporous nanorods). When the total charge passed during electrodeposition of an electrode film is kept constant, the thickness of the conformal electrode film deposited onto the current collectors is expected to reduce with the increase in total surface area of different current collectors. Hence the rate capability of the electrode is expected to improve upon increasing surface area of the current collectors. To demonstrate this important concept, we choose gold as our current collector material and PANI as our electrode material. We fabricate the nanostructured gold current collector using hard template assisted electrodeposition technique followed by polyaniline electropolymerization on the nanostructured Au. Polyaniline is chosen as our cathode material due to the high voltage w.r.t Li/Li^+ and the ease of fabrication. Also, PANI is known to change redox states between charge/discharge processes and hence exhibiting a large change in electronic conductivity between charge/discharge[19]. Hence, a nanostructured current collector morphology is expected to have a significant effect on the rate capability of the PANI electrode material.

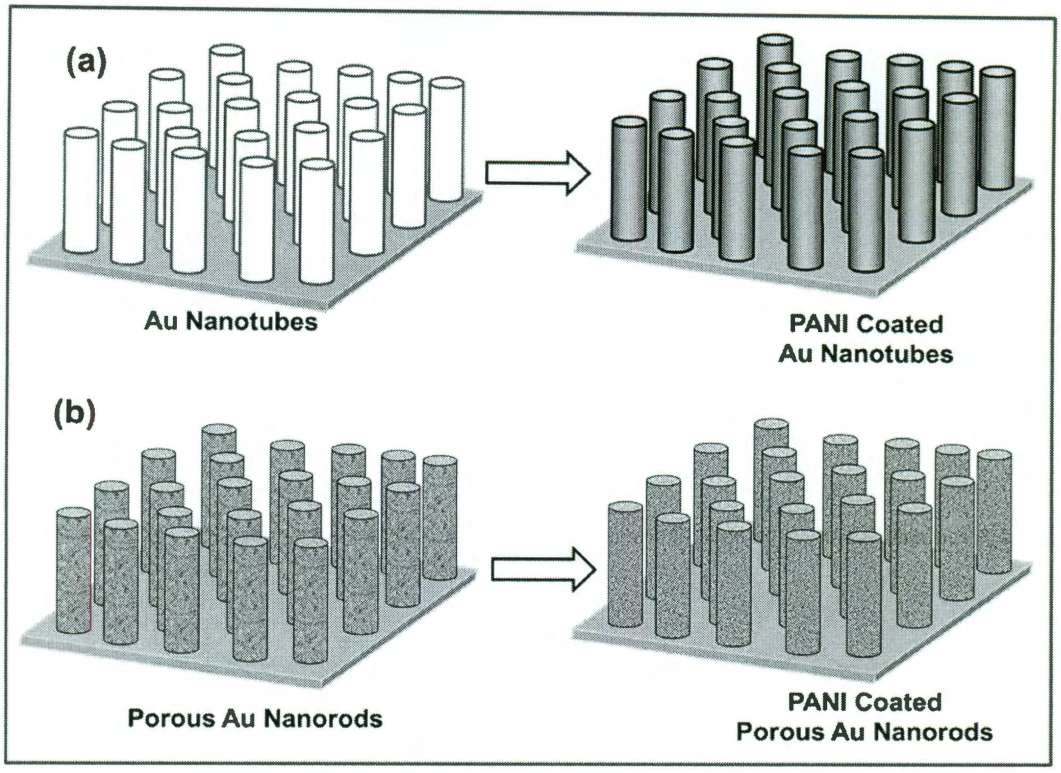

Figure 3-1: Schematic diagram of the vertically aligned array of (a) nanotubes and (b) nanoporous nanorods and the subsequent electrodeposition of the PANI layer.

3.3.2. Nanotubular current collector

Firstly we have looked at the vertically aligned nanotube based current collector as a substrate for Li battery electrodes. The vertically aligned gold nanotube array was fabricated using a hard template assisted electrodeposition technique and attached onto a stainless steel substrate (Figure 3-2a). From the SEM image in Figure 3-2a it is clear that the nanotubes have ~ 20 nm wall thickness and an inside diameter of ~180 nm. The nanotubes are separated by an average distance of around ~ 200 nm. The nanotubes are ~ 500 nm in height and have higher surface area compared to the conventionally used planar or nanorod[7] substrates due to the available inner wall surface for electrode

deposition. A PANI film was electropolymerized onto the gold nanotube array to form a conformal coating around each nanotube and SEM was used to characterize the resulting PANI/Au nanostructure. The SEM image in Figure 3-2b clearly shows that the PANI coating around the nanotubes is conformal after electropolymerization on the Au nanotubes. We have also fabricated the conventional planar design for thin film batteries by electrodepositing a thin film of Au onto a stainless steel substrate and then polyaniline electrode film onto it to compare with the nanotube based configuration. The nanotube based configuration shows improved electrode surface area and hence the electrode mass distribution per footprint area compared to the thin film PANI electrode.

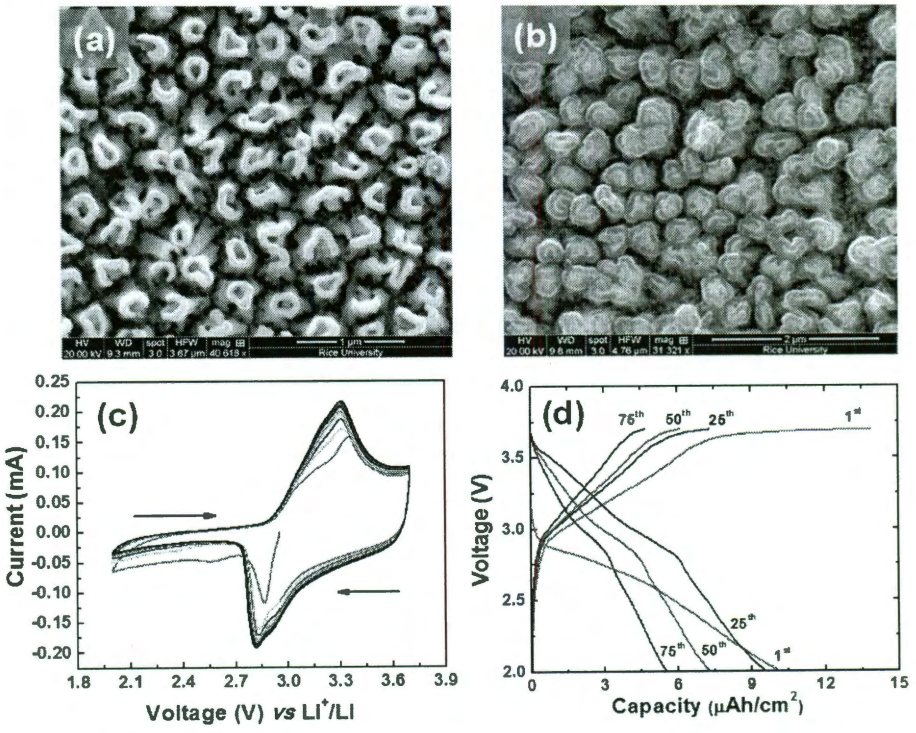

Figure 3-2. (a) SEM image of aligned array of gold nanotube current collector. (b) Polyaniline coated gold nanotube array. (c) Cyclic voltammetry of the PANI coated Au nanotube electrode (d) Voltage vs discharge capacity profile of the PANI coated Au nanotube array.

The cyclic voltammetry scans for the Au nanotube/PANI electrode is shown in Figure 3-2c. The CV scans were conducted between 2 and 3.6 V at a scan rate of ~ 0.5 mV/s. The first anodic scan was started from the open circuit voltage of the cell until 2 V vs Li/Li^+ and an anodic peak was observed around ~ 2.9 V which indicates the discharge process of the cell where the PANI electrode is reduced. The first cathodic scan shows a peak at around 3.4 V showing the charge process where the PANI electrode is oxidized. The subsequent anodic and cathodic scans show good reversibility of the PANI redox process and the peaks are shifted to 2.8 and 3.3 V respectively. Figure 3-2d shows the voltage vs discharge capacity curves for the PANI/Au nanotube configuration.

Figure 3-3 shows the voltage profile of the planar configuration of the PANI electrode. From the voltage profile of the planar configuration it can be seen that the discharge plateau is clearer from the second cycle onwards as electrolyte accessibility to the electrode is improved after the first cycle. In the case of the nanotube based configuration (Figure 3-2d) the electrolyte is better accessible to the PANI film due to the inter-tube spacing. An improvement in the reversible capacity of nanotube based configuration is observed compared to the planar configuration after 75 cycles of charge/discharge. This could be attributed to the improved mass distribution of PANI around Au nanotubes compared to a planar film.

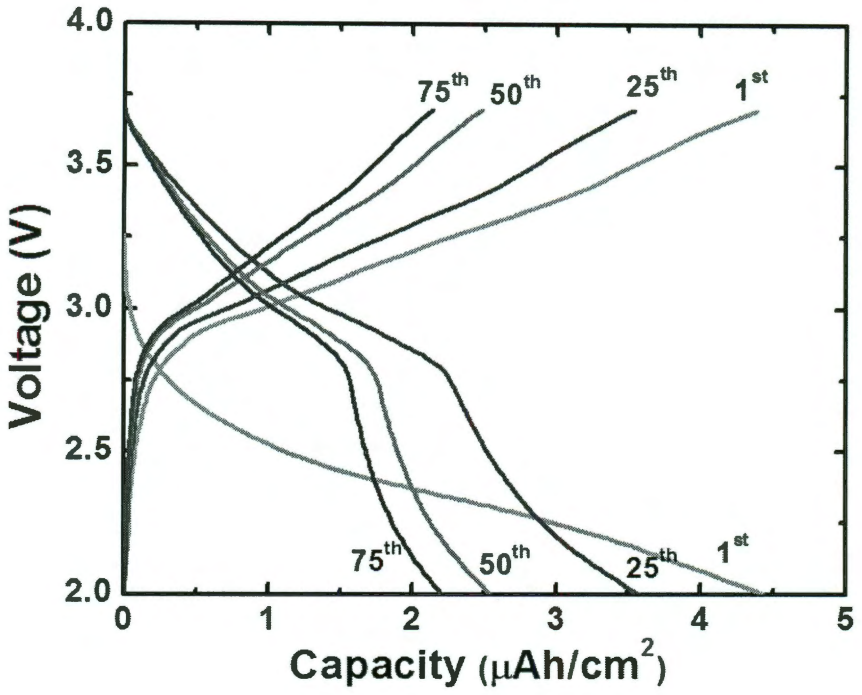

Figure 3-3: Voltage vs discharge capacity profile for the planar PANI configuration

3.3.3. Nanoporous nanorod current collector

We have also fabricated vertically aligned Au nanoporous nanorod array as a current collector to improve the electrode surface area more than the nanotube and planar based configurations. The Au nanoporous nanorod array was fabricated using a hard template assisted alloying/dealloying technique. The nanoporous nanorods are 500 nm in height and are separated by an inter-rod distance of around ~ 200 nm. We have also characterized these nanorods by TEM and they show a highly porous structure for the nanorod resulting in an interconnected network of Au nanoparticles with an internal pore size of around ~ 5-10 nm (Figure 3-3 and 3-4).

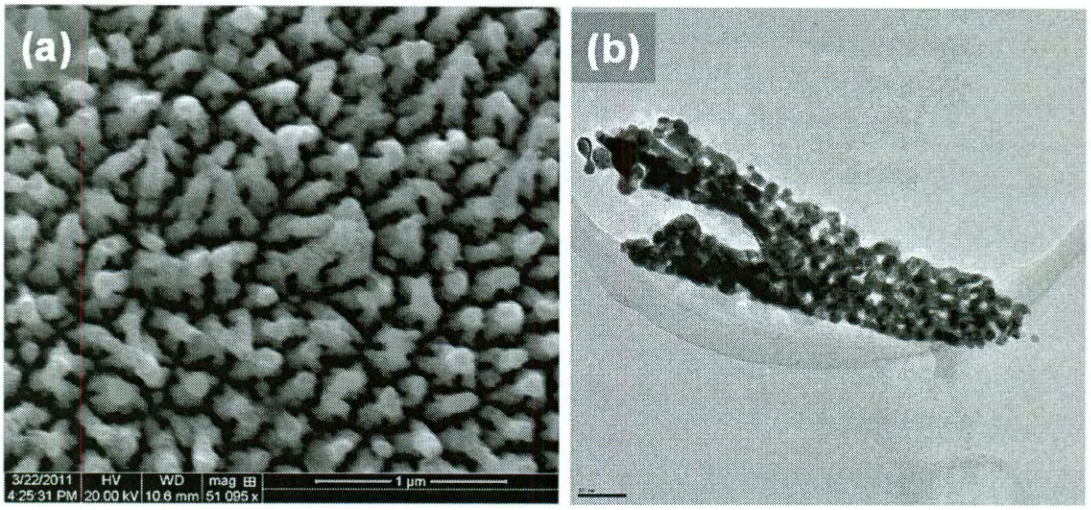

Figure 3-4: (a) SEM and (b) TEM images of porous Au nanorods

The PANI electrode was electropolymerized onto the Au nanoporous nanorod substrate and the resulting structure was characterized by SEM and TEM shown in Figure 3-5a, b and Figure 3-6. From the high magnification transmission electron microscopy image (Figure 3-6) it is clear that the polyaniline forms a conformal coating around the nanoporous nanorod substrate, and also fills the internal pores within the nanorod. This results in improved i) mass distribution (thinner layers of PANI due to higher surface for mass to deposit on) compared to the nanotube or planar based design and ii) very intimate contact of PANI electrode with the interconnected Au current collector. Galvanostatic charge/discharge measurements at current rate 0.04 mA/cm^2 were conducted and the resultant voltage vs capacity curves for the PANI coated nanoporous nanorod array are shown in the Figure 3-3c.

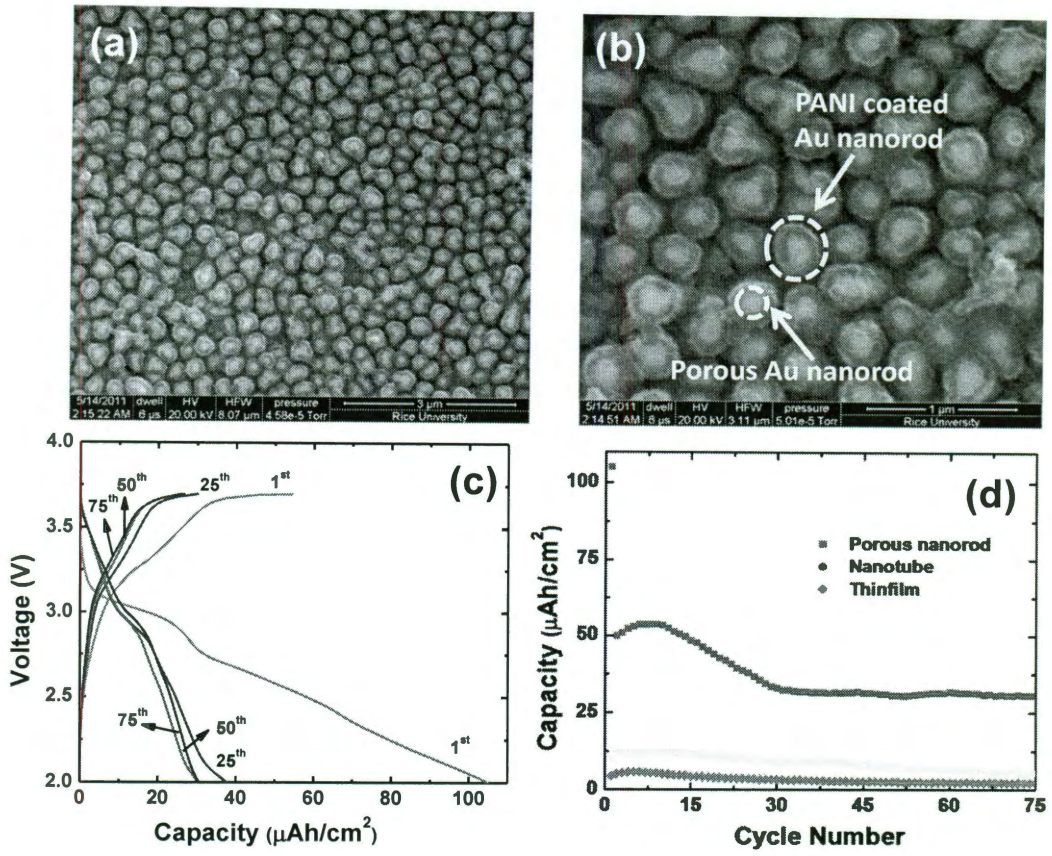

Figure 3-5. (a) Low (b) high magnification SEM image of the PANI coated nanoporous Au nanorod (c) Voltage vs discharge capacity graphs for the galvanostatic measurements conducted on the nanoporous nanorod current collector configuration. (d) Discharge capacity vs cycle number plot for the three different configurations – planar, nanotube and nanoporous nanorod upto 75 cycles.

From the voltage vs capacity profiles we can clearly observe the typical plateaus for PANI electrode during charge and discharge processes. A large irreversible capacity loss is observed after the first charge/discharge cycle for the nanoporous nanorod configuration. A reversible capacity of ~32 μAh/cm^2 was observed after 75 cycles of charge/discharge for the nanoporous nanorod configuration.

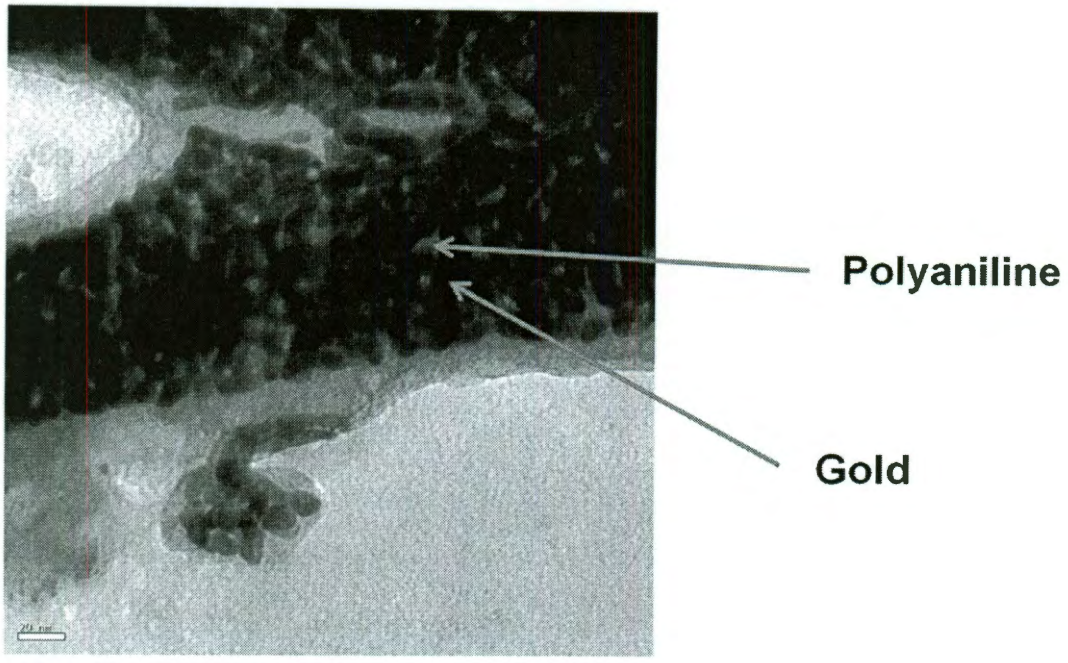

Figure 3-6: TEM image of PANI coated nanoporous gold nanorod clearly showing the both the gold (darker sections) and PANI (lighter sections) segments within the nanorod. Polyaniline can be seen within the pores of the nanoporous gold nanorod as shown. PANI layer thickness ~20 nm.

We have also conducted extended cycling tests on the three configurations at 0.04 mA/cm^2 and the discharge capacity vs cycle number was plotted as shown in Figure 3-5d. As we can observe from Figure 3-5c reversible discharge capacities of ~2 $\mu Ah/cm^2$, 8 $\mu Ah/cm^2$, 30 $\mu Ah/cm^2$ were observed for planar, nanotube and nanoporous nanorod current collector systems respectively after 75 cycles. Hence we can confirm that the nanoporous nanorods show much better rate capability compared to the planar or nanotube based current collectors. This can be attributed to the increased surface area due to the network of nanopores of size ~ 5-10 nm in the nanoporous gold nanorod, hence forming thinner conformal layers of polyaniline electrode around the current collector facilitating faster electron and ion transport from the electrode to current

collector. As the electron transport from the electrode to current collector is an important step in determining the overall rate capability of the electrode for electrodes having lower electronic conductivity, it is reflected in the difference in rate capabilities of the three configurations. Hence the novel 3D nanoporous architecture for current collectors could also be used for cathode materials such as $LiCoO_2$, $LiMn_2O_4$ etc. that suffer from low electronic conductivity, to improve rate capability of the electrode materials.

We have also conducted high rate galvanostatic charge/discharge measurements to evaluate the rate capability of the nanoporous nanorod current collector design. Polyaniline coated nanoporous Au nanorods were tested against Li foil at current rates of 40 $\mu A/cm^2$, 200 $\mu A/cm^2$, 400 $\mu A/cm^2$, 800 $\mu A/cm^2$, corresponding to C-rates 1C, 5C, 10C and 20C respectively, to evaluate the capacity retention of the 3D electrode at high current rates. From the voltage vs discharge capacity profiles (Figure 3-7a) we can observe that the polyaniline is undergoing the redox reaction to exhibit the electrochemical properties. The redox reaction is still observed as the voltage plateau even as the current rate of operation is increased. Figure 3-7b shows that the capacity of the cell is well retained upto 75 cycles of charge/discharge for the above current rates of operation. At current rates of operation, 0.2 and 0.4 mA/cm^2, it can be observed that the loss in reversible capacity is minimal. It is also observed that the 3D polyaniline electrode shows capacity retention of ~30 % of the nominal capacity even at high current rate of 0.8 mA/cm^2. The half cells showed stable discharge capacities upto 75 cycles of charge/discharge. The 3D polyaniline electrode has shown good rate capability due to the reduced electron and ion diffusion distances. Shorter ion and electron diffusion distances are a result of reduced PANI electrode thickness due to the high surface current collector design (nanoporous Au nanorod).

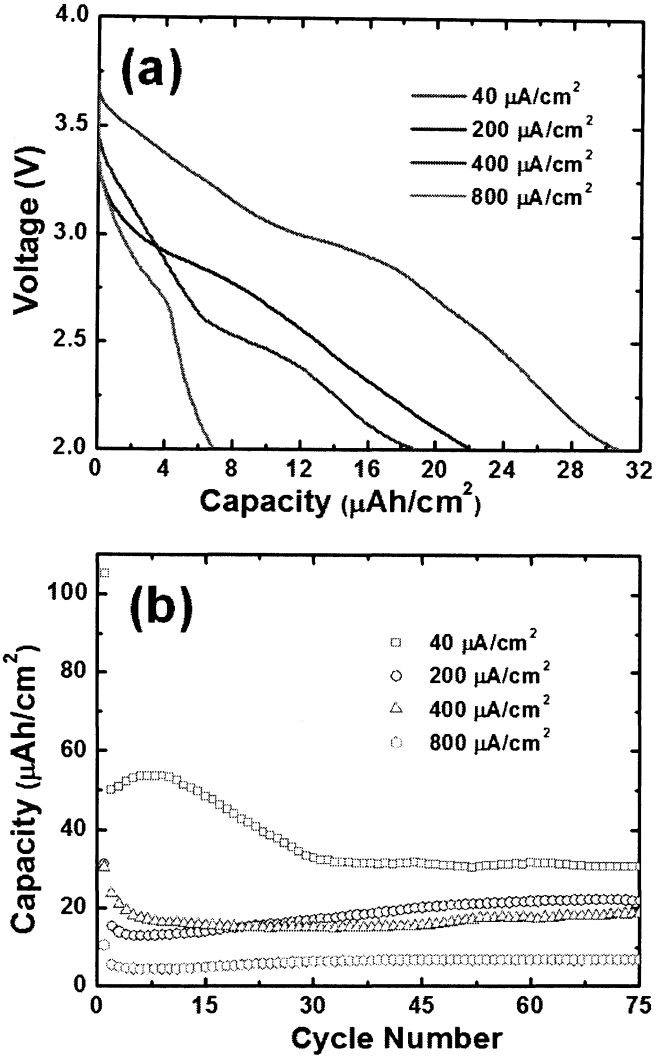

Figure 3-7. (a) Voltage *vs* discharge capacity and (b) Discharge capacity vs cycle number graphs for the galvanostatic measurements conducted on the nanoporous nanorod configuration at currents 40, 80, 200, 800 μA/cm^2.

3.4. Conclusions

In conclusion we find that 3D nanoporous designs for electrodes have resulted in improved rate characteristics than that of conventional planar thin film based designs. Polyaniline electrodes have been electropolymerized onto nanotube and nanoporous

nanorod based current collectors. The nanoporous nanorod current collector shows capacity retention of upto 30 % of the reversible capacity (32 $\mu Ah/cm^2$) even at high current rates of 0.8 mA/cm^2. The nanoporous nanorod current collectors allow for improved mass accommodation per geometric area compared to nanorod or nanotube based designs which could be important for cathode layer depositions. The nanoporous nanorod design proposed could be helpful in increasing electrode mass per unit area at high current rate of operation and still preserve the space between nanorods for subsequent electrolyte and electrode layer deposition. The nanoporous nanorod design demonstrates an example of combining aperiodicity (within pores of each nanowire) and periodicity (vertically aligned array of nanorods with constant inter-rod distance) for the design of high energy and high power 3D microbatteries.

Chapter 4: Nanoporous nickel current collectors for Li ion battery anode

4.1. Introduction

With the recent interest in development of electric vehicles, high energy density Li ion batteries are becoming a necessity.[112,113] Energy density of a Li ion cell depends on the voltage and the capacity of the cell. Hence electrode capacities play an important role in the final energy density of the battery pack. The energy demands for the operation of vehicles far surpass the energy densities obtained from commercially existing Li ion battery electrode chemistries. Hence extensive research efforts are underway in search of new battery electrodes to improve the energy density of the Li ion cell. Current electrodes used for Li ion batteries involve layered or olivine cathode materials and graphitic anode material. The graphite anode used in commercial Li ion batteries have some intrinsic drawbacks associated with it: i) low specific capacity ~ 370 mAh/g ii) very low Li intercalation potential ~ 0.1 V causing risk for Li plating and iii) large irreversible capacity loss in the first cycle due to secondary electrolyte interphase formation. Silicon on the other hand appears to be a suitable candidate with very high capacity of ~ 4200 mAh/g and slightly higher voltage of Li insertion ~0.5 V. Increase in capacity of negative electrode increases the overall energy density of the Li ion battery. But Si electrodes suffer from severe capacity fade upon cycling. The capacity fade is attributed to large volume change (~400 %; $Li_{22}Si_5$) associated with the reversible lithium insertion resulting in pulverizing/decrepitating Si from the current collector. Another issue plaguing silicon anode has been its low rate capability and associated polarization due to loss of contact with current collector surface and hence sluggish electron kinetics upon cycling. Hence recent research efforts have focused on addressing these drawbacks by

developing nanostructured morphologies for the Si anode to accommodate volume expansion and also explore better adhesion of Si to the current collector[68-73].

Nanostructured morphologies for silicon have been fabricated and half cell Li ion battery measurements have indicated some improvement over the bulk Si electrodes. Recent interest has been generated by the nanowire morphology due to its resistance to severe structural fracture/deformation upon cycling[57,61]. Nanosized silicon particle composites with polymer binder additives have received considerable attention to mitigate electrode decripitation from the current collector[57,58]. But the use of composites (polymer based composites) could increase complexity of electrode processing and reduce both – volumetric and gravimetric energy density. But, binder free nanostructured Si electrodes are susceptible to decripitation from current collector upon cycling and hence show limited cycle life. Many of research efforts involving thin film Si electrodes have been conducted to improve cycle life and Si electrode adhesion to current collector substrate. The Si films were deposited using chemical vapor deposition (CVD) or Physical vapor deposition (PVD) techniques with typical silicon film thickness ≤500 nm on various textured current collectors[68-71]. Although good cycle performance and rate capability were reported for the Si thin films, these films have low Si loading per unit area and hence the capacity per unit area is relatively low. There is a lot of interest in studying thicker Si films (> 500 nm) to increase the capacity of the Si electrode and maintain good cycle life.

In this chapter, we demonstrate the ability to fabricate scalable 3-D tubular nickel current collectors with variable pore dimension and thickness suitable for silicon electrode deposition. We fabricate two types of porous tubular nickel, type 1 and type 2, and their respective pore dimensions and thicknesses are shown in Table 3-1.

Conformal amorphous silicon films of different mass loadings have been coated using Plasma enhanced CVD technique onto the tubular nickel substrates (3D (Si,Ni)) and tested in Lithium half cells. The binder free 3D (Si,Ni) electrode is shown to have improved capacity per unit area and cyclic stability.

Type	Substrate Area (cm^2)	Average Film thickness (μm)	Average pore diameter (μm)	Typical number of pores/ μm^2
1(a)	4	1.5	0.15	50
1(b)	25	1.5	0.15	50
2	25	3	1-5	0.3

Table 4-1: Porous nickel characteristics

4.2. Experimental Details

4.2.1. Fabrication of porous type 1 and 2 nickel films

The Ni-Cu films were deposited by electrochemical method on surface roughened stainless steel (SS) foils (Type 304, 0.1 mm thick - Alfa Aesar). The stainless steel foil was polished with fine sand paper and cleaned thoroughly with deionized water before electrodeposition. The electrodepositions were carried out in a three electrode cell consisting of a Pt wire/gauge (CH Instruments) or stainless steel foil (Alfa Aesar) counter electrode, Ag/AgCl reference electrode (CH Instruments) and the stainless steel foil as working electrode using a potentiostat/galvanostat (NADA scientific). For type 1 porous nickel film SS foils of area 4 and 25 cm^2 was chosen. The counter electrode area was matched with the working electrode area to ensure uniform current distribution. Electrochemical bath consisted of 5 mL or 200 mL aqueous solution of $NiSO_4$ (1M),

$CuSO_4$ (0.05M), H_3BO_3 (0.5M) for the type 1a or type 1b porous nickel film respectively. Electrochemical deposition was conducted under potentiostatic (type 1a) or galvanostatic (type 1b) conditions of -1.1 V w.r.t Ag/AgCl reference and -4 mA/cm^2 respectively. Deposition was conducted at room temperature and at a pH of 4.1. For type 2 porous nickel film SS foils of area 25 cm^2 was chosen. The counter electrode area was matched with the working electrode area to ensure uniform current distribution. Electrochemical bath consisted of 200 mL aqueous solution of $NiSO_4$. $6H_2O$ (184 g/L), $CuSO_4.5H_2O$ (6.24 g/L), citric acid monohydrate (62.2 g/L), sodium dodecyl sulfate (0.2 g/L), saccharin (0.5 g/L) for type 2 nickel. Electrochemical deposition was conducted under galvanostatic conditions of -10 to -20 mA/cm^2 at room temperature and pH of 4.5 with magnetic stirring (200 rpm).

After the electrochemical deposition, the stainless steel foil supported Ni-Cu film was removed from the cell and cleaned with large amounts of de-ionized water followed by 80 °C drying in vacuum for 4 hours. The Ni-Cu film was then treated with copper etchant (Transene Company) for 6 hours to remove the copper component from the film. After etching the copper, the nanoporous nickel film was washed with copious amounts of de-ionized water to remove contaminants within the pores and dried at 120 °C in vacuum for 24 hrs. The mass of the electro-deposited Cu-Ni on SS before and after selective Cu etching was measured using a micro-balance (Mettler Toledo). The average thickness of the films was measured using a digital micrometer. To determine complete Cu removal after etching of nano-porous Ni on SS, powder X-ray diffraction studies was carried out (Rigaku bench top powder X-ray diffractometer with Cu Kα radiation).

4.2.2. Fabrication and structural characterization of 3D(Si,Ni) electrode.

The Si deposition process was carried out using a thermal chemical vapor deposition process (Applied Material – LPCVD) which has a capability of remotely cracking Si precursor. Silane precursor was used to deposit Si thin films. To achieve conformal Si coating on nano-porous Ni tubes and to increase the Si loading, experimental parameters such as carrier/reacting gas mixture flow, substrate temperature and chamber pressure and deposition time was varied. Here onwards we refer Si coated on nano-porous tubular Ni as 3D (Si,Ni) electrode. The surface morphology of the nano-structured tubular Ni before and after the Si deposition was performed using a scanning electron microscope (FEI, Environmental SEM).

4.2.3. Electrochemical characterization of 3D(Si,Ni) electrode.

All galvanostatic charge/discharge measurements were conducted using an Arbin battery analyzer. The electrochemical measurements of the 3D (Si,Ni) were performed in a CR2032 coin cell (Pred Materials). Li metal foil used as a counter/reference electrode and 1M solution of $LiPF_6$ in 3:7 (v/v) mixture of ethylene carbonate (EC) and diethyl carbonate (DEC) with vinylene carbonate (2%) additive as an electrolyte. Celgard 2500 polyethylene-polypropylene separator was used in this study. The cell charge/discharge was performed between 1.5 V and 0.05 V vs Li/Li^+ at different current rates. Here the discharge means going negative in potential (V) w.r.to open circuit potential (OCV) to 0.05 V before next charging step to 1.5 V. Coin cells fabricated with Li metal as anode in this study referred as coin half cells.

4.3. Results and Discussion

4.3.1 Current collector fabrication: Type 1 and Type 2 porous nickel

In this section we will discuss the fabrication of the 3-D porous current collector followed by the deposition of conformal Si electrode within the pores. Type 1 and 2 porous nickel was fabricated using a method involving the co-deposition of Ni-Cu and followed by the etching of the copper to form porous nickel structure (Figure 4-1).

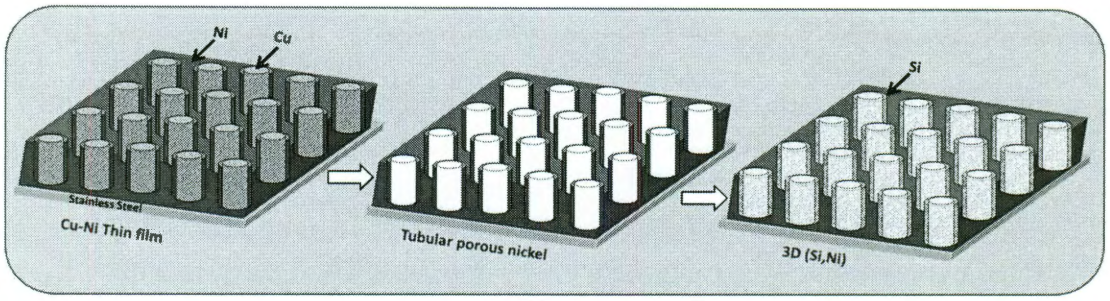

Figure 4-1: Schematic illustration of fabrication of 3D(Si,Ni) electrode. Deposition of Cu-Ni film by three electrode electrochemical deposition onto stainless steel substrate, followed by selective etching of copper component and deposition of active silicon electrode onto the porous nickel films by low pressure chemical vapor deposition.

The SEM image in Figure 4-2a shows the tubular morphology of the type 1 porous nickel. Pore diameters ranging from 100 to 300 nm are observed over the sample size and the pores are interconnected forming a tubular nickel network. The porous nickel structure implies a core-shell microstructure for the Cu-Ni film as studied in prior research work. Type 1 porous nickel films were ~1-2 μm thick. The SEM image in Figure 4-2b shows the tubular morphology of type 2 nickel, again implying a core-shell microstructure for the corresponding Cu-Ni film. But it can be observed that the pore size of the type 2 porous nickel is larger – 1- 5 μm and film thickness of ~5-6 μm. We were unsuccessful in increasing the thickness of type 1 porous nickel.

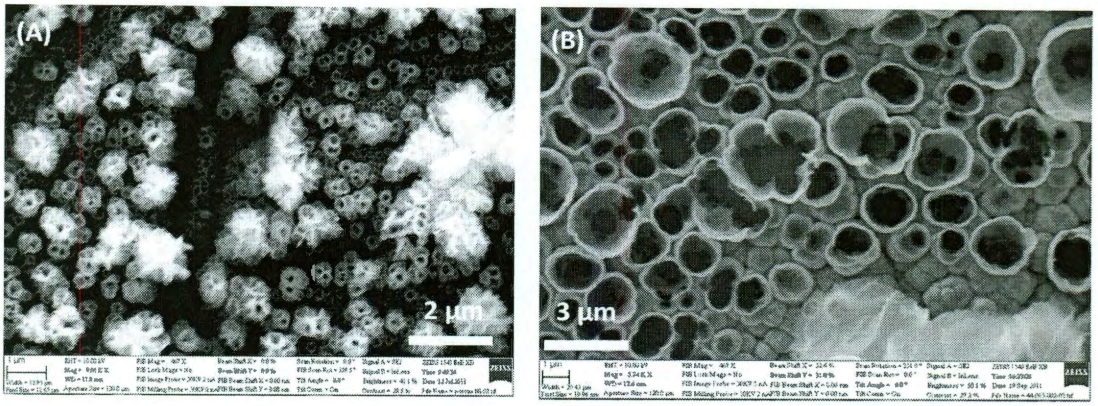

Figure 4-2: SEM image of (A) type 1 and (B) type 2 porous nickel showing interconnected tubular porous network of nickel.

Our experiments showed that on trying to grow thicker Cu-Ni films, only Copper deposition was observed under long deposition time. The enhanced Cu deposition beyond a particular thickness, was attributed to the dendritic Cu-Ni growth (high surface area) coupled with Cu deposition being mass transfer limited compared to Ni, which shows activation controlled growth.[172] On the contrary, for the type 2 porous nickel we were able to obtain thickness of the film ~6 µm. Saccharine was used as a smoothening agent to reduce dendritic Cu-Ni surface[173]. This could further enhance thickness of Cu-Ni film without the enrichment of mass transfer controlled Cu phase. The electrochemical bath was also stirred at 200 rpm to ensure uniform distribution of ions at the surface of the working electrode (stainless steel foil). This also resulted in larger Cu phases hence increasing the average pore size of the type 2 porous nickel.

Qualitative peel tests were conducted (using 3M Scotch tape) on the type 1 and 2 porous Ni substrate to ensure that the adhesion between the stainless steel substrate and the Ni film was strong. It was found that less than 1 % of the nickel mass was removed from the peel test and hence the Ni film was proved to have good adhesion

properties. To demonstrate scalability of the process we have also deposited large area (25 cm^2) type 1 and 2 porous nickel films onto stainless steel substrates using the same electrolyte under galvanostatic conditions.

4.3.2. Electrode fabrication: Type 1 and Type 2 3D(Si,Ni)

Amorphous silicon electrode is deposited onto the porous nickel substrates (type 1 and 2) using low pressure chemical vapor deposition method. The typical deposition rate for Si was around 350 Å per minute. Silane precursor is cracked thermally around a hot filament and the substrate is maintained at room temperature. This ensures no oxidation of the nickel substrate and results in conformal deposition of amorphous silicon within the pores of the nickel current collector. Figure 4-3a and b shows the typical SEM images of type 1 and type 2 3D(Si,Ni). From the images it is clear that the Si is coated within the pores of the nickel current collector being well adhered to the substrate. Silicon mass loading was varied to obtain different thicknesses of the amorphous silicon within the pores of nickel and corresponding SEM images will be shown with the respective electrochemical performance data in the next section.

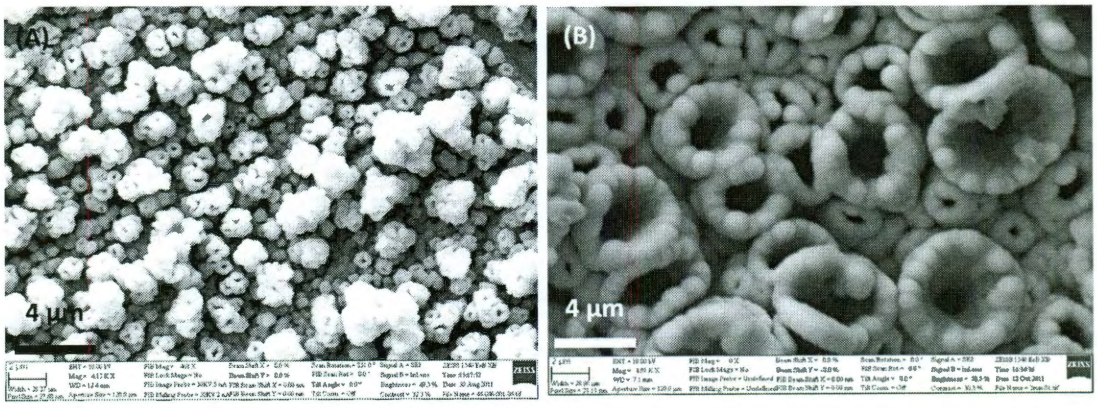

Figure 4-3: SEM images of (a) type 1 and (b) type 2 3D(Si,Ni).

4.3.3. Electrode performance – Type 1 3D(Si,Ni)

To study the performance of silicon electrode on the porous nickel current collector for Li ion battery applications, we deposited Silicon of different mass loading by a low pressure chemical vapor deposition. Table 2 shows different Si planar equivalent thicknesses (PET) on porous Ni films and their corresponding mass per unit area and theoretical capacity expected. The theoretical capacity calculation in Table 2 was done with $Li_{3.75}Si$ as the fully lithiated composition.

Sample	Si thickness	Si mass	Theoretical Capacity
	(μm)	(mg/cm^2)	($\mu Ah/cm^2$)
Type 1(a) Ni, 40 nm Si	0.04	NA	NA
Type 1(a) Ni, 100 nm Si	0.1	0.02	75
Type 1(a) Ni, 500 nm Si	0.5	0.118	410
Type 1(a) Ni, 1 μm Si	1	0.231	860
Type 1(a) Ni, 2 μm Si	2	0.441	1650
Type 2 Ni, 2 μm Si	2	0.432	1632

Table 3-2: 3D(Si,Ni) film characteristics

Firstly, we deposited very thin films (40 and 100 nm) of amorphous Si onto type 1 porous Ni film. The morphology of the 3D(Si,Ni) electrode was observed using SEM (Figure 4-4).

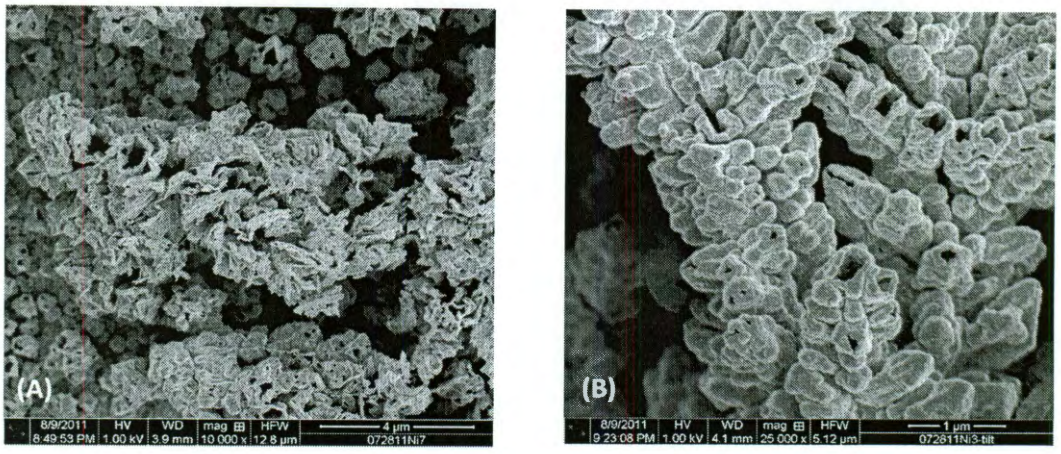

Figure 4-4: SEM images of (A) 40 and (B) 100 nm of amorphous Si onto type 1 porous Ni film

Extended cycling studies were also conducted where the capacity and coulombic efficiency have been plotted as a function of cycle number (Figure 4-5).

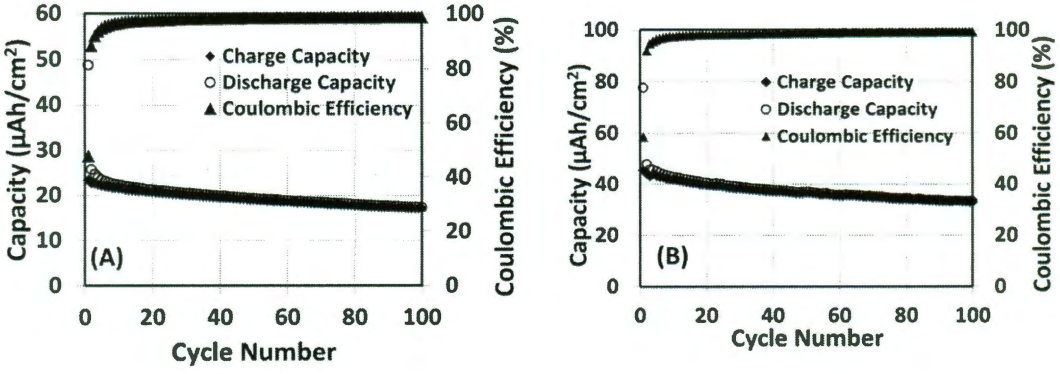

Figure 4-5: Cycling characteristics (capacity and coulombic efficiency plotted as a function of cycle number) of type 1 3D(Si,Ni) for 10 and 40 nm Si PET.

On observation of the cycling data it can be seen that there is a large irreversible loss observed after the first cycle in the discharge capacity as expected. Stable reversible discharge capacities of 30 and 50 $\mu Ah/cm^2$ were observed for the 40 and 100 nm cases respectively. Capacity loss of around 30% was observed in the discharge capacity from the 2^{nd} cycle until the 100^{th} cycle for 40, and 100 nm Si thicknesses. Yet the discharge capacity per unit area observed for the cases of 40 and 100 nm thickness is very low due to the low Si mass loading.

Hence we fabricated 3D(Si,Ni) electrodes with Si PET greater than 500 nm to increase the capacity per unit area. Figure 4-3a shows the SEM image of Si coated type 1 porous nickel with Silicon PET of 700 nm. The 700 nm type 1 3D(Si,Ni) was tested in Lithium half cells for its electrochemical performance. Figure 4-6a and b show the results of galvanostatic charge/discharge measurements conducted at a current rate of 1C (C-rate is defined as the time of discharge for the stable reversible capacity) in CR2032 coin cells.

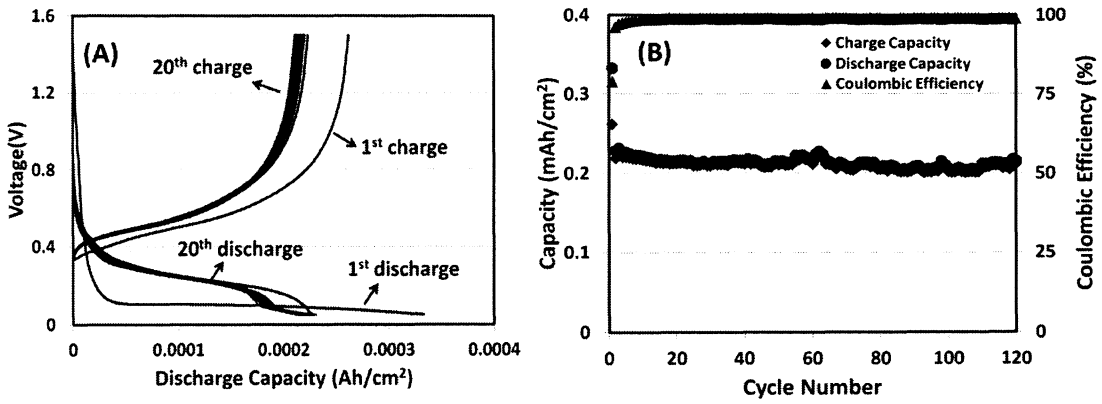

Figure 4-6: Voltage profile and Cycling characteristics (capacity and coulombic efficiency plotted as a function of cycle number) of type 1 3D(Si,Ni) for 700 nm Si PET.

From the voltage profile of the 700 nm 3D(Si,Ni) a flat discharge plateau can be observed for the first discharge whereas the subsequent charge/discharge cycles show sloping charge and discharge profiles.

Hence we can conclude that the 700 nm 3D(Si,Ni) is nanocrystalline and becomes amorphous upon Li insertion and extraction typical of silicon electrodes[1]. Figure 4-6b shows the cycling characteristics of the 700 nm 3D(Si,Ni). A first cycle capacity of 0.36 mAh/cm^2 is observed which is about 85% of the theoretical capacity expected for the corresponding Si loading (We have not employed trickle discharge - constant voltage after constant current at 0.05 V - conditions to obtain full Li insertion ($Li_{3.75}Si$ composition). Hence it can be concluded that excellent electrode utilization was observed even at a relatively high current rate of nearly 1C. An irreversible capacity loss of about ~28% was observed after the first discharge, due to secondary surface reactions, and a capacity loss of only ~5% was observed between the 2nd and 120th cycle. A stable reversible capacity of ~0.22 mAh/cm^2 was observed for the 700 nm 3D(Si,Ni). The stable cycling characteristics could be attributed to improved adhesion of active silicon electrode to nickel current collector upon repeated cycling. The internal pores in the 3D(Si,Ni) architecture help in mitigating the internal stress and subsequent fracture of silicon electrode from the current collector surface. Figure 4-6b also shows Coulombic efficiencies greater than 99 %.

We have also studied the rate capability of the 3D(Si,Ni) electrode films. Figure 4-7a shows the cycling characteristics of 500 nm 3D(Si,Ni) electrode at a current rate of ~0.8C. A stable reversible capacity of 0.18 mAh/cm^2 and coulombic efficiencies greater than 99.2 % was observed after 75 cycles of charge/discharge. Figure 4-7b shows a ragone plot for the 500 nm 3D(Si,Ni) electrode where discharge capacity after 25 cycles

are plotted at different C-rates. From the ragone plot it can be observed that the 3D silicon electrode shows a capacity retention of ~60% of nominal capacity (capacity at C-rate C/10) at a current rate of 1.1C. The 3D structure of the porous nickel allows for improved silicon mass accommodation resulting in thinner layers of Si electrode.

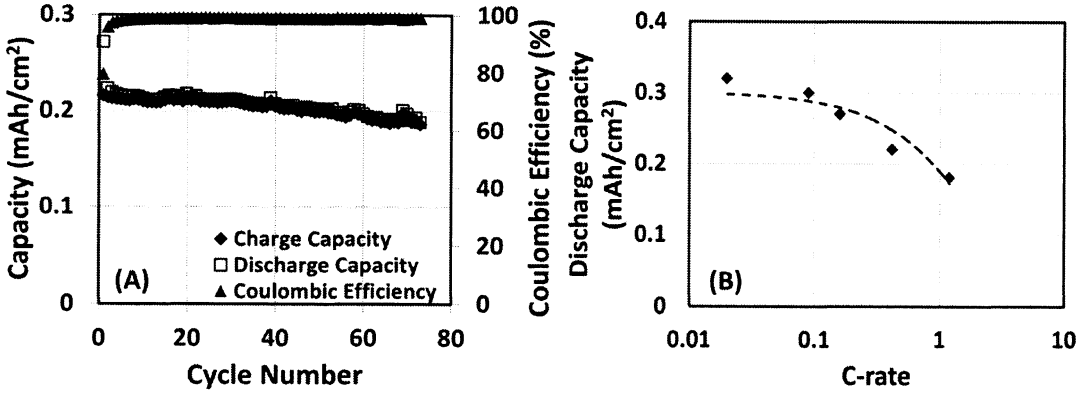

Figure 4-7: Cycling characteristics (capacity and coulombic efficiency plotted as a function of cycle number) and ragone plot of type 1 3D(Si,Ni) for 500 nm Si PET.

Thinner Si electrode layers lead to faster ion transport paths, hence improving charge/discharge capability of the electrode. Excellent adhesion of Si on Ni substrate[29,31] also leads to better electronic pathway also affecting the rate capability of the electrode. To improve the overall capacity of the electrode per unit area we further increased the Si loading per unit area on the porous nickel sample.

Silicon PET of 1 μm and 2 μm were deposited onto the type 1 porous nickel. Figure 4-8 shows the SEM images of 1 and 2 μm 3D(Si,Ni) electrode. For the 1 μm 3D(Si,Ni) we observe conformal coating of silicon with partial filling of pores in the nickel structure. Hence stable cycling characteristics are observed upon galvanostatic charge/discharge measurements. Figure 4-9a shows a stable reversible discharge

capacity of ~0.42 mAh/cm^2 at 0.9C after 70 cycles of charge/discharge, showing a doubling of capacity upon doubling the thickness of silicon (~0.2 mAh/cm^2 for Si PET 500 nm). The 1 μm 3D(Si,Ni) electrode was also cycled at higher current rate of ~2C to study its rate capability.

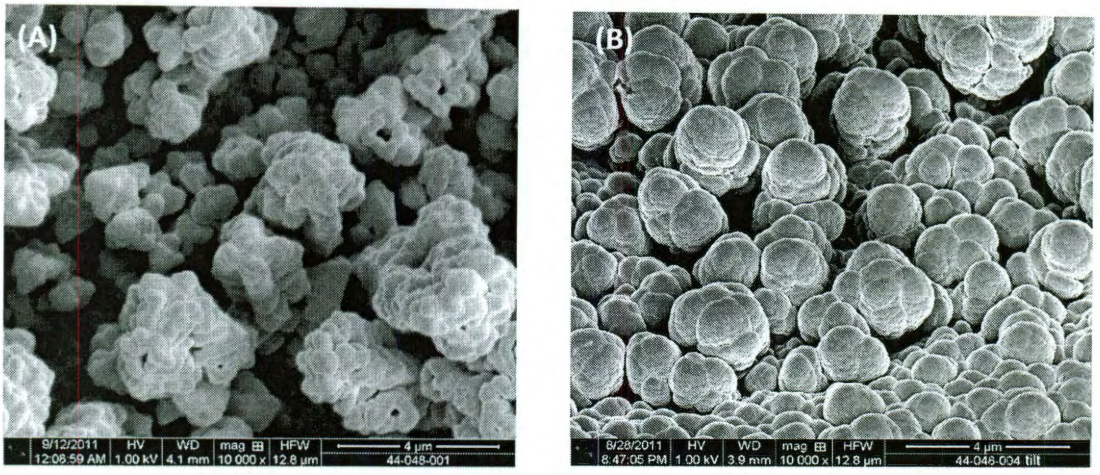

Figure 4-8: SEM images of type 1 3D(Si,Ni) for (a) 1 and (b) 2 μm Si PET.

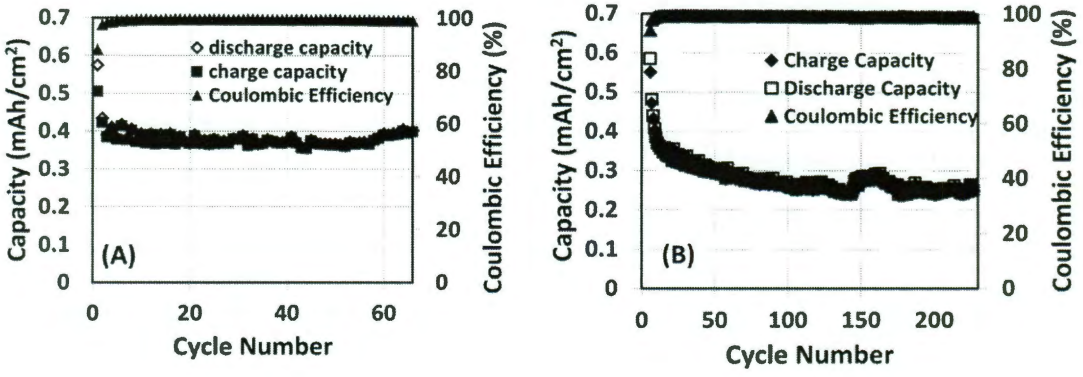

Figure 4-9: Cycling characteristics (capacity and coulombic efficiency plotted as a function of cycle number) of type 1 3D(Si,Ni) for 1 μm Si PET at (a) 1C and (b) 2C C-rate

From Figure 4-9b it can be observed that there is a 30 % capacity loss over the first 10 cycles and a stable reversible capacity of ~0.3 mAh/cm^2 after 200 cycles of charge/discharge. Hence the type 1 porous nickel served as a good current collector substrate for relatively thick (1 μm) PET of silicon. From Figure 4-8 it is clear that there is complete filling of all the pores in the type 1 porous nickel film hence resulting large microsized silicon particle overgrowth. Due to larger particle size galvanostatic charge/discharge measurements were conducted at a very low current rate (C/20) for the 2 μm 3D(Si,Ni). Figure 4-10 shows the cycling characteristics of the 2 μm 3D(Si,Ni). The 2 μm 3D(Si,Ni) shows poor cycling characteristics due to increased internal stress within the microparticles of silicon and resultant decripitation from current collector substrate. Hence it can be concluded that increase of Si PET beyond 1 μm leads to complete filling of pores (type 1 porous nickel) and hence does not increase the capacity per unit area due to severe capacity fade.

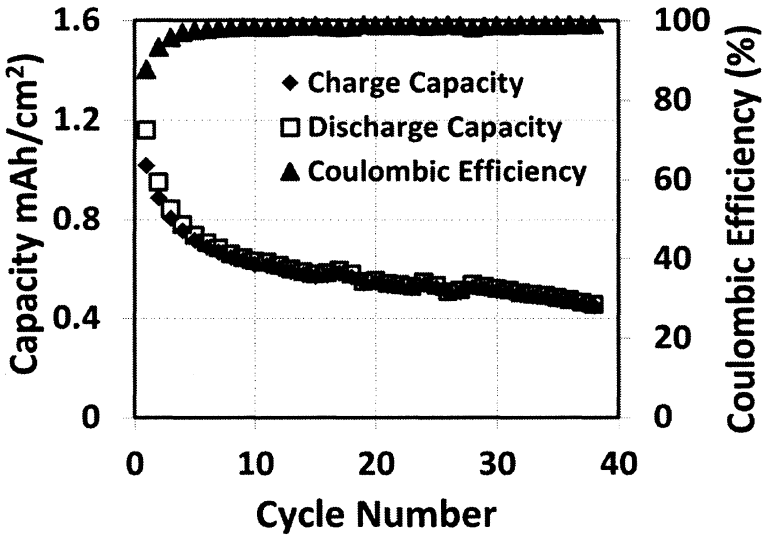

Figure 4-10: Cycling characteristics (capacity and coulombic efficiency plotted as a function of cycle number) of type 1 3D(Si,Ni) for 2 μm Si PET.

4.3.4. Electrode performance – Type 2 3D(Si,Ni)

This section of the chapter discusses the fabrication of type 2 porous nickel with larger pore diameter and film thicknesses to accommodate larger amount of silicon electrode and obtaining thinner silicon electrode films. Figure 4-11 shows the tubular morphology of the pores of type 2 porous nickel film. By engineering pore size and film thickness we have shown effective control over the electrode mass distribution for different electrode loading. The type 2, 2 μm 3D(Si,Ni) was tested for its electrochemical performance in Li half cells. Figure 11 shows the cycling characteristics of the type 2, 2 μm 3D(Si,Ni) at current rate of 0.5C. From the cycling characteristics it can be seen that stable reversible capacity of ~0.8 mAh/cm^2 is observed after 10 cycles of charge/discharge. Hence, by the use of type 2 porous nickel (larger pore diameter and film thickness) an overall increase in capacity per unit area has been accomplished even after increasing PET of Si film upto 2 μm, which was not possible with the type 1 porous nickel. Hence engineering porous Ni current collector substrates could be used as an efficient method to achieve excellent utilization of high capacity Si electrode at relatively high current rates.

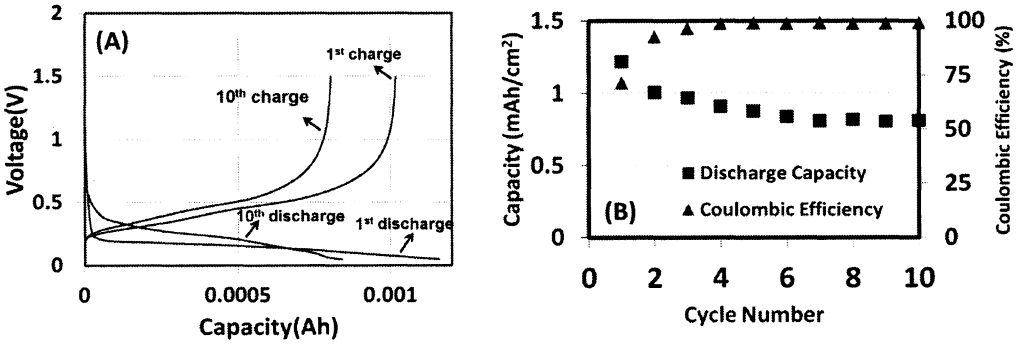

Figure 4-11: Voltage profile and Cycling characteristics (capacity and coulombic efficiency plotted as a function of cycle number) of type 2 3D(Si,Ni) for 2 μm Si (PET).

4.4. Conclusions

Porous nickel current collector was fabricated by selective leaching of Cu from the co-deposited Cu-Ni films on stainless steel substrates. Porous tubular like Ni morphology with average diameter 150 nm and height of 1.5 μm was obtained. With the use of an additive, the Ni pore size and porous Ni film thickness was increased to accommodate increased Si electrode loading. The 3D (Si,Ni) was fabricated by Si deposition on porous Ni by thermal CVD method. The electrochemical performance of the type 2 3D (Si,Ni) under constant current mode (0.5C) gave the high 1st cycle discharge capacity of 1.2 mAh/cm^2 with 70 % capacity retention after 10 cycles. The porous Ni substrates help in excellent electrode utilization for high silicon PET due to reduced internal stresses upon volume expansion an also helps in improving rate capability of Si based negative electrodes due better ionic and electronic diffusion pathways compared to planar counterpart. The electrochemical method based on pore size and film thickness engineering, is scalable and hence has the potential to control the aspect ratio of the pores whereby higher capacity Si based anode can be developed. We believe that the tubular conformal morphology for the Si electrode helps to i) accommodate the large volume changes during Li insertion/extraction and ii) better adhere to the nickel current collector substrate.

Chapter 5: Nanowire energy storage device

5.1. Introduction

The high energy Li ion battery and the high power supercapacitor are regarded as major players in energy storage[14,158,159]. Hybrid electrochemical devices (HED) form an interesting class of reversible energy storage devices which try to combine the good features of both batteries (high energy) and supercapacitors (high power)[158]. Thin planar 2D designs for batteries have dominated the field of microscale energy storage with the successful realization of high power cells[118,131]. Recently 3D designs for batteries have also attracted attention primarily due to their higher energy per footprint area compared to planar designs. Majority of 3D battery configurations have relied on the fabrication of electrode/electrolyte materials on 3D micro-patterned surfaces although a few reports exist which use nanostructured surfaces[149]. The major bottleneck still is the reliable fabrication of conformal electrolyte layers around nanostructured electrode elements[150]. The design and fabrication of a conformal single nanowire structure that embeds all components of an electrochemical storage device is still a dream and if such a structure is accomplished it could result in the ultimate miniaturization of energy storage. In addition, such devices should have advantages over conventional bulk devices due to the close proximity of electrodes between ultrathin electrolyte layers and ultra-short ion diffusion distances between the electrodes. In this chapter we demonstrate the fabrication of such a novel hybrid electrochemical device with all the active components integrated onto single nanowires and test the electrochemical performance of an array of such nanowires.

5.2. Experimental Details

5.2.1. Fabrication of Ni-Sn and polyaniline thin film

A copper foil (Nimrod Hall Copper foil company) of thickness 25 μm was used as the substrate for electrodeposition of the planar Ni-Sn film. An aqueous solution of 0.075M $NiCl_2$, 0.175M $SnCl_2$, 0.5M $K_4P_2O_7$, 0.125M Glycine and 5mL L^{-1} NH_4OH was prepared for the electrodeposition of Ni-Sn thin film. The copper foil was cleaned thoroughly with DI water before electrodeposition. The electrodepositions were carried out in a three electrode cell consisting of a Pt counter electrode, Ag/AgCl reference electrode and the copper foil as working electrode using an AUTOLAB PGSTAT 302N potentiostat/galvanostat. The Ni-Sn thin film was electrodeposited using a galvanostatic method at a current density of 6 mA/cm^2, typically for 5 minutes. After electrodeposition the copper foil was removed from the cell and cleaned with large amounts of DI water followed by drying in vacuum for 4 hours. The cathode was made of PANI (emeraldine base 5k MW, SIGMA ALDRICH), carbon black and PVDF binder in the weight ratio of 85: 10: 5. The slurry was prepared by mixing the above mixture of PANI, carbon black and PVDF in Dimethylformamide thoroughly, followed by casting onto an Aluminium foil (Alfa Aesar, thickness of 0.01 mm). The coated cathode was dried in a vacuum oven at 80°C for 24 hours.

5.2.2. Fabrication of nanowire hybrid electrochemical device

Alumina templates (ANODISC 13) were purchased from WHATMAN which had an average pore diameter of around 200 nm. A thin (100 nm) copper layer was sputtered onto the branched side of the alumina template which served as the electrical contact for the electrodeposition of nanowires. Ni-Sn nanorods of ~500 nm length were grown within the alumina templates using the same electrolyte solution as used for the Ni-Sn

thin film growth on the copper foil current collector. The Ni-Sn nanowires were electrodeposited using a galvanostatic method at a current density of 6 mA/cm^2, typically for 3 minutes. The pores of the alumina templates were widened chemically using 3M NaOH for 2 minutes. A 1 wt % polyethylene oxide (100k Molecular weight, SIGMA ALDRICH) solution in methylene chloride was used to wet the walls of the widened alumina template. The solution was dropped onto the surface of the template and the extra liquid was wiped of using soft tissue paper. A solution of Polyaniline (emeraldine base 5k MW, SIGMA ALDRICH), PVDF and carbon black (2: 0.1: 0.05 wt %) was made in dimethyl formamide solvent and was used to fabricate the cathode within the pores of the alumina template. The polyaniline solution was dropped onto the surface of the template, allowed to infiltrate for an hour and then the solution was vacuum dried. This left a thin polyaniline layer on the surface of the alumina template for electrical contact. A 200 nm thick Al current collector layer was sputter coated onto the PANI electrode layer. The alumina template was soaked in 1 M solution of $LiPF_6$ in 1:1 (v/v) mixture of ethylene carbonate (EC) and dimethyl carbonate (PC) for 1 h for impregnation of ions into the polymer (PEO) matrix. The excess liquid was wiped off from the surface of the template.

5.2.3. Electrochemical Measurements

All galvanostatic charge/discharge measurements were conducted using an ARBIN BT 2000 Battery Analyzer. The electrochemical measurements of the Ni-Sn thin film were performed in a Swagelok-type cell using Ni-Sn thin film as the working electrode, Li metal foil as a counter/reference electrode and 1M solution of $LiPF_6$ in 1:1 (v/v) mixture of ethylene carbonate (EC) and dimethyl carbonate (DMC) as an electrolyte. A glass microfiber filter was used as the separator. The cells were charged

and discharged between 1.5 V and 0.02 V vs Li/Li^+ at current rates 0.2, 0.3 and 0.4 mA/cm^2. The electrochemical measurements for the hybrid device was conducted again in the Swagelok-type cell using Ni-Sn thin film as the anode and PANI:PVDF:C (85:10:5, wt%) film as the cathode and celgard separator soaked in 1M solution of $LiPF_6$ in 1:1 (v/v) mixture of ethylene carbonate (EC) and dimethyl carbonate (DMC) as an electrolyte. The cells were charged and discharged between 1.5 and 3.4 V at current rates 0.2, 0.3 and 0.4 mA/cm^2. The electrochemical measurements for the nanowire design was conducted in a Swagelok-type cell in which the copper back coated side of the template served as the counter and reference electrode and the Al coated side of the alumina template served as the working electrode. Before the alumina template, which encased the nanowire electrochemical devices, was loaded into the Swagelok cell we wetted the template in the liquid electrolyte ($LiPF_6$ in 1:1 (v/v) mixture of ethylene carbonate (EC) and dimethyl carbonate (DMC)) to activate the PEO separator. The cells were charged and discharged between 0.02 and 3.4 V at current rates 0.03 mA/cm^2, 0.05 mA/cm^2, 0.07 mA/cm^2.

5.3. Results and Discussion

5.3.1. Thin film hybrid PANI/NiSn electrochemical device

Early work on HEDs, reported by Scrosati and co-workers, described the Polyaniline/Carbon dion battery. More recent research in the field of HEDs (which combine battery and the electrochemical double layer capacitor electrodes) has focused on using lithium titanate (LTO) anodes and activated carbon cathodes[158, 159]. Nanosized LTO, has been used as the anode based on its good cyclic stability and rate capability. But due to the low specific capacity of LTO (160 mAh/g) and high Li insertion voltage (1.5 vs Li/Li^+) there are limitations on the energy density that can be achieved. Also the

high temperature synthesis for LTO makes it an expensive fabrication process. Metallic/Intermetallic based anode materials such as Sn, Ni-Sn, Cu-Sn, Cu-Sb have been shown to have very high specific capacity and good cyclic stability[120]. The room temperature electrodeposition fabrication process for Ni-Sn makes it an attractive candidate for building thin film devices. Polyaniline on the other hand, is well known for its pseudocapacitive behavior due to the numerous oxidation states it can exist in by doping/undoping processes[173]. Polyaniline can also be synthesized easily by a variety of chemical and electrochemical polymerization techniques[173]. Hence we chose Ni-Sn and polyaniline as the electrodes for our thin film energy storage device. Ni-Sn was fabricated by electrochemical deposition directly onto a copper current collector substrate and characterized by X-ray diffraction (Figure 1) and the polyaniline electrode was drop coated onto Al current collector.

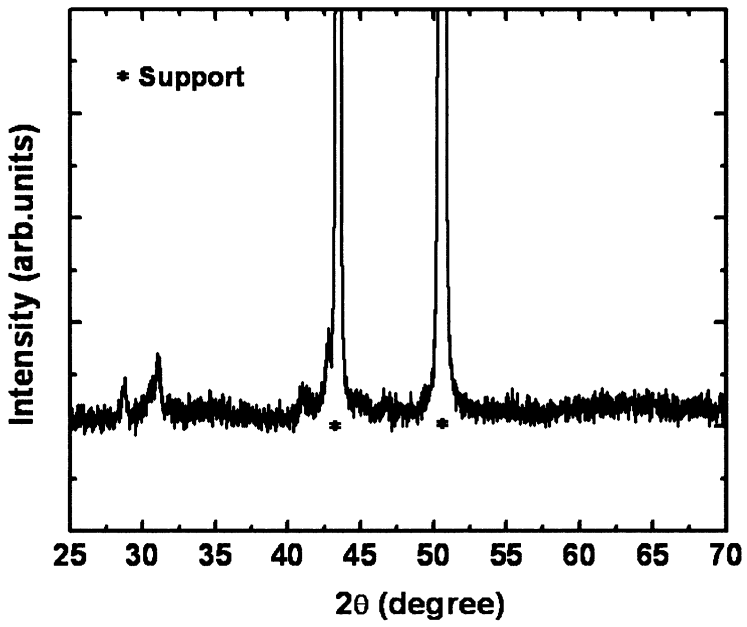

Figure 5-1: X-ray diffraction pattern of Ni-Sn thin film electrodeposited on Cu foil

The total device area was ~ 0.5 cm^2. The voltage vs time and cycling characteristics for the Ni-Sn thin films against Li foil showed the typical Li insertion/de-insertion behavior and initial and reversible capacity of ~ 800 mAh/g and 350 mAh/g respectively at current rate ~0.2 mA/cm^2 (Figure 5-2). Polyaniline is known to show a reversible capacity of around ~30mAh/g with an initial capacity of ~60 mAh/g for the redox doping/undoping process. Based on the initial specific capacities observed for the two electrodes we constructed a full cell consisting of Ni-Sn anode and polyaniline cathode with a cathode to anode mass ratio typically around ~14, hence taking into consideration the irreversible losses of the electrodes.

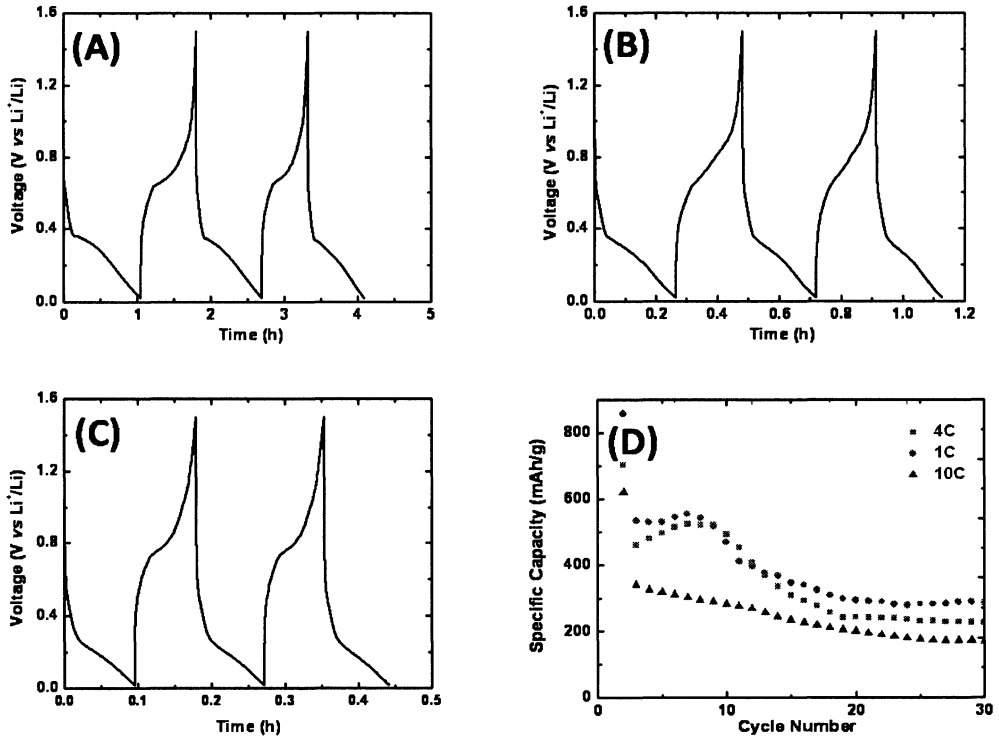

Figure 5-2: A. 0.2 mA/cm^2, **B.** 0.3 mA/cm^2 and **C.** 0.4 mA/cm^2, **D.** Specific Discharge capacity vs cycle number plot for Ni-Sn vs Li foil at current rates "●" 1C, "■" 4C and "▲" 10C

Galvanostatic charge/discharge experiments were conducted on the Ni-Sn/PANI full cell between 1.5 and 3.4 V at a current rate of ~0.2 mA/cm^2 and the voltage vs. time curves were recorded (Figure 5-3A). The cells were cycled for ~ 25 cycles and a stable reversible capacity of ~100 μAh/cm^2 was obtained at coulombic efficiencies of ~90%

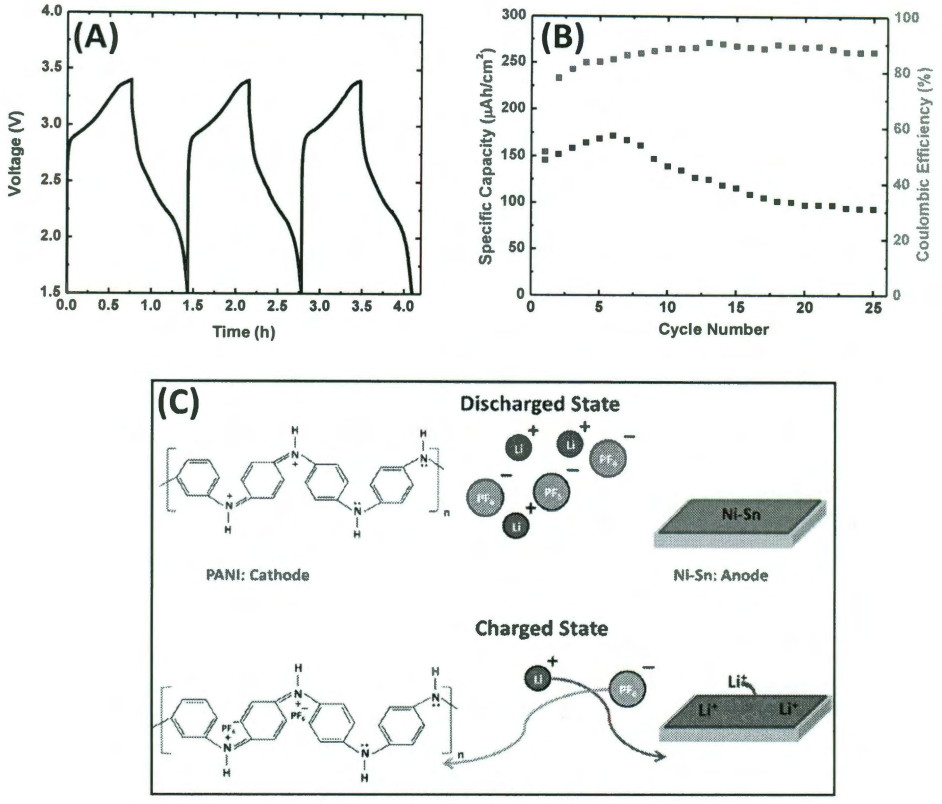

Figure 5-3. (a) Voltage vs time curves of the thin film hybrid electrochemical device using polymer gel electrolyte (PEO soaked in solution of 1M $LiPF_6$ in EC:DMC (1:1 by volume)) cycled at current rate ~0.2 mA/cm^2. (b) Galvanostatic charge/discharge measurements conducted at current rate of ~0.2 mA/cm^2 for 25 cycles showing a reversible capacity of ~100 μAh/cm^2 at a coulombic efficiency of ~90% (c) Schematic diagram of the mechanism of the energy storage device operation showing Li ion insertion/deinsertion at the Ni-Sn anode and PF_6^- ion doping/undoping at the PANI cathode during charge and discharge processes

(Figure 5-3B). To confirm the electrochemistry of this novel energy storage device we conducted ex-situ XPS analysis after the first charge process for both electrodes (Figure 5-4 and 5). Li 1s, Ni 2p and Sn 3d peaks appear in the Ni-Sn electrode material after the first charge process. Consequently C 1s, N 1s, Cl 2p and O 2p peaks are seen in the PANI electrode material after the first charge process. From these observations we confirm that the Li ion insertion takes place into the Ni-Sn electrode through electrochemical alloying mechanism during the charge process and simultaneously the PF_6^- ions doped into the polyaniline electrode. During discharge process we expect Li ion de-insertion and PF_6^- ion undoping from Ni-Sn and PANI electrodes respectively back into the electrolyte (Figure 5-3C).

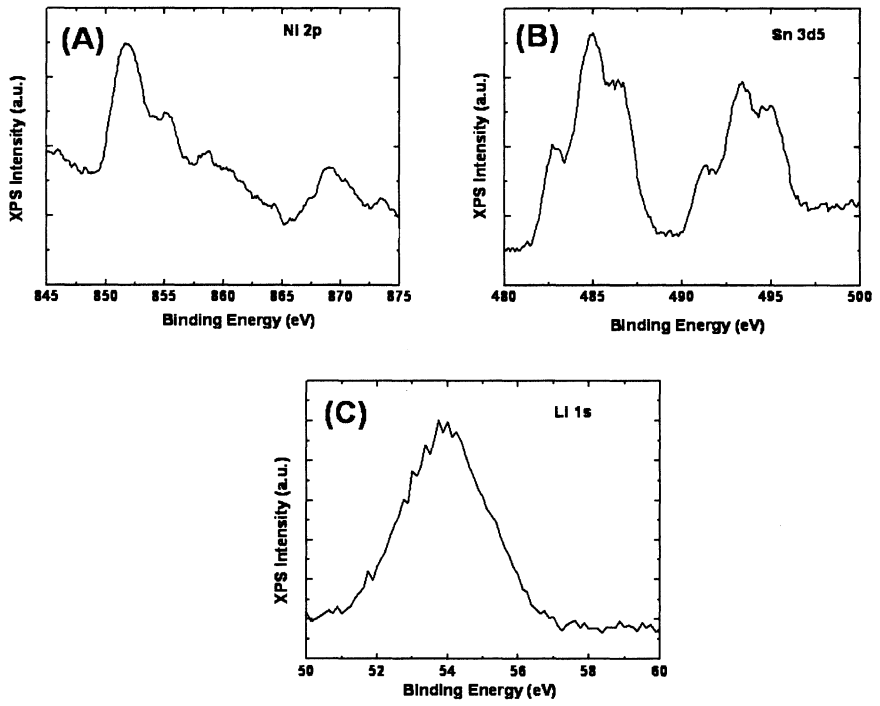

Figure 5-4. X-ray photoelectron spectroscopy data for Ni-Sn thin film after first charge process showing **A.** Ni 2p, **B.** Sn 3d and **C.** Li 1s peaks.

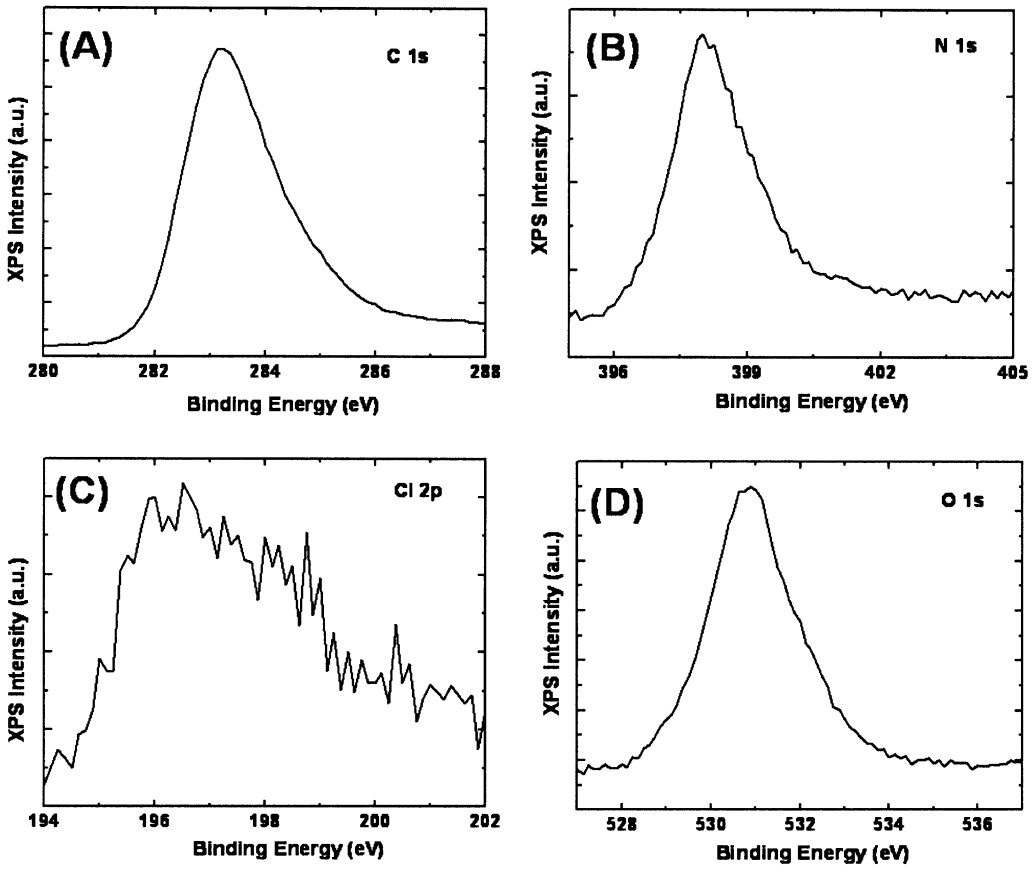

Figure 5-5. X-ray photoelectron spectroscopy data for PANI thin film after first charge process showing, **A.** C 1s, **B.** N 1s, **C.** Cl 2p and **D.** O 1s peaks.

The electrochemical cells were fabricated and tested as shown in the schematic in Figure 5-6A where the thin film Ni-Sn anode and PANI cathode were stacked on each other separated by a Celgard separator soaked in $LiPF_6$ based electrolyte. Galvanostatic charge/discharge tests were conducted at rates ~0.2, 0.3 and 0.4 mA/cm^2 and reversible capacities of ~100 μAh/cm^2, 75 μAh/cm^2 and 56 μAh/cm^2 were obtained after ~ 20 cycles of charge/discharge (Figure 5-6B).

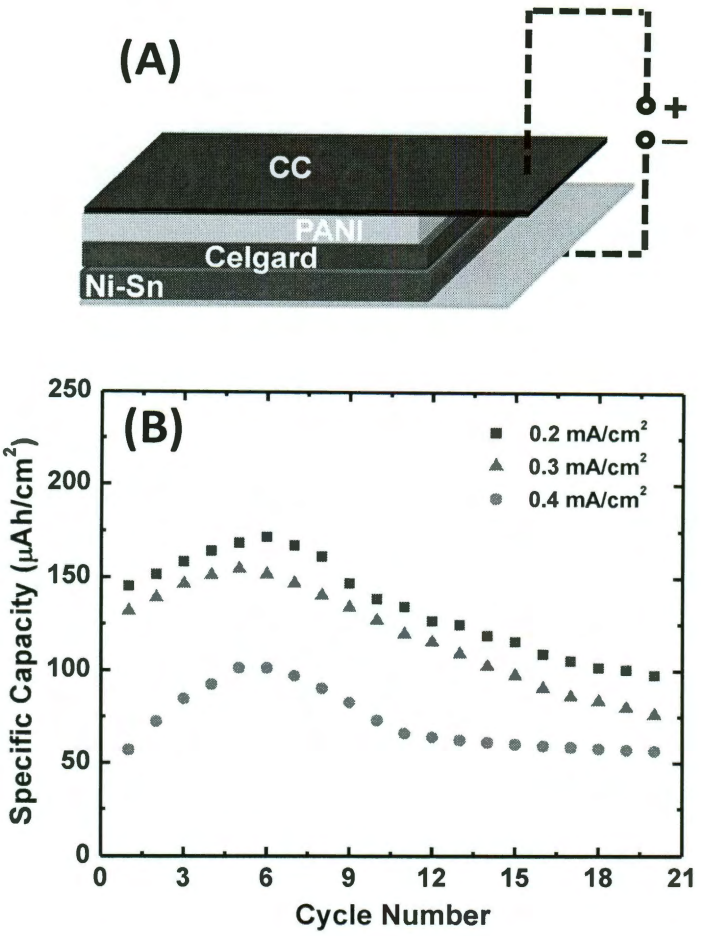

Figure 5-6. (a) Schematic representation of thin film device showing anode - Ni-Sn and cathode - PANI separated by a thin celgard film. (b) Discharge capacity vs cycle number plots for galvanostatic charge/discharge conducted on thin film Ni-Sn/PANI device at current rates 0.2 mA/cm^2, 0.3 mA/cm^2, 0.4 mA/cm^2 for 20 cycles.

Voltage vs time plots for the galvanostatic tests conducted at current rates 0.3 and 0.4 mA/cm^2 are shown in Figure 5-7. From the charge/discharge curves at different rates we can infer that the device shows good rate capability upon cycling at different current rates. We were able to obtain fast current rates of operation for our hybrid device due to the pseudocapactive (fast redox reaction) nature of our cathode material hence

delivering high capacity per unit area at high power. At the PANI cathode of our hybrid devices, PF_6^- ion intercalation takes place which is based on a fast doping/undoping process. Also the increase in the specific capacity of the anode and the lower Li insertion potential hence could improve the energy density of the device. It is also noteworthy to mention that our device is based on a room temperature fabricated, Li free, polymer cathode (PANI) which makes the device a very cost effective. It is important to note that we are able to achieve good rate capability with a thick celgard separator (~20μm thick). The fabrication of our hybrid devices using nanostructured electrodes and ultrathin separators could result in improved rate capabilities suitable for ultrahigh power applications.

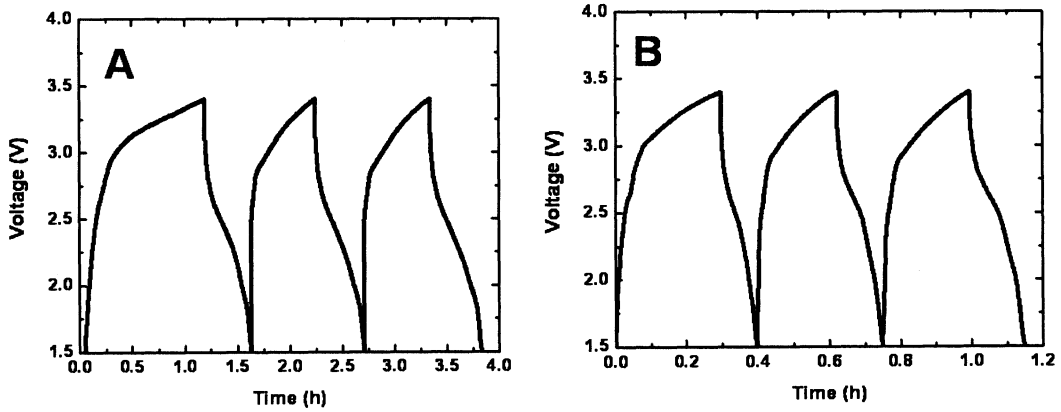

Figure 5-7. Voltage vs time plots for thin film hybrid device at current rates **A.** 0.3 mA/cm^2 and **B.** 0.4 mA/cm^2

5.3.2. Nanowire energy storage device

The electrodes we have chosen (Ni-Sn and PANI) can be easily synthesized at room temperature using simple, scalable techniques such as electrodeposition and drop coating, hence making it ideal for fabricating nanostructured microscale energy storage

devices. We utilize an anodic alumina membrane as the template for the fabrication of the nanowire hybrid energy storage. By a combination of electrodeposition of Ni-Sn, chemical widening of the pores of the anodic alumina and drop coating of separator (polyethylene oxide - PEO) and cathode (polyaniline) layers, we are able to fabricate a full electrochemical device on individual nanowires (Figure 8A). Transmission electron microscopy is used to characterize the interfaces between electrode and electrolyte layers. Figure 8B, C, D clearly depicts the conformal electrode/electrolyte configuration for both the cathode and anode. The anode (Ni-Sn) is coated with a thin electrolyte (PEO) layer as shown in Figure 8B and the cathode (PANI) is also coated with a thin layer of electrolyte (PEO) as shown in Figure 8D.

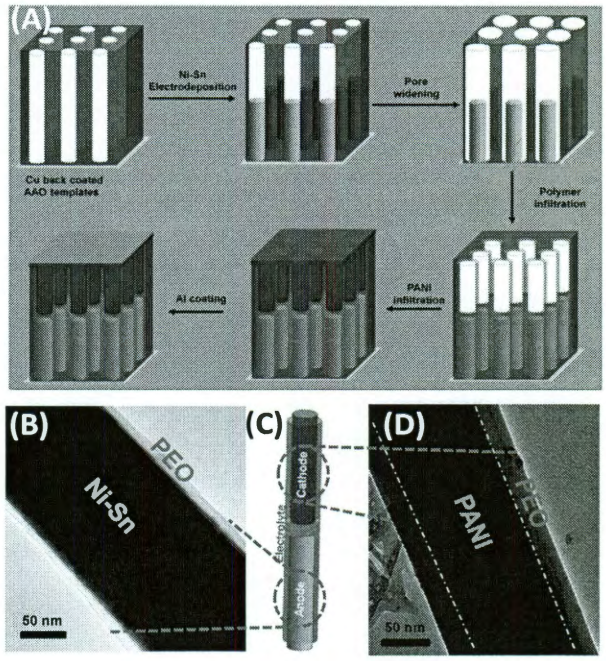

Figure 5-8. (a) Schematic representation of the fabrication process for the nanowire energy storage device. (b) TEM image of the anode/electrolyte core/shell nanowires. (c) Schematic representation of the nanowire energy storage device. (d) Transmission electron microscope (TEM) image of the cathode/electrolyte core/shell nanowires.

The anode and the cathode are separated by a ~20 nm layer of PEO electrolyte (Figure 5-9). A schematic of the final nanowire structure for the hybrid energy storage device is shown in Figure 8C. The conformal wrapping of the PEO layer around both cathode and anode of the device ensures radial ion diffusion and excellent ion accessibility to the electrodes. The ability to coat thin conformal layers of electrolyte around electrodes with different lengths allows control of the capacity per unit area of the device.

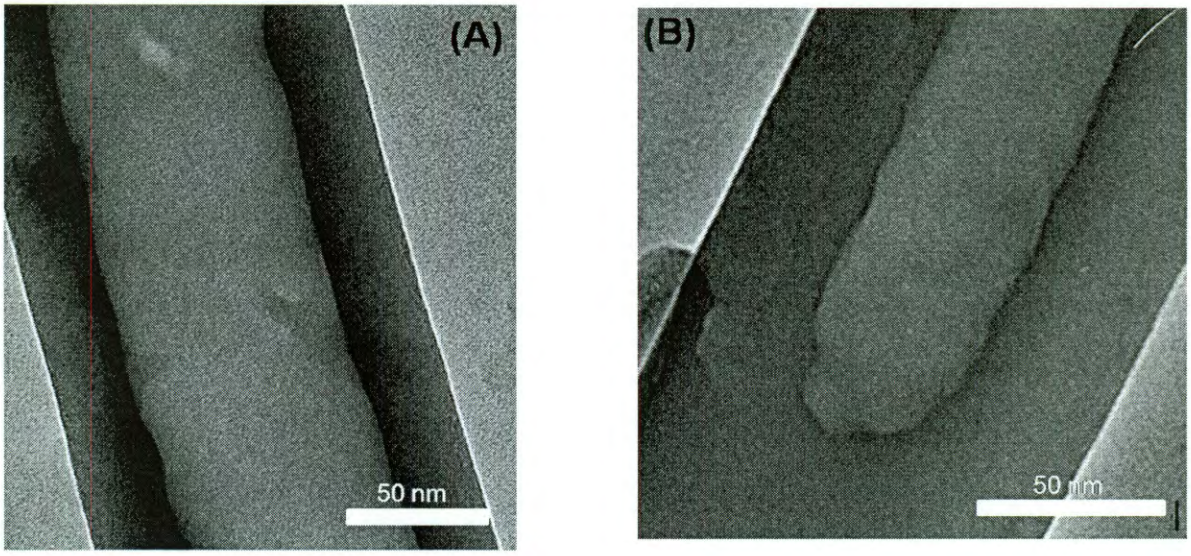

Figure 5-9: A. Transmission electron microscopy image showing the empty PEO nanotube structure before filling of the PANI cathode. **B** Transmission electron microscopy image showing the thickness (~30 nm) of the PEO nanotube interface with Ni-Sn nanowire before filling of the PANI cathode.

Vertically aligned arrays of the nanowire devices were tested for their electrochemical performance. The mass of the electrodes in the cell is determined by the thickness of the alumina template (the length of the nanowires) used hence defining the capacity delivered by the device. We have used 60 μm thick anodic alumina templates

for this study and due to vast density difference between Ni-Sn and polyaniline we had to grow short nanorods (~500 nm in length) of Ni-Sn and fill the rest of the template with polyaniline cathode to ensure close to optimum cathode to anode mass ratio. The total device area was measured to be ~ 0.4 cm^2. The voltage vs time plot for the galvanostatic measurement at current rate 0.03 mA/cm^2 between 0.02 and 3.4 V depicts the Li ion electrochemistry and is shown in Figure 5-10A. It is interesting to observe that the discharge behavior in the nanostructured device is slightly different from the thin film device. It is observed in Figure 5-10A that there exists voltage drops at higher voltage ranges and most of the discharge capacity is observed below 2V unlike the case of the thin film design. This could be attributed to the inherent self discharge phenomena associated with the nanostructured device due to the ultrathin nature of the separator used. As it has been suggested by Rolison *et al.*[149], self discharge is a serious hurdle in batteries with ultrathin separators due to the leakage current associated with such devices. To help hold the charge better the use of polymer separators with minute electronic conductivity and optimal thickness is critical. Rate capability of the nanowire based hybrid device was studied by conducting the galvanostatic measurements at different current rates. Cycling characteristics at the current rates 0.03, 0.05 and 0.07 mA/cm^2 are shown in Figure 5-10B. Stable reversible capacities of ~ 3, 1.5 and 1 $\mu Ah/cm^2$ have been achieved at current rates 0.03, 0.05 and 0.07 mA/cm^2 respectively upto 30 cycles of charge/discharge. Coulumbic efficiencies of ~65 % have been obtained for these nanowire based hybrid energy storage devices. This could be attributed to the ultrathin (~20 nm) nature of the separator used which could thereby lead to potential drops due to self discharge phenomenon[149]. An optimized thickness for the separator layer between the two electrodes could help in achieving higher columbic

efficiencies. The discharge capacity per unit area of the nanowire device is smaller compared to the thin film data, due to the smaller thickness of electrodes used and the

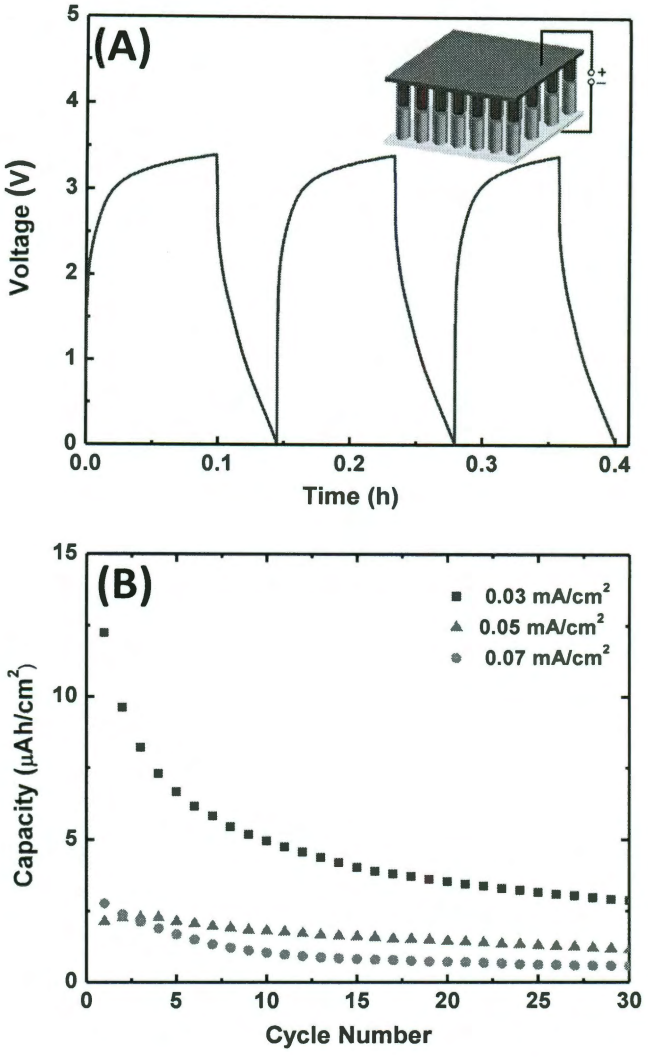

Figure 5-10: (a) Voltage vs time graphs for the galvanostatic measurements conducted on the conformal nanowire energy storage device. *Inset*: Schematic representation of vertically aligned array of the nanowire hybrid device. (b) Discharge capacity vs cycle number plot showing reversible capacities at three different current rates (0.03 mA/cm^2, 0.05 mA/cm^2, 0.07 mA/cm^2) upto 30 cycles.

reduced coloumbic efficiency. By increasing electrode lengths (using alumina templates of different thicknesses) of cathode and anode it could be possible to improve capacity per unit area of the device. The nanostrucured design exhibits short Li ion diffusion distance, i) within the Ni-Sn electrode due to conformal wrapping of the PEO electrolyte and ii) between the two electrodes due to the ultrathin separator (~20 nm PEO) layer. This allows for fast Li ion diffusion within the battery (Ni-Sn) electrode and within the electrolyte layer between the anode and cathode resulting in fast charge/discharge capability and with optimized separator thickness the electrochemical performance of the nanowire device could be further enhanced.

5.4. Conclusions

In conclusion, we have fabricated a new hybrid energy storage device on a single nanowire and tested a parallel array of such functional nanowire devices for their electrochemical performance. The nanowire design for the Ni-Sn/PANI system was fabricated using a conformal electrode/electrolyte configuration and had an ultrathin, ~20 nm, separator (PEO) between the electrodes to improve rate capability characteristics. The hybrid nanowire device built using Li free electrodes showed good charge/discharge characteristics with a discharge capacity of 3 $\mu Ah/cm^2$ at a current rate of 0.03 mA/cm^2. Such nanowire energy storage devices could be useful in better understanding Li ion electrochemistry at the nanoscale and to power nano-electronic devices.

Chapter 6: Summary

The development of Lithium ion batteries is critical to satisfy the ever increasing demand for mobile electronics and the recent emergence of electric vehicle technology. The need for higher energy and higher power batteries is tremendous. Two general approaches, namely i) new materials chemistry, and ii) new engineering design can be employed to address performance issues that face the current battery technology. This thesis focusses on the development of the three dimensional nanostructured design for Lithium ion battery. We have engineered materials at the nanoscale to develop 3D designs for current collectors, electrodes and electrolyte of Li ion batteries.

Designing nanostructured electrolytes to separate electrodes of Li ion batteries could have profound effect on the rate capability and cycle life of the batteries. But the task of designing ultrathin solid state electrolyte layers is quite challenging. One aspect of this thesis presents a new and economical process to develop such ultrathin separator coatings around nanostructured material. The coatings play an important role in stabilizing SEI formation around high surface area electrode (a problem which is preventing widespread nanomaterials in battery components) by reducing electrode/electrolyte interactions. Future work could entail studying different high capacity intermetallic based anode systems to achieve stable cycling behavior. Carbon anodes suffer from low capacities making current batteries expensive for use in electric vehicle applications. Hence by optimization of higher capacity anodes such as Si and Sn one could realize more affordable battery pack cost for next generation electric vehicles. Polymer coatings could play an important role in the development of Si based anodes by controlling SEI formation.

This thesis also focusses on 3D current collector architectures to accommodate more electrode mass, and controlling electrode thickness. The designs developed in this thesis allow for significant increase in energy per footprint area (an important metric for battery performance). We have developed an interesting thin film current collector architecture which incorporates both order and disorder (Au nanoporous nanorods) into the same current collector system which could be instrumental in achieving high energy devices. Electrode current collector adhesion is improved due to conformal nature of electrode coatings around the current collector. By adopting the 3D design, we have also developed porous electrodes with ability to engineer pore dimensions. This has helped in alleviating strain built up within high volume of expansion materials such as silicon and thereby improving cycling characteristics. Further increasing the thickness of the porous current collector films could improve energy per footprint area of the devices. The approach which was intended for thin film battery applications could be seamlessly extended to higher energy applications such as electric vehicles by varying film thicknesses of the current collectors.

In the final segment of this thesis, we look at the interesting problem of engineering all essential components of a Li based energy storage device – anode, cathode and electrolyte – onto a single nanowire. We have achieved the fabrication of such a device using Ni-Sn as the anode, Polyaniline as the cathode and PEO based electrolyte. We have observed a very important phenomenon, of rapid self-discharge for cells built in this fashion, where the electrodes are separated by nanometer thick separators. Future work could focus on optimizing separation distances to reduce self discharge and current leakage problems.

In closing the author hopes that this chapter provides a summary of research results pursued as part of this thesis and future directions and applications. This chapter underlines how nanostructured bottom up approach for battery design development could be crucial for obtaining high performance batteries to satisfy increasing energy demands.

References

1. Linden, D.; Reddy, T. B. (eds) Handbook of Batteries, 3rd edn (McGraw-Hill, **2002).**

2. Nagaura, T.; Tozawa, K.; Prog. Batteries Sol. Cells **1990** 9, 209

3. Takeshita, H. Worldwide. Proc. Conf. Power **2000**, San Diego.

4. Ikeda, H.; Saito, T.; Tamura, H. *Proc. Manganese Dioxide Symp. Vol. 1 (eds Kozawa, A. & Brodd, R.H.)* **1975**

5. Broahead, J.; Butherus, A.D. US Patent 3791867.

6. Whittingham, M. S. *Science* **1976** *192*, 1226

7. Tarascon, J. M.; Armand, M. *Nature* **2001** 414, 359

8. Lazzari, M.; Scrosati, B. *J. Electrochem. Soc.* **1980** *127*, 773

9. Armand, M.; Tarascon, J.M. *Nature* **2008** *451*, 652

10. Whittingham, M. S. *US Patent* 4009052.

11. Kezuka, K.; Hatazawa, T.; Nakajima, K *Journal of Power Sources* **2001** *97–98*, 755

12. M. Stanley Whittingham *Chem. Rev.* **2004,** 104, 4271

13. Mitzushima, K.; Jones, P. C.; Wiseman, P. J.; Goodenough, J. B. *Mater. Res. Bull.* **1980** *15*, 783

14. Amatucci, G. G.; Tarascon, J. M.; Klein, L. C. *J. Electrochem. Soc.* **1996** *143,* 1114

15. Van Schalkwijk, W.; Scrosati, B. *Advances in Lithium-Ion Batteries* (Kluwer Academic/Plenum, New York) **2002**

16. Rossen, E.; Reimers, J. N.; Dahn, J. R. *Solid State Ionics* **1993** 62, 53.

17. Gabrisch, H.; Yazimi, R.; Fultz, B. J. El*ectrochem. Soc.* **2004** 151, A891.

18. Li, N.; Martin, C. R.; Scrosati, B. *Electrochem. Solid-State Lett.* **2000** *3*, 316

19. Ozawa, K. *Solid State Ionics* **1994** *69*, 212

20. Goodenough, J. B.; Mizuchima, K. *U.S. Patent* 4302518

21. Imanishi, N.; Fujiyoshi, M.; Takeda, Y.; Yamamoto, O.; Tabuchi,M. *Solid State Ionics* **1999** *118*, 121

22. Levasseur, S.; Menetrier, M.; Suard, E.; Delmas, C. *Solid State Ionics* **2000**, *128*, 11

23. Kang Xu *Chem. Rev.* **2004** *104*, 4303

24. Koch, V. R.; Goldman, J. L.; Mattos, C. J.; Mulvaney, M. *J. Electrochem. Soc.* **1982** 1, 129

25. Koch, V. R.; Young, J. H. *Science* **1979** *204*, 499.

26. Goldman, J. L.; Mank, R. M.; Young, J. H.; Koch, V. R.; Young, J. H. J. *Electrochem. Soc.* **1980** *127*, 1461.

27. Desjardins, C. D.; Cadger, T. G.; Salter, R. S.; Donaldson, G.;Casey, E. J. *J. Electrochem. Soc.* **1985**, 132, 529

28. Foos, J. S.; McVeigh, J. *J. Electrochem. Soc.* **1983** *130*, 628

29. Foos, J. S.; Stolki, T. J. *J. Electrochem. Soc.* **1988** *135*, 2769

30. Abraham, K. M.; Goldman, J. L.; Natwig, D. L. *J. Electrochem.Soc.* **1982** *129*, 2404.

31. Dampier, F. W. *J. Electrochem. Soc.* **1981** *128*, 2501

32. Abraham, K. M.; Pasquariello, D. M.; Martin, F. J. *J. Electrochem. Soc.* **1986** *133*, 661.

33. Aurbach, D.; Gofer, Y.; Langsam, J. J. *Electrochem. Soc.* **1989** *136*, 3198.

34. Newman, G. H.; Francis, R. W.; Gaines, L. H.; Rao, B. M. *J.Electrochem. Soc.* **1980** *127*, 2025.

35. Scrosati, *B. Nature Nanotechnology* **2007** *2*, 598 - 599

36. Endo M.; Nakamura J.; Sasabe Y.; Takahashi T.; Inagaki M. T. *IEEE Jpn.* **1995** *115-A*, 349.

37. Endo M.; Nakamura J.; Sasabe Y.; Takahashi T. ; Inagaki M. *TANS0* **1994** *165*,282

38. Yata S.; Kinoshita H.; Komori M.; Ando N.; Kashiwa- mura T.; Harada T.; Tanaka K. ; Yamabe T. *Synth. Metals* **1994** *62*, 153.

39. Mabuchi A., Tokumitsu T., Fujimoto H. and Kashu T., *Extended Abstracts of 7th Int. Meeting on Lithium Batteries, Boston,* **1994** *205*, 15

40. Sato K.; Noguchi M.; Demachi A.; Oki N.; Endo M. *Science* **1994** *264*, 556

41. Sato K.; Noguchi M.; Demachi A.; Oki N.; Sasabe Y.; Endo M., *Proc. Int. Workshop on Advanced Battery,* **1995** *219*, 11

42. Kasavajjula, U.; Wang, C.; Appleby, J. A. *Journal of Power Sources* **2007**, *163* 1003

43. Aricò, A. S.; Bruce, P.; Scrosati, B.; Tarascon , J. M.; Schalkwijk, W. V. *Nature Materials* **2005** *4,* 366

44. Huggins, R. A. *in Handbook of Battery Materials* (ed. Besenhard, J. O.) Part III, Chapter 4 (Wiley-VCH, Weinheim, **1999**).

45. Winter, M.; Besenhard, J. O. *Electrochim. Acta* **1999** *45*, 31

46. Nazar, L. F.; Crosnier, O. In Lithium Batteries Science and Technology (eds Nazri,G.-A. & Pistoia, G.) 112–143 (Kluwer Academic/Plenum, Boston, **2004**).

47. Idota, Y.; Kabuto, T.; Matsufuji, A.; Maekawa, Y.; Miyasaki, T. *Science* **1997** *276*,1395

48. Mao, O.; Dahn,J. R. *J. Electrochem. Soc.***1999** *146*, 423

49. Beaulieu, L. Y.; Dahn, J. R. *J. Electrochem. Soc.* **2000** *147*, 3237

50. Graetz, J., Ahn, C. C., Yazami, R. & Fuetz, B. *Electrochem. Solid-State Lett.* **2003** *6*, A194

51. Yang, J. et al., *Electrochem. Solid-State Lett.* **2003** *6*, A154

52. Novak, P. et al. *in Int. Meeting Li Batteries IMLB12 Nara, Japan Abstract 9* **2004.**

53. Ikeda, H. et al. in *Proc. 42nd Battery Symposium, Yokohama, Japan 282* **2001**.

54. Green, M.; Fielder, E.; Scrosati, B.; Wachtler, M.; Serra Moreno, J. *Electrochem. Solid-State Lett.***2003** *6*, A75

55. J. Yang, M. Winter, J.O. Besenhard *Electrochem. Solid-State Lett.* **1996** *90*, 281

56. Chan, C. K.; Peng, H.; Liu, G.; McIlwrath, K.; Zhang, X. F.; Huggins, R. A.; Cui *Nature Nanotechnology* **2008** *3,* 31

57. Green, M.; Fielder, E.; Scrosati, B., Wachtler, M. & Moreno, J. S. *Electrochem. Solid-State Lett.* **2003,** *6*, A75

58. Ryu, J. H.; Kim, J. W.; Sung, Y.-E.; Oh, S. M. *Electrochem. Solid-State Lett.* **2004** *7*, A306

59. Graetz, J.; Ahn, C. C.; Yazami, R.; Fultz, B. *Electrochem. Solid-State Lett.* **2003***, 6*, A194

60. Gao, B.; Sinha, S.; Fleming, L.; Zhou, O.*Adv. Mater.* **2001** *13*,816

61. Kim. Y. L.; Lee, H. Y.; Jang, S. W.; Lim, S. H.; Lee, S. J.; Baik, H. K. *Electrochim. Acta* **2003** *48*, 2593.

62. Kim, J. B.; Lee, H. Y.; Lee, K. S. *Electrochem. Commun.* **2003** *5*, 544.

63. Kim, J. B.; Lim, S. H.; Lee, S. M.J. Electrochem. Soc. **2006**, *153* A455.

64. Jung, J. Y.; M.H. Kim, H.S. Moon, J.W. Park, *Mater. Sci. Forum* **2005** *486*, 558.

65. Park, Y. S.; Baik, H. K.; Lee, S. M.; Oh, J. Y. *US Pat. 6,828,063* (**2004**) (to Samsung SDI Co.).

66. Lee, S. J.; Lee, H. Y.; H.-K. Baik, S.-M. Lee*, J. Power Sources* **2003** *113* 119

67. Takamura, T.; Ohara, S.; Uehara, M.; Suzuki, J.; Sekine, K. *J. Power Sources* **2004** *96*, 129

68. M. Uehara, J. Suzuki, K. Tamura, K. Sekine, T. Takamura, *J. Power Sources* **2005** *441*, 146

69. Ahn, H. J.; Y.-S. Kim, K.-W. Park, T.-Y. Seong, *Chem. Commun.* **2005** *43*, 162.

70. Hatchard, T. D.; Dahn, J. R. J. *Electrochem. Soc.* **2004** *151*, A1628.

71. Dahn, J. R.; Trussler, S.; Hatchard, T. D.; Bonakdarpour, A.; MuellerNeuhaus, J. R.; K.C. Hewitt, M. Fleischauer, *Chem. Mater.* **2002** 14, 3519.

72. Fleischauer, M. D.; Hatchard, T. D.; Rockwell, M.; Topple, J. M.; Trussler, S.Jericho, S. K.; Jericho, M. H.; Dahn, J. R. *J. Electrochem. Soc.* **2003,** *150* A1465.

73. Beaulieu, L. Y.; Eberman, K. W.; Turner, R. L.; Krause, L.J.; Dahn, J. R. *Electrochem. Solid-State Lett.* **2001 4,** A137.

74. Beaulieu, L. Y.; Hatchard, T. D.; Bonakdarpour, A.; Fleischauer, M. D. Dahn, J. R.; *J. Electrochem. Soc.* **2003** *150*, A1457.

75. Hatchard, T. D.; Dahn, J. R. *J. Electrochem. Soc.* **2005** *152*, A1445.

76. Hatchard, T. D.; Obrovac, M. N.; Dahn, J. R. *J. Electrochem. Soc.* **2005** *152*, A2335.

77. Song, S. W.; Striebel, K.A.; Reade, R. P.; Roberts, G.A.; Cairns, E. J. J. *Electrochem. Soc.* **2003** 150, A121.

78. Magasinski, A.; Dixon, P.; Hertzberg, B.; Kvit, A.; Ayala, J.; Yushin, G. *Nature Materials* **2010** *9,* 353

79. Armstrong, A. R., Armstrong, G., Canales, Garcia, J. R.; Bruce, P. G. **2005** 2 862

80. Whittingham, M. (Ed.), *Solid State Ionics* **1994** 69, 402

81. Winter, M.; Besenhard, J.; Spahr, K.; Novak, P. *Adv. Mater.* **1998** *10,* 402

82. Dahn, J. R.; Zhang, T.; Liu, Y.; Xue, J. S. *Science* **1995** *270*, 402

83. Avdeev, V. Nalimova, K. Semenenko, *High Pressure Res.* **1990** *11*, 402

84. Frackowiak, E.; Gautier, S.; Gaucher, H.; Bonnamy, H.; Beguin, F. *Carbon* **1999** *37*, 61

85. Wu, G. T.; C. S. Wang, X. B. Zhang, H. S. Yang, Z. F. Qi, P. M. He, W. Z. Li, *J. Electrochem. Soc.* **1999** *146*, 1696

86. Claye, A..; R. Lee, Z. Benes, J. Fischer, *J. Electrochem. Soc.* **2004** *402*,403

87. Gao, B.; Kelinhammes, A.; Tang, X. .; C. Bower, Y. Wu, O. Zhou, *Chem. Phys. Lett.* **1999** *307*, 153

88. Claye, A. S.; Fischer, J. E.; Huffman, C. B.; Rinzler A. G.; Smalley, R. E. J. *Electrochem. Soc.*, **2000** *147*, 2845

89. Mukhopadhyay, I.; S. Kawasaki, F. Okino, A. Govindaraj,; C. N. R. Rao; H. Touhara, *Physica B*, **2002** *323*, 130

90. Ng, S. H.; J. Wang, Z. P. Guo,; J. Chen,; G. X. Wang; H. K. Liu, *Electrochim. Acta*, **2005** *51*, 23

91. Gao, B.; Kleinhammes, A.; Tang, X. P.; Bower, C.; Fleming, L.; O. Zhou, Chem. Phys. Lett., **1999** *307*, 153

92. Gao, B.; Shimoda, H.; X. P. Tang, A. Kleinhammes, L.; Fleming,Y. Wu.; O. Zhou, *AIP Conf. Proc.,* **2001** *590*, 95

93. Shimoda, H.; Gao, B.; Tang, X.P., Kleinhammes, A.; L. Fleming, Y. Wu and O. Zhou, *Phys. Rev. Lett.,* **2002** *88*, 5502.

94. Eom J. Y.; H. S. Kwon, *J. Mater. Res.*, **2008** *23*, 2458

95. Jeong, S.K.; M. Inaba,; R. Mogi, Y. Iriyama,; T. Abe.; Z. Ogumi, *Langmuir*, **2001** *17*, 8281

96. Landi, B. J.; Ganter, M. J.; Schauerman, C. D. Cress.; R. P. Raffaelle, *J. Phys. Chem. C,* **2008** *112*, 7509.

97. Landi, B. J.; M. J. Ganter; C. M. Schauerman; R. A. DiLeo; C. D. Cress; R. P. Raffaelle, in *Mobile Energy*, **2008**

98. Amaratunga, G. Nathan, A.; Nookala, M.; Smart, M. C., Eds. *Mater. Res. Soc. Symp. Proc.*, **2009**, 1127E, 1127-T03-06.

99. DiLeo, R. A.; Landi, B. J.; Raffaelle, R. P. *J. Appl. Phys.* **2007** *101*, 0643071

100. Landi, B. J.; DiLeo, C. M.; Schauerman, C. D.; Cress, M. J.; Ganter, M. J.; Raffaelle, R. P. *J. Nanosci. Nanotechnol.*, **2009** *9,* 3406.

101. Zhang, Z.; Peng, J.; Zhang, H. *Appl. Phys. Lett.*, **2001** *79*, 3515

102. Landi, B. J.; Raffaelle, R. P.; Heben, R. P.; J. L. Alleman, W. VanDerveer and T. Gennett, *Nano Lett.,* **2002** *2,* 1329

103. Li, X.; Kang, F.; Shen, W. *Carbon*, **2006** *44,* 1334

104. Guoping, W.; Qingtang, Z.; Zuolong. Y.; MeiZheng, Q. *Solid State Ionics*, **2008** *179*, 263

105. Jin, E. M.; B. Jin, Park, K. H.; Gu, H. B.; Park. G. C.; Kim, K. W. *J. Nanosci. Nanotechnol.,* **2008** *8*, 5057

106. Lee, D.-W. Kim.; J.-G. Park, *Cryst. Growth Des.,* **2008**, 8, 4506

107. Lee, J. H.; Kim, G. S.; Choi, Y. H.; Park, W. I.;Rogers. J. A.; Paik, U. *J. Power Sources*, **2008** *184*, 308

108. Li, X.; Kang, F.; Bai X.; Shen, W. *Electrochem. Commun.*, **2007**, 9, 663

109. Li, X.; Kang, F.; Shen, W. *Electrochem. Solid-State Lett.*, **2006**, 9, A126

110. Sotowa, C.; Origi, G.; M. Takeuchi, Y.; Nishimura, K.; Takeuchi, Y.; Jang, Y. J.; Kim, T.; Hayashi, Y. A.; Kim, M.; Endo, M.; Dresselhaus, M. S. *ChemSusChem*, **2008**, *1*, 911

111. Chung, S. Y., Bloking, J. T & Chiang, Y. M. *Nature Mater.* **2002** *1*, 123

112. Padhi, A. K., Najundaswamy, K. S. & Goodenough, J. B. *J. Electrochem. Soc.* **1997** *144*, 1188

113. Padhi, A. K., Najundaswamy, K. S., Masquelier, C., Okada, S.; Goodenough, J. B. *J. Electrochem. Soc.* **1997** *144*, 1609

114. Najundaswamy, K. S.et al. *Solid State Ionics* **1996** *92*, 1

115. Andersson, A. S.; Kalska, B.; Häggström, L.; Thomas, J. O. *Solid State Ionics* **2000** *130,* 41

116. Prosini, P. P., Zane, D.; Pasquali, M. *Electrochim. Acta* **2001** *46,* 3517

117. Bates, J. B.; Dudney, N. J.; Neudecker, B.; Ueda, A.; Evans, C. D. *Solid State Ion*ics **1999** *135*, 33

118. Golodnitsky, D.; Nathan, M.; Yufit, V.; Strauss, E.; Freedman, K.; Burstein, L.; Gladkich, A.; Peled, E. *Solid State Ionics* **2006** *177*, 26

119. Hassoun, J.; Panero, S.; Simon, P.; Taberna, P. L.; Scrosati, B. *Adv. Mater.* **2007** *19*, 1632

120. Nam, K. T.; Kim, D-W.; Yoo, P. J.; Chiang, Y. –C.; Meethong, N.; Hammond, P. T.; Chiang, Y. –M.; Belcher, A. M. *Proc. Natl. Acad. Sci. USA* **2008** *105,* 17227

121. Powers, R. A. *Proc. IEEE* **1995** *83*, 687

122. Nathan, M.; Golodnitsky, D.; Yufit, V.; Strauss, E.; Ripenbein, T.; Shechtman, I.; Menkin, S.; Peled, E. *J. Microelectromech Syst.* **2005**, *14*, 879

123. Hassoun, J.; Panero, S.; Scrosati, B. *J Power Sources* **2006**, *160*, 1336

124. Owen, J. R. *Chem. Soc. Rev.* **1997**, *26*, 259

125. NanoMarkets Report, Thin-Film and Printed Batteries Market, White Paper, March **2008**, www.nanomarkets.net.

126. W. C. West, J. F. Whitacre, V. White, B.V. Ratnakumar, *J. Micromech. Microeng.*, **2002** *12*, 58

127. N. J. Dudney, *Mat. Sci. Eng. B*, **2005** *116*, 245.

128. Cho, Y. K.; Wartena, R.; Tobias, S. M.; Chiang. Y. -M. *Adv. Funct. Mater.* **2010**, *17*, 379

129. Dillon, A. C.; Mahan, A. H.; Deshpande, R.; Parilla, P. A.; Jones, K. M.; Lee. S. H. *Thin Solid Films* **2008**, *516*, 794

130. Bates, J. B.; Dudney, N. J.; Gruzalski, G. R.; Zuhr, A. Choudhury, C. F. Luck, and J. D. Robertson, *Solid State Ionics*, **1992** 53, 647

131. Bates, J. B.; Dudney, N. J.; Gruzalski, G. R.; Zuhr, R. A.; Choudhury, A.; Luck. C. A.; Robertson, J. D. *J. Power Sources* **1993** *103,* 43

132. Yu, X.; Bates, J. B.; Jellison, Jr., and F. X. Hart, *J. Electrochem. Soc.*, **1997** *144*, 524

133. http://www.excellatron.com/high.html

134. C. N. Li, J. M. Yang, V. Krasnov, J. Arias, and K. W. Nieh, *Electrochem. Solid-State Lett.,* **2008** 11, A81

135. N. J. Dudney, J. B. Bates, and C. D. Evans, *Ceramics Transactions*, **2000** *109*, 341

136. Lee, S. H.; Liu, P.; C. E. Tracy, *Electrochem. Solid-State Lett.*, **2003** 6, A275

137. Inaguma, Y. et al.; *Solid State Commun.* **1993** *86*, 689

138. Kanno, R..; Maruyama, M. *J. Electrochem. Soc.* **2001** *148*, A742

139. Mizuno, F., Hayashi, A., Tadanaga, K. & Tatsumisago, M. *Adv. Mater.* **2005** *17*, 918

140. Hayashi, A., Minami, K., Mizuno, F. & Tatsumisago, M. *J. Mater. Sci.* **2008**, *43*, 1885

141. Kondo, S., Takada, K.; Yamamura, Y. *Solid State Ion.* **1992** *53*, 1183

142. Takada, K., Aotani, N.; Kondo, S. *J. Power Sources* **1993** *43*, 135

143. Inada, T. et al. J. *Power Sources* **2009** *194*, 1085

144. Kobayashi, T. et al. *J. Power Sources* **2008**, *182*, 621

145. Kobayashi, T., Yamada, A.; Kanno, R. *Electrochim. Acta* **2008**, *53*, 5045

146. Alpen, U. V., Rabenau, A.; Talat, G. H. Ionic *Appl. Phys. Lett.* **1977** *30*, 623

147. Lapp, T.; Skaarup, S.; Hooper, A. *Solid State Ion.* **1983** *11*, 103

148. Long, J. W.; Dunn, B.; Rolison, D. R.; White, H. S. *Chem. Rev.* **2004**, *104*, 4463

149. Cheah, S. K.; Perre, E.; Rooth, M.; Fondell, M.; Harsta, A.; Nyholm, L.; Boman, M.; Gustaffson, T.; Lu, J.; Simon, P.; Edstrom, K. *Nano Lett.* **2009**, *9*, 3230

150. Madou, M. J.; Jornet, F. G. *US Patent 11837286* **2007**.

151. Bazin, L.; Mitra, S.; Taberna, P. L.; Poizot, P.; Gressier, M.; Menu, M. J.; Barnabe, A.; Simon, P.; Tarascon, J. –M. *J. Power Sources* **2009**, *188*, 578

152. Long, J. W.; Rhodes, C. P.; Young, A. L.; Rolison, D. R. *Nano Lett.* **2003**, *3*, 1151

153. Rhodes, C. P.; Long, J. W.; Doescher, M. S.; Fontanella, J. J.; Rolison, D. R. *J. Phys. Chem. B* **2004**, *108*, 13079

154. Dewan, C.; Teeters, D. *J. Power Sources* **2003**, *119*, 310

155. Pushparaj, V. L.; Shaijumon, M. M.; Kumar, A.; Murugesan, S.; Ci, L.; Vajtai, R.; Linhardt, R. J.; Nalamasu, O.; Ajayan, P. M. *Proc. Nat. Acad. Sci. U.S.A.* **2007**, *104,* 13574

156. Spila, E.; Panero, S.; Scrosati, B. *Electrochim. Acta.* **1998,** *43,* 1651.

157. Amatucci, G. G.; Badway, F.; Du Pasquier, A.; Zheng, T. *J. Electrochem. Soc.* **2001,** *148,* A930.

158. Du Pasquier, A.; Laforgue, A.; Simon, P.; Amatucci, G. G.; Fauvarque, J.-F *J. Electrochem. Soc.* **2002**, *149*, A302.

159. Simon, P.; Gogotsi, Y. *Nature Mater.* **2008**, *7,* 845.

160. Yang, C. M.; Kim, Y-J.; Endo, M.; Kano, H.; Yudasaka, M. *et al.* **2007**, *129*, 20.

161. Gowda, S. R.; Reddy, A. L. M.; Manikoth, S. M.; Zhan, X.; Ci, L. *et al., Nano Lett.* **2011***, 11*, 101.

162. Prieto, A. L.; Mosby, J. M.; Arthur, T. S. US Patent App. 12/391,197, **2009.**

163. Pasquier, A. D.; Plitz, I.; Menocal, S.; Amatucci, G. *J Power Sources* **2003***, 115,* 171.

164. Winter, M.; Besenhard, J. O. *Electrochim. Acta* **1999**, *45*, 31

165. Roberts, M.; Johns, P.; Owen, J.; Brandell, D.; Edstrom, K.; Enany, G. E.; Guery, C.; Golodnitsky, D.; Lacey, M.; Lecoeur, C.; Mazor, H.; Peled, E.; Perre, E.; Shaijumon, M. M.; Simon, P.; Taberna, P-L. *J Mater. Chem,* **2011**, *21*, 9876.

166. Zhang, H.; Yu, X.; Braun, P. V. *Nature Nantoech* **2011**, *6*, 277.

167. Taberna, P. L.; Mitra, S.; Poizot, P.; Simon, P.; Tarascon, J. M. *Nature Mater.* **2006**, *5,* 567.

168. Shin, H-C.; Liu, M.; *Adv. Funct. Mater.* 2005*, 15*, 582.

169. Lytle, J. C.; Wallace, J. M.; Sassin, M. B.; Barrow, A. J.; Long, J. W.; Dysart, J. L.; Renninger, C. H.; Saunders, M. P.; Brandell, N. L.; Rolison, D. R. *Energy Environ. Sci.*, **2011**, *4*, 1913

170. Johns, P.; Roberts, M.; Owen, J. *J Mater. Chem.* **2011**, *21*, 10153

171. Zhang, S.; Xing, Y.; Jiang, T.; Du, Z.; Li, F.; He, L.; Liu, W. *J.PowerSources* **2011**, *196*, 6915.

172. Yu, Y.; Gu , L.; Lang, X.; Zhu, C.; Fujita, T.; Chen, M.; Maier, M. **2011,** *23*, 2443.

173. Gowda, S. R.; Reddy, A. L. M.; Zhan, X.; Ajayan, P. M. *Nano Lett.* **2011***, 11*, 3329.

174. Novak, P.; Müller, K.; Santhanam, K. S. V.; Haas, O. *Chem. Rev.* **1997**, *97*, 207.